2003

The compative research on the ag-alloy sheathed bi-2223 tapes

Zhongmin Zhang
University of Wollongong

The Compative Research on the Ag-alloy Sheathed Bi-2223 Tapes

A thesis submitted in fulfillment of the requirements
for the awarded of the degree

Honours Master of Engineering

From

University of Wollongong

By

Zhongmin Zhang

At

Institute for Superconducting and Electronic Materials

Faculty of Engineering

November 2003

Preface

This thesis describes work carried out at the Institute of Superconducting Engineering Materials (ISEM), Faculty of Material Engineering, University of Wollongong, from January 2002 to June 2003, under the supervision of Professor Hua Kun Liu and Dr. Miles Apperley from the Australian Superconductor Company.

Acknowledgements

Firstly, I would like to thank my supervisor, Professor Hua Kun Liu and Dr. Miles Apperley, for the guidance and advice they provided me, throughout the development and accomplishment of the research work. Secondly, I would like to thank Dr. Rong Zeng, for the help he provided me when I conducted tensile strain measurements at the Australian Superconductor Company. I also need to thank Dr. Joseph Horvat and Dr. Xiaolin Wang for the help he provided me on critical current density (J_c) – magnetic field (H) dependence measurements. In particular, I would like to thank John Volf, for his work in preparing all the samples for this research.

I would like to express sincere gratitude to Dr. T. Silver for providing great help in proof reading this thesis. It has been a pleasure to work at the ISEM, University of Wollongong. I would like to thank Matthew Lindesay, Saeid Soltanian, Sihai Zhou, Jiazhao Wang, Caiyun Wang, Yao Chen, Aihua Li, Yao Chen and all other colleagues at the ISEM for their general help and support.

Contents

Preface I

Contents II

Abstract V

Chapter 1. Introduction 1

Chapter 2. Literature Review 7

2.1. Application of Bi-2223 Materials 7
2.1.1 Introduction to the Application of Bi-2223 Materials 7
2.1.2 Superconducting Current Leads 8
2.2. Bi- based HTS Materials 11
2.2.1. Crystal Structure of Bi-based HTS 11
2.2.2. Phase Equilibrium in the Bi-based Oxide Ceramic System 13
2.3. Properties of Bi-2223 Tapes 14
2.3.1. Electrical Properties 14
2.3.2. Mechanical Properties 16
2.4. Powder-In-Tube Technique 18
2.4.1. Configurations of Precursor and Restack Sheath Materials 20
2.4.2. Deformation 22
2.4.3 Heat Treatment 24
2.5 Summary 27
References 29

Chapter 3. Introduction to Earlier Stage Work 34

3.1. 37-filament Bi-2223 Tape Configurations 34
3.2. Fabrication of Ag and Ag-alloy Sheathed Bi-2223 Tapes 35
3.2.1. Packing Bi-2223 Precursor Powder into the Tubes 37
3.2.2. Deformation Processing 37
3.2.3 Heat Treatment 39
3.3. X-ray Diffraction (XRD) 40

Reference 41

Chapter 4. Experimental Work 42

4.1. Electrical Properties 42
4.1.1. Critical Current Measurement 42
4.1.2. Critical Current Density (J_c) – Magnetic Field (H) Dependence Measurement 43
4.2. Mechanical Properties 44
4.2.1. Sheath Hardness 44
4.2.2. Tensile Strength 45
4.2.3. Bending Strain 46
4.3. Microstructure Analysis 46
4.3.1. XRD for Phase Analysis 46
4.3.2. Optical Microscopy 47
4.3.3. Scanning Electron Microscopy (SEM) 48

Chapter 5. Results 49

5.1. Phase Compositions 49
5.2. Electrical Properties 50
5.2.1. I_c and Sheath Configuration 50
5.2.2. Normalized J_c - Field Dependence and the Sheath Materials 51
5.3. Mechanical Properties 53
5.3.1. Bending Strain and the Sheath Materials 53
5.3.2. Hardness Profiles and the Sheath Materials 54
5.3.3. Tensile Profiles and the Sheath Materials 55
5.4. Microstructure Analysis 56
5.4.1. Optical Microscope Analysis 56
5.4.2. Scanning Electron Microscopy Analysis 60
Reference 72

Chapter 6. Discussion and Conclusion 73

6.1. Phase Composition 73
6.2. Electrical Properties 75

6.2.1. Optimized Critical Current I_c (at 77 K, 0 T) 75
6.2.2. Normalized J_c - Field Dependence and the Sheath Materials 76
6.3. Mechanical Properties 76
6.3.1. Bend Strain and the Sheath Materials 76
6.3.2. Hardness Profiles and the Sheath Materials 78
6.3.3. Tensile Strength and the Sheath Materials 79
6.4. Conclusion 80
References 81

Abstract

The work conducted for this thesis focuses on the effects of Ag-alloy materials on electrical properties, mechanical properties and microstructures of Bi-2223 tapes. In this work, Ag, AgAu, AgSb and AgMg were chosen as the precursor and restack sheath materials. The objectives of the work include: to investigate the phase formation of different alloy sheathed tapes fabricated using the powder-in-tube technique and heat treated at various temperatures; to measure the electrical properties of the alloy sheathed tapes; to characterise the mechanical properties of the alloy sheathed tapes and to observe the microstructures of the Bi(Pb)-Sr-Ca-Cu-O material inside the alloy sheathed tapes.

To fulfill these objectives, 7 kinds of 37 filament tapes with Ag, AgAu7wt%, AgSb0.6wt% and AgMg0.2wt% as precursor and restack sheaths were fabricated using the Powder In Tube (PIT) technique. These tapes were heat-treated at a temperature range of 832°C to 846 °C for the first stage (HT 1), followed by a second stage (HT 2). An intermediate roll pass was performed between the heat treatments.

The phase compositions (Bi-2223, Bi-2212, Bi-2201 and Bi-3221) were determined from X-ray diffraction data. It is seen that after HT 1 about 80% of the core was converted into Bi-2223 phase with the rest remains phases in most cases, because the major phase was Bi2212 in the green tapes and there was almost no Bi-2223 phase. The main purposes of sintering are to convert Bi-2212 into Bi-2223 and to achieve grain growth and grain connectivity. With HT 2, the fraction of Bi-2223 phase can reach to about 95% for higher J_c tapes. Bi-2201 is converted into superconducting phase during sintering at lower temperature (810 °C--825 °C), and slow cooling eliminated Bi-3221.

Analysis of the I_c and volume fractions of the Bi-2223, Bi-2212, Bi-2201 and

Bi-3221 phases indicated that volume fractions of Bi-2223 ~ 83-95%, Bi-2212 ~ 5%, Bi-2201 ~ 0% and Bi-3221 < 2% normally result in tapes with the highest I_c.

The normalized J_c dependence on magnetic field of the tapes at 77 K at H//c and H//ab were compared. The relationship between J_c and magnetic field was characteristic of multifilamentary Bi-2223 tapes. No conclusive correlation between alloy type or configuration and I_c performance in fields was established.

Bend strain tolerance was investigated by measuring the critical current at zero field (I_{co}) of a short sample and the I_c after one-way bending of the sample around progressively smaller diameter formers in the range of 110 to 20 mm. It was clearly observed that the tolerance of I_c to bending was quite different for the various tapes. The critical bend strain, ε_{crit} (bend strain when $I_c/I_{co} = 0.95$), of tapes with restack/precursor sheath Ag/Ag or Ag/AgSb was approximately 0.3%; the ε_{crit} of tapes with AgSb/Ag and with AgSb/AgAu was 0.42% and 0.47%, respectively. Tapes with AgAu/AgAu and with AgAu/AgSb sheath had ε_{crit} value of 0.28% and 0.25%, respectively. Tape with AgMg/AgAu possessed the highest ε_{crit} of 0.73%, displaying best performance of I_c tolerance to bend strain. From these results it was concluded that tapes with like restack sheath materials had similar bend strain properties and that the improved tolerance to bend strain could be related to the mechanical properties of the sheath materials.

The sequence of the sheath hardness from highest to lowest was AgMg0.2wt%, AgSb0.6wt%, AgAu7wt% or Ag. These results are consistent with the bend strain performance. Harder restack sheaths, such as those with Mg or Sb, may provide a mechanism by which the tolerance of the Bi-2223 to bend strain can be improved.

The best strengthening effect was shown in tapes with the restack sheath containing Mg. Tapes with the restack sheath containing Sb had the next best strengthening effect. Tapes with the sheath containing Au were similar to tape with pure Ag sheath,

indicating that the use of Au has a negligible effect on tensile strength. This trend was also consistent with the assessment of the bend strain tolerance.

To understand the mechanism behind the effects of different alloys, optical microscopy (OM) and scanning electron microscopy (SEM) were used to analyze the microstructures of the superconducting core and sheath of Bi-2223 tapes. The microstructure analysis showed that Sb will react with the core oxide when Ag-alloy is the precursor sheath and significantly reduce the electrical performance of the tape. In contrast, this reaction will not be so serious when pure Ag is used as the precursor sheath.

Chapter 1. Introduction

Superconducting materials have two characteristics. The first one is the total loss of electrical resistance when the superconductor is cooled below the Critical Transition Temperature (T_c) [1] discovered by H. K. Onnes in 1911. The second characteristic is perfect diamagnetism, such that an applied external magnetic field will be completely expelled from the interior of the superconductor, as found by Meissner in 1933 [2].

The existence of the superconducting stage is dependent on three interdependent parameters of the material. These are the critical temperature, the critical magnetic field strength and the critical current.

Critical Temperature (T_c) is defined as the particular temperature at which the material loses its resistance to become superconducting. This is a property of the material and the superconducting phase present; so one of the main focuses of superconductivity research is to discover new materials that become superconductors at higher temperatures [3].

Critical Magnetic Field (H_c) is another parameter of superconducting materials. Due to the lack of resistance in a superconducting material, eddy currents persist within a finite penetration depth, λ, from the surface. Because the eddy currents shield the superconductor from the external magnetic field, at a depth λ from the surface of the superconductor the magnetic field tends to zero. However, the superconductivity of the material will break down if the strength of the applied and self magnetic fields becomes greater than the critical magnetic field strength.

Critical Current Density (J_c) is a parameter related to critical current (I_c), the maximum current that can be passed without loss of superconductivity. The passing of a large DC current through the material at temperatures below T_c can also cause the superconductor to return to its normal state. The amount of current that a material can carry per cross sectional area is called the critical current density, J_c, which is usually measured in amperes per cm^2. The critical current

density is the current carrying ability of the superconductor and is a very important parameter for practical applications. At current densities higher than J_c the superconductivity breaks down and the material will show resistance. J_c is a function of the temperature and the magnetic field, and it strongly depends on the microstructure of the superconductor [4].

The first type of superconducting materials, such as mercury, which was discovered in 1911 and has a T_c of 4.2 K, require cooling by liquid He. Because of the very low temperatures required for the onset of superconductivity, these materials are commonly referred to as low temperature superconductors (LTS).

In 1986, Bednorz and Muller [5] discovered a new types of superconducting material, $(LaBa_2)CuO_{4-x}$ that had a T_c of 34 K. Many researchers began to focus on this new class of superconductors, which are named high temperature superconductors (HTS). As a consequence, materials with T_c values up to 130 K were discovered [6]. These discoveries indicate that superconductivity might be applied more cheaply and simply to a broad range of applications compared to the LTS that had been discovered much earlier and developed since the 1950's. With increased T_c values, there was now potential to use liquid nitrogen with a boiling point of 77 K as a cheaper and safer refrigerant.

Since the discoveries of Bednorz and Muller, several families of HTS material have been discovered. These include Y-Ba-Cu-O (T_c = 90 K) [7], Bi-Sr-Ca-Cu-O (T_c = 110 K) [8], Tl-Ba-Ca-Cu-O (T_c = 125 K) [9] and $HgBa_2Ca_2Cu_3O_x$ (T_c = 134 K) [10]. The Bi-Sr-Ca-Cu-O series of materials has attracted considerable research when they were quickly demonstrated to be easily fabricated into long lengths of wire suitable for power applications because the crystal lattice of BSCCO compounds shears easily along the bismuth oxide planes. This allows BSCCO compounds to be deformed and shaped with less difficulty than the other ceramic superconductors by the Powder In Tube (PIT) method [11-13].

BSCCO HTS material is typically synthesized as a polycrystalline material that is relatively hard and brittle. Because of the layered structure, the crystal tends to cleave along the

Cu-O planes (a-b planes of the crystal structure) producing crystals with a "mica like" or platy morphology. These physical characteristics of BSCCO material mean that the fabrication of long lengths of wire requires the material to be encapsulated by a metal cladding or sheath. This manufacturing process is known as the powder-in-tube (PIT) technique [11-13]. The sheath material should fulfill the following requirements:

- Compatible with BSCCO oxide, i.e. must not react with the HTS core
- Stable in the ambient atmosphere and does not oxidize in oxygen
- Provides mechanical strength and support to the HTS core
- Similar coefficient of thermal expansion to the HTS core
- Preferably be abundant and cheap.

To satisfy most of these requirements, silver (Ag) is widely used as the sheath material. Pure Ag on its own, however, is inadequate in providing all these requirements, and alloying is required to improve the properties of the sheath [12]. Tapes sheathed with Ag alloy have the following advantages:

- Improvement in the mechanical properties that enable the tape to withstand the stresses developed during fabrication and service. Stresses developed in the material could lead to the degradation of the transport properties [13].
- Strength to withstand the electromagnetic/magnetic hoop stresses developed as a consequence of Lorentz forces in large and/or high-field magnets [12].
- Resistance to "sausaging" along the length of tapes. Sausaging of the HTS core reduces the effective superconducting cross-sectional area and disrupts the grain alignment near the silver/core interface, which is believed to carry most of the current passing through the tape. This can produce microcracks that block the current path.

A series of silver alloys including AgSb, AgAu, AgAl, AgCu, AgMg, AgNi, AgMn, AgPd, AgPt, AgNiMg, etc. [12, 14-25] have been used as sheath materials. However, the J_c values observed in PIT tapes fabricated from these alloys were lower than for pure Ag sheathed tapes,

highlighting the importance of investigating the effect of such sheath alloys on the phase formation of Bi-2223 in PIT tapes.

In this work, Ag and AgAu, AgSb and AgMg alloys were chosen as the precursor and restack sheath materials. The objectives of the work were:

1. To investigate the optimum I_c corresponding to volume fraction of phases (Bi-2223, Bi-2212, Bi-2201 and Bi-3221).
2. To measure the electrical properties of Ag and Ag-alloy sheathed tapes and to find out the optimum I_c dependence on alloy sheath configurations and the relation of the normalised J_c-field dependence and the sheath materials.
3. To characterise the mechanical properties of Ag and Ag-alloy sheathed tapes and to find out the relationship between bend strain and the sheath material, hardness profiles and the sheath material and tensile strength and the sheath material
4. To investigate the microstructures of the superconducting core (BSCCO) and the alloy sheath and to find out the relationship between microstructure and superconductivity, microstructure and mechanical properties, microstructure and Bi2223 phase formation.

Reference

[1] H. Kamerlingh Onnes, *Leiden Comm.*, 1206 (1911) 1226.

[2] W. Meissner and R. Ochsenfield, Nalurwissenschaften, 21 (1933) 787.

[3] A. J. Bourdillon and N. X. Tan, *High Temperature Superconductors: Processing and Science.* 1994, New York: Academic Press, Inc. p288.

[4] Y. C. Guo, W. M. Chen, H. K. Liu, S. X. Dou and A. V. Lukashenko, Physica C 355 (2001) 163.

[5] J.G Bednorz and K. A. Muller, Z. Phys. B64 (1986) 189.

[6] T. P. Sheahen, *Introduction to High-temperature Superconductivity*, Plenum Press, 1994.

[7] M. K. Wu, J. R. Ashburn, C. J. Torng et al, Phys. Rev. Lett., 58 (1987) 908.

[8] M. Maeda, Y. Tnanaka, m. Fukutomi and T. Asano, Jap. J. Appl. Phys. 27 (1988) L209.

[9] Z.Z. Sheng, A. M. Herman, Nature, 332 (1988) 55.

[10] C. H. Park, P. L. Anyder, J. Am. Ceram. Soc. 78, 3(7) (1995).

[11] Heine, K., J. Tenbrink and M. Thoner, Appl. Phys. Lett., 55 (1989) 2442.

[12] M. Apperley, R. Zeng, F. Darmann, G McCaughey, *Cryogenics*, 40, (2000) 319-324.

[13] S. X. Dou and H.K. Liu, Supercond. Sci.Technol., 6, (1993) 297.

[14] W. Goldacker, E. Mossang, M. Quilitz, M. Rikel, *IEEE Transactions on Applied Superconductivity*, 7 (1997) 1407.

[15] H. Fujishiro, M. Ikebe, K. Noto, M. Matsukawa, T. Sasaoka, J. Sato, S. Kuma, *IEEE Transactions on Magnetics*, 30 (4 Part 2), (1994) 1645.

[16] L. Martini, F. Barberiis, R. Berti, L. Bigoni, F. Curcio, G Volpini, *International Journal of Modern Physics B*, 13 (1999) 1357.

[17] Sasaoka, K. Nomura, J. Sato, S. Kuma, H. Fujishiro, M. Ikebe, K. Noto, *Applied Physics Letters*, 64 (1994) 1304.

[18] J. Yoo, H. Chung, J. Ko, H. Kim, *IEEE Transactions on Applied Superconductivity*, 7 (1997) 1837.

[19] K. Fischer, T. Fahr, A. Hütten, U. Schläfer, M. Schubert, C. Rodig, H-P. Trinks, *Supercond. Sci. Technol.* 11 (1998) 995.

[20] M. Ishizuka, Y. Tanaka, T. Hashimoto, H. Maeda, *Physica C*, 290 (1997) 265.

[21] Y. Tanaka, F. Matsumoto, H. Maeda, M. Ishizuka, *IEEE Transactions on Applied Superconductivity*, 5 (1995) 1158.

[22] R.P. Aloysius, A. Sobha, P. Guruswamy, U. Syamaprasad, *Supercond. Sci. Technol.* 14 (2001) 85.

[23] M. Putti, M.R. Cimberle, C. Ferdeghini, G Grasso, A. Manca, W. Goldacker, *IEEE Transactions on Applied Superconductivity*, 11 (2001) 3285.

[24] R. Zeng, Y.C. Guo, Y. Tanaka, J. Horvat, M. Ionescu, T.P. Beales, M. Apperley, H.K. Liu, S.X. Dou, *Physica C*, 307 (1998) 229.

[25] J. D. Cotton, G N. Riley and Jr., M. D. Teplitsky, *High temperature superconductors: synthesis, processing, and large-scale applications*, in U. Balachandran, P. J. McGinn

and J. S. Abell, eds. The Minerals, Metals and Materials Society, 1996, p89.

[26] R. N. Lumley, A. J. Morton and I. J. Polmear, *Acta Materialia*, Vol. 50, Issue 14 (2002) 3597.

Chapter 2. Literature Review

Utilization of Bi-2223 material requires the development of manufacturing technologies that can produce high performance, low-cost high-T_c superconducting wires. The achievement of this goal can only occur through an understanding of the basic relationships between processing, properties, and microstructures of the complex ceramic superconductors.

2.1. Application of Bi-2223 Materials

2.1.1 Introduction to the Application of Bi-2223 Materials

The vast research interest in high temperature superconductivity is due to the potential to apply the technology to a broad range of applications [1]. There are strong "techno-economic" drivers for the application of HTS technology. High temperature superconductivity is potentially the greatest technology in the field of power and communications. This innovation will impact on many aspects of our lives including electricity supply and utilisation, motors, generators, medicine and transportation.

It is important to note that all these applications must exhibit a reliability and maintenance profile, within the utility environment, that is not only comparable but also essentially identical to their conventional counterparts.

Ag-alloy sheathed BSCCO tape is typically cooled using liquid nitrogen, and various devices such as power cables, current leads and coils in transformers and motors [2]. Despite high J_c, tapes sheathed by pure Ag [3-6] are quite weak and require extra reinforcement in order to bear the tensile and bending stresses that are likely to occur during handling. A variety of Ag alloys, such as Au, Mg Pd, Mn, Al, Cu, Ni Ti and Sb have been examined as possible sheath materials to improve the mechanical

strength [7-22].

2.1.2 Superconducting Current leads

Current leads have become the first commercially available large scale application made of HTS. High temperature superconducting (HTS) current leads can minimise energy loss, cut refrigeration costs and raise efficiency of magnet systems. The advantages of using HTS's is their capacity to carry an electrical current below a critical temperature without any resistive loss while the thermal heat load is suppressed due to the low thermal conductivity. European industry has developed a 5kArms/50 kV current lead [23]. A16 kA current lead has been designed at Argonne National Laboratory for the SEMS project [24], Oxford Instruments and CERN have announced the successful test of an experimental 13 kA HTS current lead. Forschungszentrum Karlsruhe, Germany, and the Centre de recherches en Physique des Plasmas, Switzerland have constructed a 60 kA HTS binary current lead.

Replacing copper leads with HTS can drastically reduce the heat leakage into a cryogenic system. The theoretical optimum of the heat leakage per ampere (Q/I) for copper leads is 1.04 W/kA for vapour-cooled leads, and 47 W/kA for conduction-cooled current leads [25]. With HTS current leads, 100 – 500 mW/kA has been achieved [26- 28]. Both bulk (sintered or melt textured) HTS and HTS tapes have been utilized for current leads. While bulk rods or tubes usually have very low thermal conductivity and are cheaper to produce, Ag-sheathed HTS tapes are advantageous in terms of engineering safety, as the silver sheath acts as (i) a mechanical and chemical protection, (ii) an emergency current carrier, and (iii) current contacts because of the low resistance of the silver sheath. However, the major disadvantage of Ag-sheathed HTS tapes is the heat leakage due to the high thermal conductivity of the silver sheath.

Numerous efforts to produce efficient HTS current leads have basically diverged into two directions. Bulk rods or tubes of HTS such as Y-Ba-Cu-O (123) [26, 29, 30], Bi-2212 [29-31], Bi-2223 [29, 31, 32], can be produced with a rather low J_c but very low thermal conductivity [33]. Another possibility is to utilise silver sheathed HTS tapes [29, 34, 35], with high J_c and high thermal conductivity of the silver sheath. In the latter case the thermal conductivity can be drastically reduced by using alloyed silver [34]. So far, the current leads based on HTS tapes have been designed as conduction cooled leads (i.e. they are only cooled at the lower end) [27].

1.5 kA class current leads made of Bi-2223 Ag and Ag-alloy sheathed tapes have been manufactured and tested at Australian Superconductors Ltd and the University of Wollongong. The HTS current leads were constructed by binding of Ag, AgAu and AgAuMg alloy sheathed tapes, a non-magnetic stainless steel former and copper caps. I_c of the HTS current leads ware 1540 A, 1346 A and 980 A for AgAuMg, AgAu and Ag sheathed Bi-2223 current leads at 77 K, respectively. Using a mass flow loss measurement instrument, the heat leakage was estimated to be 2.4 W, 1.1 W and 1.0 W/lead, respectively over a temperature range from 77 K to 300 K. Using an empirical formula for thermal conductivity, the heat leakage was calculated to be 9 W, 0.21 W and 0.20 W/lead when the warm end temperature was 77 K [36]. Table 2.1 summarizes the characteristics of current leads made using Bi-2223 bulks or tapes.

Table 2.2. Review of Research Activities on Bi-2223 HTS Current Leads

Research Groups	Material(s)	Length (cm)	I_c (A)	J_c (A/cm^2)	Heat Leakage (mW/kA)		Ref.
Rhone Poulence (FR)	2223 bulk	40	1000		90		[37]
GERN Geneva (CH)	2223 tape (ASC)	50			140		[28]
TCSUH	2223 bulk	15	800	530			[38.39]
Argonne National Lab	2223 bulk	12-25	1500	1000	300		[40-42]
Babcock & Wilcox Co.	2223 tape (Ag-Au)	55 (HTS)	16000		100W/16kA		[43,44]
Naval Research Lab Washington	2223 bulk	20	250	250			[45]
Railway Technical Research Institute	2223 tape (Ag-Au)	43	600		500		[46]
Sumitomo Heavy Industry & Tohoku University	2223 bulk	10	1000	>1000	150		[47-49]
Sumitomo Electric Ind.	2223 tape	55	500- 2000	10^4	300		[50-53]
Showa Electric Wire	2223 bulk	10	1130	2500	100		[54]
NIRM, Japan	2223 tape (Ag-Cu)			$3.5*10^4$			[55]
IMR, China & IMM, Korea	2223 tape Ag-Au-Mg			$2.85*10^4$			[56]
				J_c (A/cm^2)	77-300K	4.2-77K	[36]
Australian Superconductors Ltd & University of Wollongong	2223 tape Ag		980	5400 (J_c)	1.0	9	
	2223 tape AgAu/AgAu4%		1350	4200 (J_c)	1.1	0.2	
	2223 tape AgAu7%/AgAu7%			4000 (J_c)			
	2223 tape Ag/AgSb			6000 (J_c)			
	2223 tape AgAu/AgAuMg		1540	4500 (J_c)	2.4	0.25	

2.2. Bi- based HTS Materials

2.2.1. Crystal Structure of Bi-based HTS

The Bi-Sr-Ca-Cu-O system comprises a series of $Bi_2Sr_2Ca_{n-1}Cu_nO_{2n+4+y}$ compounds. The best-known compounds with n = 1 to 3 are $Bi_2Sr_2CuO_{6+y}$ (Bi-2201), $Bi_2Sr_2CaCu_2O_{8+y}$ (Bi-2212) and $Bi_2Sr_2Ca_2Cu_3O_{10+y}$ (Bi-2223). Maeda et al. first reported superconducting transition temperatures between 80 K and 110 K in the Bi-Sr-Ca-Cu-O system, for the Bi-2212 and Bi-2223 phases [57].

Some research shows that doping with Pb substantially enhances the formation rate of Bi-based superconductors, especially for Bi-2223 [57]. Doping can slightly increase T_c [59] because Pb^{4+} has a larger ionic radius (1.2 Å) compared with Bi^{3+}. Therefore, the substitution of Bi by Pb may support the crystallisation of Bi-2223 [60,61] and, in addition, Pb doping shifts the phase stability to lower temperatures (unleaded Bi-2223: 840-890°C; Pb-doped Bi-2223: 830-880°C). Investigations of the Pb solubility in Bi-2223 show that the single-phase region of Bi-2223 within the BiO-SrO-CaO-CuO system is an irregularly shaped area that is characterized by a decreasing Pb content with increasing temperature [61].

The crystal structures of $Bi_2Sr_2Ca_{n-1}Cu_nO_{2n+4+y}$ (n = 1, 2, 3) play a very important role in forming HTS. Bi-2201 phase has a pseudo-tetragonal symmetry with lattice parameters a = b = 5.4 Å and c = 24.4 Å [62]. The unit-cell of Bi-2201 contains four formula units and is a stack of atomic planes in the sequence of:

$(BiO)_2/SrO/CuO_2/SrO/(BiO)_2/SrO/CuO_2/SrO/(BiO)_2$.

Bi-2212 phase has a pseudo-tetragonal structure with lattice parameters a = b = 5.4 Å and c = 30.8 Å [64]. The unit-cell of Bi-2212 contains four formula units and is a stack of atomic planes in the sequence of:

$(BiO)_2/SrO/CuO_2/Ca/CuO_2/SrO/(BiO)_2/SrO/CuO_2/Ca/CuO_2/SrO$.

Bi-2223 phase has a pseudo-tetragonal symmetry with lattice parameters a = b = 5.4 Å and c = 37 Å [64]. The unit-cell of Bi-2223 contains four formula units and is a stack of atomic planes in the sequence of:

$(BiO)_2/SrO/CuO_2/Ca/CuO_2/Ca/CuO_2/SrO/(BiO)_2/SrO/CuO_2/Ca/CuO_2/SrO$.

The structures of Bi-2201, Bi-2212 and Bi-2223 are similar as they all contain one or more immediately adjacent Cu-O planes in the unit cell. These planes are perpendicular to the c axis and hence parallel to the a-b planes as shown in Figure 2.1.

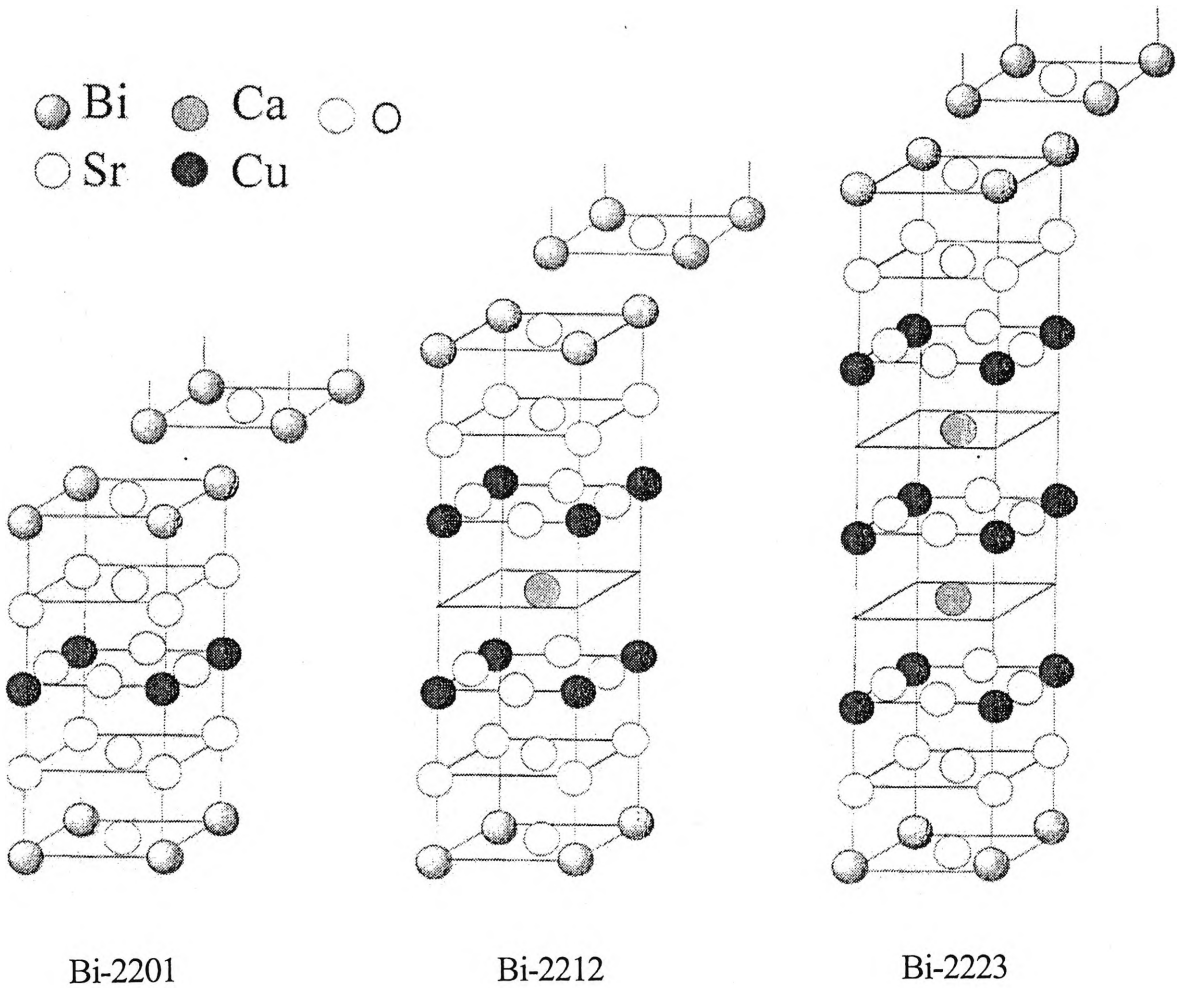

Figure 2. 1 Crystal structure of Bi-2201, Bi-2212 and Bi-2223 [66]

As a consequence of this layered crystal chemistry, all the BSCCO superconductors (n = 1-3) have grains that grow in a platelike form. Plates of Bi-2223 are typically submicrometre in thickness (c axis) but with larger lateral dimensions (a and b axes) that typically measure several micrometres.

It is considered that T_c is a function of the content of O, Ca, and Bi. It decreases with increasing Ca and Bi content [66, 72, 87]. T_c of Bi-2201 is less than 20 K. T_c of Bi-2212 varies between about 60 K and 94 K. This may depends on the chemical composition of the phase. Pb doped Bi-2212 has a T_c up to about 98 K. The T_c of Bi-2223 can reach to110 K. T_c also slightly decreases with increasing content of O, Bi, and Ca in the phase [66-69], but there is no dependce on the Pb content of the phase [70]. It seems that the oxygen content of the Bi-2223 depends on the temperature, oxygen partial pressure, and cation concentration of the phase during synthesis.

2.2.2. Phase Equilibrium in the Bi-based Oxide Ceramic System

Based on knowledge of phase equilibrium in the BiO-SrO-CaO-CuO system, it is considered that Bi-2212 can be observed easily because it is thermodynamically stable over a wide temperature range. The fact that Bi-2223 was detected in multiphase samples is due to its signal in resistivity and AC susceptibility measurements even for small concentrations [71, 72].

The formation of Bi-2223 can be considered to be the result of a reaction between Bi-2212 and a molten impurity phase like Ca_2PbO_4 or Ca_2CuO_3 [73]. Some evidence shows that partial melting (near 825°C) is crucially important to the formation of Pb-substituted Bi-2223, and that the formation takes a long time because of slow kinetics. Takada et al [74] have studied the wettability of the liquid for Bi-2201, Bi-2212, and Bi-2223 and suggested that a reaction with the liquid converts the Bi-2212 into the Bi-2223. They designed an important experiment where a mixture of Bi-2201 and Ca_2PbO_4 (in a 7:3 ratio) was put on pellets of Bi-2201, Bi-2212, and

Bi-2223 and then heated at 825°C for 1 hour. They found that the Bi-2223 was hardly wetted at all by the liquid, whereas both the Bi-2201 and Bi-2212 pellets were wetted immediately. This means that Bi-2212 can convert into Bi-2223 under certain condition.

2.3. Properties of Bi-2223 Tapes

2.3.1. Electrical Properties

The transport critical current density, J_c, of silver alloy sheathed Bi-2223 tapes is typically measured using the four-probe dc technique. The critical current, I_c, is determined from the recorded I-V curve using the 1 μV/cm criterion. The critical current density, J_c, is then calculated by dividing I_c by the sample cross-sectional area. The highest recorded J_c of a Bi-2223 tape was 73,000 A/cm^2 reported by American Superconductor Corporation (ASC) [75] in short samples. For long-lengths of tape I_c of 28 A and J_c of 5.2 kA/cm^2 were achieved for a 1250 m long tape manufactured by Nordic Superconductor Technologies (NST) [76].

Several studies have shown that only part (approximately10% of the superconductor cross section) of the filament carries any super-current [77]. These regions have been shown to occur at the sides of the tapes and they appear to exhibit no appreciable field dependence [79]. The J_c values in these regions are up to five times the average J_c for the tape. These high values may be attributed to the relatively higher compression that occurs at the sides of the tapes than at the center of the tape, thus producing a greater degree of grain alignment in the BSCCO close to the edges of single filament tapes.

Yamada et al. [78] investigated the depth profile of the texture in multifilament Bi-2223 tapes. It was found that the density and degree of grain alignment in the central filaments of a multifilament tape are higher than in the two sides of the tape. As a result, the central portion of the tape carries a higher critical current density than the edge portions [79-81]. At 77 K it was

found that the innermost filament carries a J_c of 53 KA cm^{-2}, much larger than for all the filaments of the outer shell where J_c ranges between 25 and 40 $KAcm^{-2}$ [82].

This means that J_c is higher towards the outside or edges of a single filament of BSCCO because that is where the alignment and density are greatest, i.e. lower density and alignment are found towards the centre. In a multifilament tape, the filaments towards the center of the cross section have greater grain alignment compared to the filaments toward the edges, so that the J_c values of the filaments in the center of the tape are higher compared to the filaments on the edges.

J_c dependence on an applied magnetic field, H, in Bi-2223 superconducting tapes is a major indication of the suitability of the material to a specific application. It is principally measured in two directions normally denoted H//ab and H//c -- parallel and perpendicular to the broad surface of the tape, respectively. The value of J_c drops rapidly with increasing H in both directions; however, the property is anisotropic so that the drop in J_c is most severe for the H//c direction, with J_c almost vanishing at a field of 0.5T [84]. The anisotropic behaviour of J_c in a magnetic field is due to the difference in flux pinning strength between the a-b planes and along the c-axis as shown in Figure 2.2.

Being ceramic materials, BSCCO contains grains, grain boundaries, twins, voids and other imperfections. Grain boundaries can effectively pin magnetic flux, and are partially responsible for high critical current densities. However, the short coherence lengths of the oxides make the electrical/magnetic properties exceedingly sensitive to microstructural in homogeneities [83]. For H//ab, due to the Lorentz force the flux lines are forced to move along the c-axis (crossing the a-b planes), which has strong intrinsic flux pinning strength while for H//c, the flux lines are forced to move within the a-b planes, which has weak pinning strength [84].

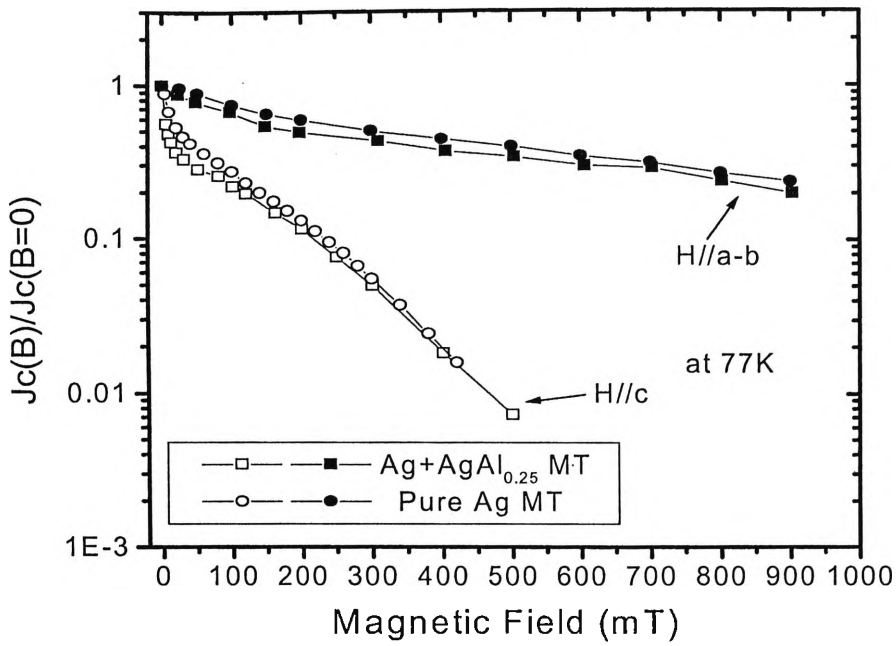

Figure 2. 2 J_c dependence on the magnetic field at 77 K in Ag and Ag-alloy sheathed Bi-2223 PIT tapes [84]

2.3.2. Mechanical Properties

The most common mechanical properties of PIT Bi-2223 tapes that are characterized are the tensile strength, the resistance of J_c to bending strain and the hardness of the sheath.

Bending is very common in the construction of superconducting devices such as magnets, generators, motors, transformers, and fault current limiters. The bending strain increases with decreasing radius of the bending curvature. If the change in the thickness of the specimen during bending is neglected, the strain, ε , on the tension surface (top surface) of the specimen is equal to the strain on the compression surface (bottom surface) and is given by,

$$\%\varepsilon = t/\Phi_f \times 100 \qquad (1)$$

where t is the tape thickness and Φ_f is the former diameter.

It has been observed that as the bend strain of a tape is increased, a point is reached at which the J_c of the tape will begin to degrade. This point is known as the critical bend strain, ε_{crit}.

Further bending beyond this point will result in continuing degradation of I_c as shown in Figure 2.3 [13]. The results indicate that bending properties were improved as the alloying element Mg increased from 0.2% to 0.5%. The reduction in J_c with bend strain is a consequence of cracking of the BSCCO filaments [86]. The cracks cut off paths of current flow and largely reduce the current-carrying capacity of the tape.

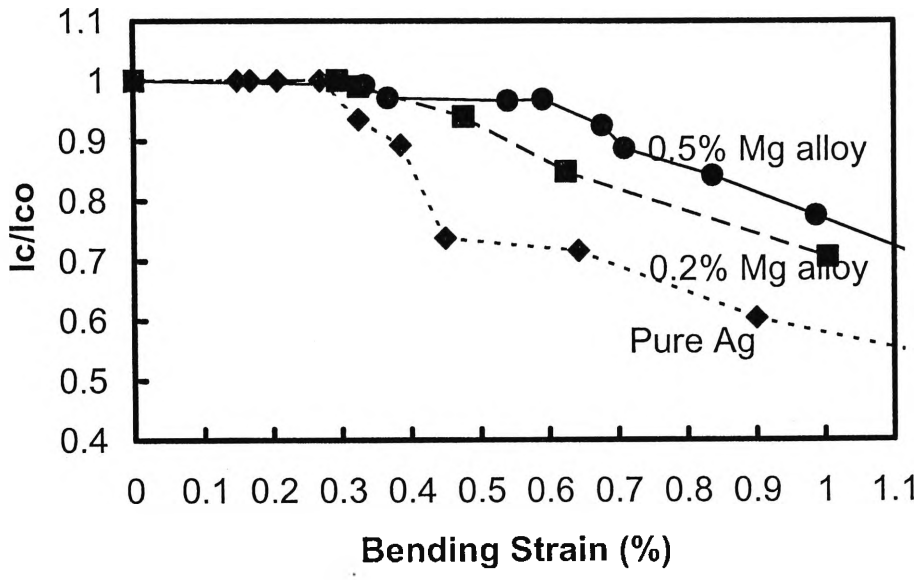

Figure 2. 3 Relative I_c/I_{c0} as a function of bend strain [13]

Apperley et al. [13] reported that increasing the alloying element Mg from 0.2% to 0.5%, increased the maximum axial stress before degradation in I_c occurred (Figure 2.4). Yoo et al. reported that alloying with Au or Pb is not very effective in increasing hardness, but that the addition of a small quantity of Mg to Ag-Au or Ag-Pb increases the hardness significantly due to dispersion hardening [87].

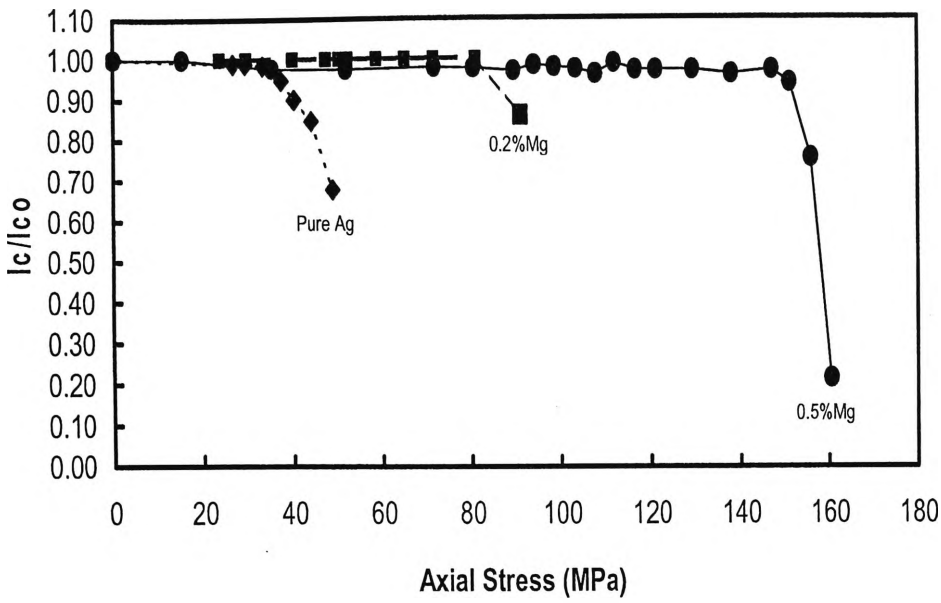

Figure 2. 4 Relative I_c/I_{c0} as a function of axial (tensile) stress [13]

2.4. Powder-In-Tube Technique

The crystal lattice of BSCCO compounds can be sheared easily along the bismuth oxide planes and this allows the material to be deformed and shaped with less difficulty than other ceramic superconductors. In 1989 K. Heine et al. [88] developed a technique, called the "Powder-in-Tube" (PIT) technique, to produce long BSCCO wires. In most PIT techniques, the process consists of powder packing, swaging, drawing, pressing or rolling and thermal treatment stages. A schematic diagram of PIT is shown in Figure 2.5 [118].

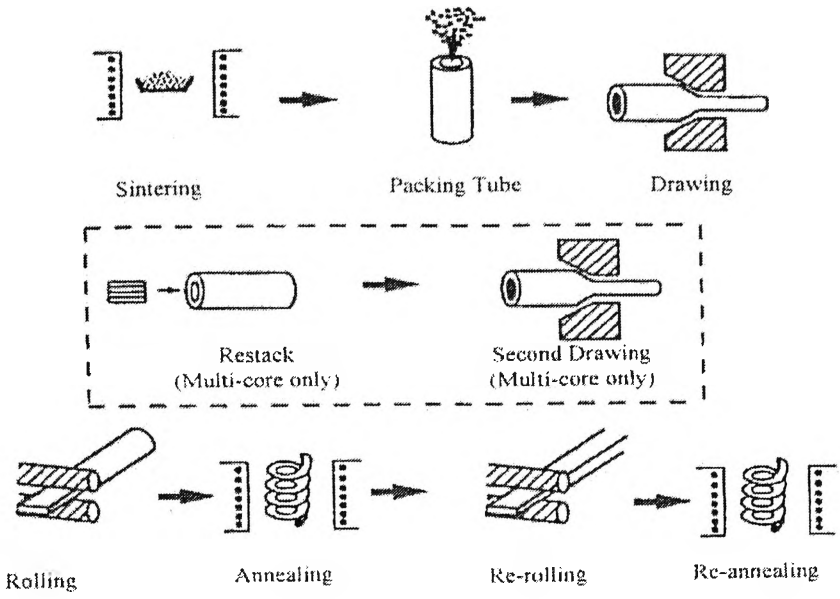

Figure 2. 5 Schematic diagram of the power-in-tube method to make wire and tapes [118].

BSCCO precursor powder is finely ground, mixed and packed into a silver or silver alloy tube. The composite is then swaged and drawn to the desired wire size through a series of dies. The wires can be annealed to relieve some of the stresses that build-up during these steps.

The standard procedure for heat treatment of silver-sheathed Bi-2223 superconducting tapes is a thermomechanical process, which consists of alternate thermal sintering and mechanical deformation. The process starts and finishes with a sintering step. Mechanical deformation is carried out between sintering steps and is, therefore, called intermediate deformation.

There are two major goals to be achieved by the heat treatment. The first goal is to form as pure as possible Bi-2223 phase. Before heat treatment, the green tapes consist of a major phase of Bi-2212 and other minor phases. Bi-2212 phase is gradually converted into Bi-2223 phase during the process of heat treatment. The second goal is to form a desirable microstructure in the superconductor core in order to enable the tapes to carry a large current.

There are a number of parameters, which affect the superconducting properties of

Bi-2223/Ag tapes. The important parameters include sintering temperature, sintering time, healing and cooling rate, oxygen partial pressure, method of mechanical deformation, thickness reduction rate, and number of sintering and intermediate deformation cycles [82, 83]. These parameters have to be optimized in order to achieve a pure Bi-2223 phase and desirable microstructure in the heat-treated tapes.

2.4.1. Configurations of Precursor and Restack Sheath Materials

There are several reasons why silver is used as precursor and restack sheath material in the composite. The first is that the metal provides some strength and ductility during the drawing process. The second is it also serves as a parallel electrical conduction path to carry current in case local superconductivity is lost. The third is that it provides thermal stabilization to minimize local heating and prevent catastrophic loss of superconductivity as well as providing protection from the surrounding environment. The forth is that it acts as mechanical protection for the brittle superconducting oxide. Most importantly, silver is used because it does not react with the superconducting oxide during the heat treatment stages of the PIT process nor does it form an oxide layer preventing oxygen diffusion through the sheath to the core [89, 90].

Pure Ag is chemically compatible with Bi-2223, and it has been found to be beneficial for the formation and stabilisation of Bi-2223 [91-93]. Furthermore, oxygen can diffuse through it very quickly at elevated temperatures [94, 95]. Although the strength of cold worked pure Ag is usually sufficient to withstand the forces involved in PIT composite fabrication, Ag becomes very soft after the heat treatment, which is typically performed at 825°C for periods of up to 100 hours. The mechanical properties of the sheaths after heat treatment are inadequate to withstand the stresses developed during fabrication and service of superconducting components. Stresses developed in the material could lead to the degradation of transport J_c. Such forces are likely in devices such as power cables, motors, transformers and coils, and especially high field magnet

insert coils, which will be subject to large hoop stresses on the windings.

Another problem with the pure silver sheath is the sausaging effect along the length of tapes. The sausaging of tapes reduces the effective superconducting cross-sectional area and disrupts the grain alignment near the interface of the silver and the superconducting core. More seriously, microcracks are often found to accompany sausaging, and these block the current. In order to minimize sausaging, it has been observed that the extent of mechanical deformation during tape processing should be reduced and the mechanical strength of the sheath should be enhanced [83].

One way to increase the strength of the sheath is to use Ag alloys [96-98]. In order to improve the mechanical characteristics of tapes, and thus to create a more robust final product with minimal sausaging, alternative sheath materials are required. The choice of sheath material will be dictated by its mechanical strength, chemical inertness with the superconducting core, and electrical conductivity. In recent years, a variety of Ag-alloys, such as Ag-Mn [99, 100], Ag-Al [101], Ag-Cu [102], Ag-Ti [103] and Ag-Mg-Ni alloys [104] have been used as the sheathing material. With Ag-Mg-Ni alloy, the Mg is intended to form oxide particles for hardening, while the Ni is added as a grain-refining agent. In practice, it was found that Mg and Ni tend to form Mg-Ni-O particles [104]. It is also probable that these alloy elements (or oxides) influence Bi-2223 formation [99-103].

In monofilament Ag-X alloy sheathed tapes (X = Cu, Al, Ti, Ni and Au), the formation of Bi-2223 was influenced by the reactivity of X with oxygen. Even very small alloying additions caused a significant change in the microstructure of the oxide core and phase formation kinetics of Bi-2223. In multifilament tapes, composed of an inner Ag sheath surrounding the BSCCO filaments and an outer alloy sheath surrounding the bundle of single filament wires, there was no such significant influence on the phase formation of Bi-2223 [105].

To control the thermal conductivity of Ag-alloy sheathed tapes is absolutely necessary in a variety of different applications [17]. Ag or Ag-alloy sheathed Bi-2223 tapes used for current

leads for superconducting magnets, carrying energy without Joule effect losses from the liquid nitrogen bath to the liquid helium bath, must have low thermal conductivity to minimize the heat flow to the cryogen. However, Ag or Ag-alloy sheathed Bi-2223 tapes used for the superconducting magnet coil should have high thermal conductivity and good mechanical properties to sustain the stress arising from Lorentz forces.

Jang et al. [104] reported that the thermal conductivities for AgMg, AgSb and AgAu at 40 K are 411.4, 142.3 and 109.7 W/(m.K) respectively, which are approximately 2 to 9 times lower than that of Ag (1004.6 W/(m.K)). The calculated thermal conductivity of a tape from the corresponding value of sheath and core was close to the measured one, suggesting that the thermal conductivity of BSCCO tape made of various sheath materials can be practically estimated. Australian Superconductors Ltd and the University of Wollongong have reported that AgAuMg alloy sheath material significantly improved the performance of Bi-2223 current leads, because Mg significantly improved the mechanical properties and Au significantly reduced the thermal conductivity [36].

2.4.2. Deformation

An optimal amount of deformation is required to achieve adequate grain alignment and avoid defects such as micro-cracks and sausaging. It has been shown that an optimal amount of deformation also exists for the phase content that develops in tape. However, this is also strongly dependent on additional factors such as time, temperature and the deformation technique [84].

Oota et al. [106] found that the thickness dependence of J_c at 77 K was different in three distinctive stages. At the first stage (0.2 mm – 1.0 mm), J_c was increased gradually as d decreased, by the co-deformation between the Ag sheath and the ceramic core. At the second stage (0.1 mm – 0.2 mm), J_c was raised sharply with decreasing d, by the densification of the ceramic core itself in the tape. Both of the stages resulted in an improved degree of grain

alignment. At the third stage (0.05 mm – 0.1 mm), J_c was lowered by the distortion of the Ag/ceramics interface, which was caused by the extreme densification of the ceramic core. A peak of $J_c = 1.53\times10^4$ A/cm^2 (77 K, 0 T) at $d = 0.1$ mm was explained by a competition between the improvement in grain connectivity and the disturbance in the transport current path. This also led to "sausaging" of the composite tape and reduced the J_c. This behaviour was thought to be due to the increased local densities of the powder, which creates a 'lump' that the silver sheath passes over. This created a wavy morphology at the interface between the Ag sheath and the oxide core. It led to a reduced effective cross section of the current path and disturbed the desired texture of the grains [107].

Li et al. [108] also studied the deformation, particularly the differences between rolling and uniaxial pressing, and observed the formation of sausage and crack defects. It was shown that the mass flow characteristics of pressing and rolling are significantly different. This was predominantly due to the stress state being rotated 90° between the two techniques. When the tape was rolled, mass flow was mainly along the length of the tape with little material flow across the width. This resulted the formation of microstructural defects, such as sausaging and micro-cracks across the width of the tape. Conversely, microstructural defects were observed along the length of pressed tapes because the majority of material flow was across the width of the tape. The higher J_c values obtained in pressed tapes have been attributed to the powder flow profile, because the defects lie parallel to the current path and not across the current path.

Deformation of the sheath and BSCCO composite is influenced by the manner in which the precursor is packed into the sheathing tube. Yamada et al. [78] have studied the effect of the packing procedure. Filling the Ag tube with loose powder leads to an irregular shape of the oxide core in the green tape and hence a low J_c, whereas a high J_c was achieved by packing high-density cylindrical rods prepared by swaging. The interface between the Ag and the oxide core was smooth, contributing to the higher J_c.

The common problems of sausaging and cracks that arise during deformation of the sheath

and BSCCO composite can severely limit the overall current in the tapes. The occurrence of these defects is due in part to the mismatch between the deformation properties of the sheath and the BSCCO precursor core. This mismatch leads to inhomogeneous deformation of the composite structure. To improve the homogeneity of deformation, a deformation process called "sandwich" rolling was developed to prevent the formation of sausaging and cracks in the longitudinal direction [109]. "Sandwich" rolling means that the tape is deformed between two steel sheets. The stress-strain state of a tape processed by "sandwich" rolling is similar to that produced during uniaxial pressing of tapes, because the deformation of steel sheets is negligible in comparison to that of Ag-clad Bi-2223 tape. The stress-strain distribution in the superconducting oxide core can be controlled by changing the curvature of the steel sheets. The J_c of sandwich rolled tape is improved in comparison with flat rolled tape.

2.4.3 Heat Treatment

The thermal treatment of BSCCO tapes is a crucially important part of the PIT process. Heat treatment of the tape results in the transformation of the Bi-2212 phase in the precursor material to Bi-2223, accompanied by grain alignment, grain growth and densification of the microstructure. In order to improve J_c, many researchers have focused on getting pure 2223 phase in Ag or Ag-alloy sheathed tapes because of the importance of a highly aligned, pure 2223 microstructure to achieve high J_c [110].

A number of parameters can affect the results of heat treatment of Ag or Ag-alloy sheathed BSCCO tapes. These are sintering temperature, sintering time, heating and cooling rate, oxygen partial pressure, mechanical deformation method, thickness reduction rate, and number of sintering and intermediate deformation cycles [83]. It has been found that the presence of Ag itself decreases the partial melting temperature of BSCCO and therefore decreases the sintering temperature of tape up to 10-15°C [112]. Ahn et al. reported that the temperature window for

processing could be widened and the volume fraction of Bi-2223 in the tape increased under low oxygen partial pressure. Using an atmosphere of N_2-7.5% O_2, nearly pure Bi-2223 phase was obtained by proper control of a multi-step annealing temperature [110]. The tapes annealed in N_2-7.5% O_2 retained their J_c values well over a wide annealing temperature range of 785-805°C with only 10% deviation from the highest value. Because the wide temperature range of heat treatment is advantageous for large-scale production, a low oxygen partial pressure of around 7.5% is commonly used for heat treatment instead of air.

It is commonly believed that there are different mechanisms for the formation and alignment of the Bi-2223 phase during heat-treatment. The presence of liquid phase is one of the essential factors for the formation and grain alignment of Bi-2223 [112]. It has been suggested that Bi-2223 forms by depositing dissolved cations from the liquid onto ledges of solid Bi-2212 or existing Bi-2223 platelets [113]. Alternatively a nucleation and growth mechanism has been proposed [114]. What has been realized is that regardless of the actual formation mechanism, the reaction process is dependent on the amount of liquid present and the processing route used to synthesize the precursor powder.

During the cooling process, the conversion of the liquid phase has a significant effect on the phase composition in the final tape and consequently J_c. According to Wang and Parrell's work, slow cooling and two-step annealing procedures at the end of the final thermal cycle have shown clear advantages in terms of critical current densities and flux pinning over conventional processing [115, 116]. It was found that the cooling rate influences both the intergranular connectivity and the intragranular flux pinning strength of the polycrystalline filaments.

Slow cooling eliminated Bi-2201 phase although it increased Bi-2212 and Bi-3221 phases. The elimination of Bi-2201 phase gave rise to a substantial enhancement in J_c and improved J_c behaviour in magnetic fields. These improvements in the superconducting properties occurred despite partial decomposition of the Bi-2223 phase into non-superconducting impurity phases during the slow cooling.

In order to reduce the amount of Bi-2201 amorphous phase, a two-step sintering procedure was used for the final heat-treatment cycle. Figure 2.6 shows a typical schedule for thermal treatment of Bi-2223 tapes. In this process, the final sintering is divided into two steps, with the first step at about 840°C for 30 h, followed by the second step at a low temperature (810-825°C) for 20-40 h, before finally cooling down to room temperature. The period of sintering at lower temperature allows the Bi-2201 and amorphous phase to be converted into superconducting phase or other less detrimental non-superconducting phases [83].

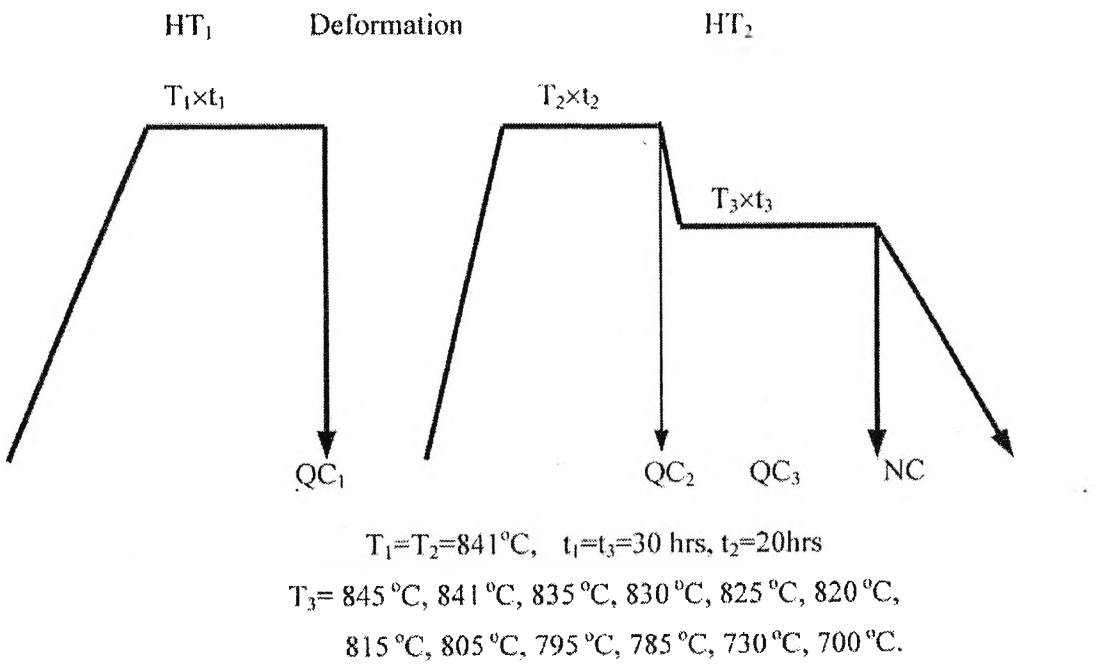

Figure 2. 6 Schedule for thermal treatment of Bi-2223 tapes

In Figure 2.5, the sintering time is shown by t_n, whre n = Number of thermal cycle and t is the number of hours for heat-treatment, NC means normal cooling rate of 2 K/min, QC means quenching from temperature T.

The maximum volume fraction of Bi-2223 phase occurs around 825°C. Above 825°C, liquid phase coexists with Bi-2223 and Ca-Sr-Cu-O, and its amount increases with increasing

temperature [83]. When the annealing temperature is set at 845°C, there is a large fraction of liquid present. On quenching, the liquid phase is converted to amorphous phase. If the annealing temperature is set at 825°C, the lowest temperature at which liquid forms and which leads to the formation of Bi-2223, the liquid phase is largely converted to Bi-2223 through reaction with Ca-Sr-Cu-O, until all the liquid phase is exhausted [117]. These results suggest that 825°C is the optimum temperature at which the liquid phase is largely converted to Bi-2223 with minimum Bi-2201 and Bi-2212.

2.5 Summary

Since the discovery of BSCCO system superconductor, a significant amount of research has been undertaken to investigate the microstructure, phase equilibrium and electrical properties of the BSCCO materials. Ag-alloy sheathed Bi-2223 tapes have been identified as the main form in which the material can be applied and the, powder-in-tube method has been extensively developed as the preferred manufacturing process for Bi-2223 tapes.

Current leads are an early stage application of BSCCO where the benefits of superconductivity can be clearly identified. These minimise energy loss, cut refrigeration costs and raise the efficiency of magnet systems. The advantages of using HTS's are their capacity for carrying an electrical current below a critical temperature without any resistive loss while the thermal heat load is suppressed due to the low thermal conductivity. The application of PIT tapes to current lead designs has shown some potential but the need for the use of Ag alloys as the sheathing materials is essential. The use of alloys will result in providing some strength and ductility during the drawing process, as well as a parallel electrical conduction path to carry current in case local superconductivity is lost.

As the properties of Ag-alloy sheathed BSCCO tapes for current leads applications are the

subject of this thesis, a number of parameters affecting the superconducting properties of Bi2223/Ag tapes, including the sintering temperature, sintering time, cooling rate, oxygen partial pressure, method of mechanical deformation, thickness reduction rate, and number of sintering and intermediate deformation cycles are reviewed. An attempt has been made to investigate the effect of the heat-treatment temperature on the phase formation of Ag alloy sheathed tapes and to show experimentally the effects of Ag-alloy sheath on the electrical properties and mechanical properties of Bi-2223 tapes. Bi-2223 tapes with Ag and Ag alloys (AgAu, AgMg, AgSb) sheaths were characterized in this study. The properties of the tapes were ranked so that the most suitable PIT BSCCO tapes for current leads applications could be identified.

References

[1] A.C.Rose-Innes and E.H.Rhoderick, "Introduction to Superconductivity", PERGAMON, 194 (1994) 23.

[2] R. D. Blaugher, The 1998 international workshop on superconductivity, Okinawa, Japan, July 12-15, (1998).

[3] K. Sato, T. Hikata, H. Mukai, M. Veyama, K. Iwata, T. Kato, T. Masada, M. Nagata and T. Mitsui, IEEE Trans. Magn. 27 (1991) 1231.

[4] Y. Yamada, B. Obst and R. Flukiger. Supercond. Sci. Technol. 4 (1991) 165.

[5] S.X. Dou and H.K. Li,. Supercond. Sci. Technol. 6 (1993) 297.

[6] Q. Li, K. Brodersen, H.A. Hjuler and T. Ferltoft. Physica C, 217 (1993) 360.

[7] H. Fujishiro, M. Ikebe, K. Noto, M. Matsukawa, T. Sasaoka, J. Sato and S. Kuma, IEEE Transactions on Magnetics, 30 (4 Part 2), (1994) 1645.

[8] L. Martini, F. Barberiis, R. Berti, L. Bigoni, F. Curcio and G Volpini, International Journal of Modern Physics B, 13 (1999) 1357.

[9] Sasaoka, K. Nomura, J. Sato, S. Kuma, H. Fujishiro, M. Ikebe and K. Noto, Applied Physics Letters, 64 (1994) 1304.

[10] W. Goldacker, E. Mossang, M. Quilitz, and M. Rikel, IEEE Transactions on Applied Superconductivity, 7 (1997) 1407.

[11] J. Yoo, H. Chung, J. Ko and H. Kim, IEEE Transactions on Applied Superconductivity, 7 (1997) 1837.

[12] K. Fischer, T. Fahr, A. Hütten, U. Schläfer, M. Schubert, C. Rodig and H. P. Trinks, Supercond. Sci. Technol. 11 (1998) 995.

[13] M. Apperley, R. Zeng, F. Darmann and G McCaughey, Cryogenics, 40, (2000) 319-324.

[14] M. Ishizuka, Y. Tanaka, T. Hashimoto and H. Maeda, Physica C, 290 (1997) 265.

[15] .Y. Tanaka, F. Matsumoto, H. Maeda and M. Ishizuka, IEEE Transactions on Applied Superconductivity, 5 (1995) 1158.

[16] R.P. Aloysius, A. Sobha, P. Guruswamy, U. Syamaprasad, Supercond. Sci. Technol. 14 (2001) 85.

[17] M. Putti, M.R. Cimberle, C. Ferdeghini, G Grasso, A. Manca and W. Goldacker, IEEE Transactions on Applied Superconductivity, 11 (2001) 3285.

[18] R. Zeng, Y.C. Guo, Y. Tanaka, J. Horvat, M. Ionescu, T.P. Beales, M. Apperley, H.K. Liu, S.X. Dou, Physica C, 307 (1998) 229.

[19] R. N. Lumley, A. J. Morton and I. J. Polmear, Acta Materialia, 50 (14) (2002) 3597.

[20] H.K. Liu, Z. Zhang, R. Zeng, J. Horvat and M. Apperley, IEEE Trans. Appl. Suppercon. 20003, in press.

[21] E. Quilmean, B. Andrzewski, G Desgardin, Physica C, 377 (2002) 304.

[22] E. Béghin, J. Bock, G Duperray, D. Legat and P. F. Herrmann, Applied Superconductivity, 3 (1995) 339.

[23] P.F. Herrmann, C. Cottevieille, A. Leriche, S. Elschner, IEEE Trans, Magn 32 (1996) 2724.

[24] R. C. Niemann, Y. S. Cha, J. R. Hull, W. E. Buckles, B. R. Weber, S. T. Yang, Proc, of CEC/ICMC 95, Columbus, July 17-21, 1995, Adv. In Cryogenic Eng. 41 (1996) 611.

[25] M. N. Wilson, Superconducting Magnets, Clarendon Press, Oxford, 1983.

[26] P. F. Herrmann, E. Beghin, G Bottini, C. Cottevieille, A. Leriche, T. Verhaege and J.

Bock, Cryogenics, 34 (1994) 543.
[27] T. Kato, K. Sato, T. Masuda, T. Shibata, Y. Hosoda, S. Isojima, S. Terai, T. Kishida, E. Haraguchi, in: T. Fujita, Y. Shiohara (Ed.s), Advances in Superconductivity IV, Vol. 2. Tokyo 1994.
[28] M. Teng, A. Ballarino, R. Herzog, A. Tjspeert, C. Timlin, S. Harrison, K. Smith, Proc. Of EUCAS 97, Eindhoven, The Netherlands, June 30 - July 3, 1997.
[29] D. Ponnusamy, Z. Li and K. Ravi-Chandar, IEEE Trans. Appl. Supercond. 5 (1995) 769.
[30] N. Alford, T. W. Button, S. J. Penn, P. A. Smith, IEEE Trans. Appl. Supercond. 5 (1995) 809.
[31] P. F. Herrmann, P. F. et al., IEEE Trans. Appl. Supercond. 3 (1993) 876.
[32] T. Hasebe, T. Tsuboi, K. Jikihara, S. Yasuhara, J. Sakaraba, M. Ishihara and Y. Yamada, IEEE Trans. Appl. Supercond. 5 (1995) 821.
[33] C. Uher, J. Supercond., 5 (1995) 821
[34] R.C. Niemann, Y. S. Cha, J. R. Hull, C. M. Rey and K. D. Dixon, IEEE Trans. Appl. Supercond. 5 (1995) 789.
[35] H. Fujishiro, T. Manabu, K. Noto, M. Matsukawa, T. Sasaoka, K. Nomura and J. Sato, S. Kuma. IEEE Trans. Magn. 30 (1994) 1645.
[36] H. K. Liu, The Final Report of ARC SPIRT Project in 2002, http://www.arc.gov.au.
[37] E. Beghin, J. Bock, G Dupperay, D. Legat, and P. F. Herrmann, Appl. Supercond. 3 (1995) 339.
[38] D. Ponnusamy, Y. Coulter, M. Daugherty, K. Ravi-Chander and K. Salama, Appl. Supercond. 4 (1997) 247.
[39] D. Ponnusamy, Z. Li and K. Ravi-Chandar, Proc. Of ASC 1994, IEEE Trans. Appl. Supercond. 5 (1995) 769.
[40] Y.Y. Cha, R.C. Niemann, C.A. Youngdahl, M.T. Lanagan, M. Nakade, T. Hara, Proc. Of CEC/ICMC 1995, Adv. Cryogenic Eng. 41A (1996) 603.
[41] M.P. Chudzik, B.J. Polzin, R. Thayer, J.J. Picciolo, B.L. Fisher and M.T. Lanagan, Proc. Of ASC 1996, IEEE Trans. Appl. Supercond. 7 (1997) 2102.
[42] B. L. Fisher, M.T. Lanagan, U. Balachandran, S. Honjo, and T. Hara, Proc. Of ASC1996, IEEE trans Appl. Supercond. 7 (1997) 711.
[43] R. C. Niemann, Y. S. Cha, J.R. Hull, C.M. Rey, K.D. Dixon, and J.M. Pfotenhauer, Proc. Of OEC/ICMC 1995, Adv. Cryogenic Engg. 41A (1996) 619.
[44] R. C. Niemann, Y.S. Cha, J. R. Hull, C. M. Rey and K. D. Dixon, Proc. Of ASC 1994, IEEE Trans. Appl. Supercond. 5 (1995) 789.
[45] D. U. Gubser, M. M. Miller, L. Toth, R. Rayne, S. Larence, N. Alford, T. W. Buttons, IEEE Trans. Mag. 27 (1991) 1854.
[46] E. Suzuki, M. Kurihara, Proc of EUCAS 97, IoP Publishing Conference Series No 158 (1997) 1219.
[47] T. Hasebe, T. Tsuboi, K. Jikihara, S. Yasuhara, J. Sakuraba, M. Ishihara, Y. Yamada, Proc of ASC 1994, IEEE Trans. Appl. Supercond. 5 (1995) 821.
[48] T. Hasebe, H. Mitsubori, J. Sakuraba, M. Ishihara, S. Awaji, K. Watanabe, Proc of ASC 1996, IEEE Trans. Appl. Supercond. 7 (1997) 707.
[49] K. Watanabe, S. Awaji, J. Sakuraba, K. Watazawa, T. Hasebe, T. Tsuboi, K. Jikihara, Y. H. Yamada, M. Ishihara, Cryogenics 36 (1996) 1019.
[50] T. Kato, K. Sato, T. Masuda, T. Shibata, Y. Hosoda, S. Isojima, S. Terai, T. Kishida, E. Haraguchi, T. Fujita, Y. Shirohara (Eds): Advances in Superconductivity IV, Proc. Of 6th ISS Hirohama 1993, Vol 2, Spring, Tokyo 1994.

[51] T. Kato, S. Sato, T. Ando, T. Isono, H. Tsuji, Proc. Of ISS 1995.
[52] T. Kato, N. Shibuta, K. Sato, T. Masuda, Y. Hosoda, S. Terai, E. Haraguchi, Proc of 5th Int. Symp. On Supercond. 1992.
[53] T. Masuda, Ch. Suzawa, T. Shibata, S. Isojima, T. Kato, S. Sato, Proc of ISS 1994.
[54] T. Honjo, S. Miyake, Y. Kamisada, Proc. Of ASC 1994, IEEE Trans. Appl Supercond. 5 (1995) 1486.
[55] Y. Tanaka, T. Asano, T. Yanagiya, M. Fukutomi, K. Komori and H. Maeda, Japn. J. Appl. Phys., Part 2 (Letters), 31 (1992) L235.
[56] L. Hua, J. Yoo, J. Ko, H. Kim, H. Chung and G Qiao, Physica C, 337 (1999) 236.
[57] H. Maeda, Y. Tanaka, M. Fukutomi and T. Asano, Jan. J. Appl. Phys. 27 (1988) 209.
[58] M. Takano, J. Takada, K. Oda, H. Kitaguchi, Y. Miura, Y. Ikeda, Y. Tomii, and H. Mazki, Jpn. J. Appl. Phys. 27 (1988) L1041.
[59] Y. Yamada, S Murase, Jpn. J. Appl. Phs. 27 (1988) L996.
[60] M. Takano, J. Takada, K. Oda, H. Kitaguchi, Y. Miuta, Y. Ikeda, Y. Tomii, and H. Mazaki, Jpn. J. Appl. Phys. 27 (1988) L1041.
[61] P. Strobel, J.C. Toledano, D, Morin, J. Schneck, G Vacquier, 0. Monnereau, J. Primot, and T. Fournier, Physica C 201 (1992) 27.
[62] J. C.Grivel、R.Flukiger、Journal of Alloys & Compounds, 241 (1996) 127.
[63] J. L. MacManus-Driscoll, J.C. Bravman, R. J. Savoy, G Gorman, B. R. Beyers, Journal of the American Ceramic Society, 77 (1994) 2305.
[64] C. Michel, M. Hervieu, M.M. Borel, A. Grandin, F. Deslandes, J. Provost and B. Ravesu, Phys. Rev. B, 68 (1987) 421.
[65] I. Harrington, C. Korn, S. D. Goren, H. Shaked and G Kimmel, Physica C, 226(1994) 255.
[66] P. Majewski, H.L. Su, and B. Hettich, Adv. Mater. 4 (1992) 508.
[67] P. Majewski, B. Hettich, and K. Schuize, Physica C 185-189 (1991) 469.
[68] K. Sato, N. Shibuta, H. Mukat, T. Hikta, M. Ueyama, and T.J. Kato, Appl. Phys., 70 (1991) 6484.
[69] B.W. Statt, Z. Wang, M.J.G Lee, J.V. Yakomie, P.C. de Camargo, J.F. Maya, and J.W. Rutter, Physica C, 157 (1988) 251.
[70] P. Strobel, J.C. Toledano, D. Morin, J. Schneck, G Vacquier, O. Monnereau, J.Primot, and T. Fournier, Physica C, 201 (1992) 27.
[71] K. Schuize, P. Majewski, B. Hettich, and G Prtzow, Z Metallkde. 81 (1990) 836.
[72] P. Majewski, B. Hettich, H. Jaeger, and K.Schuize, Adv. Mater. 3 (1991) 67.
[73] T. Hatano, K. \aota, S. Ikeda, K. Nakamura, and K. Owaga, Jpn. J. Appl. Phys. 27(1988) L2055.
[74] Y. Takeda, R. Kanno, F. Tanigawa, O. Yamamoto, Y. Ikeda, and M. Takano, Physica C, 159 (1989) 789.
[75] A. P. Malozemoff, et al., Applied superconductivity Conference 1998, Palm Desert, Sept. 13-18 1998, USA, IEEE Trans. Appl. Supercond., 9 (1999) 2537
[76] Z. Han, P. Bodin, W. G Wang, M. Bentzon, P. Skov-Hansen, J. Goul, P. Vase, Applied Superconductivity Conference 1998, Palm Desert, Sept. 13-18 1998, USA, 319.
[77] R. Hawsey, and J. Daley, JOM, 47 (1995) 56.
[78] Y. B. Yamada, B. Oberst and R. Flukiger, Supercond. Sci. Technol., 4 (1991) 165.
[79] D. Larbalestier, X.Y. Cai, Y. Feng, H. Edelman and A. Umezawa, Physica C, 221 (1994) 299.
[80] G Sivakov, A. V. Lukashenkoo, D. Abraimov, P. Muller, A. V. Ustinov, M. Leghissa,

Appl. Phys lett. 76 (2000) 2597.
[81] G Sivakov, A. V. Lukashenkoo, O. G Turutanov, I. M. Dmitrenko, D. V. Abraimov, P. Muller, A. V. Ustinov, Physica B. 284-288 (2000) 2071.
[82] G Strano, A. S. Siri and G Grasso, Supercond Sci. Technol. 13 (2000) 1470.
[83] H. K. Liu, M. Ionescu, Y. C, Guo, Handbook Adv. Elec. And Photonic Mat. And Devices—High Tc Superconductors and Organic Conductors, Edit: H. S. Nalwa, 3 (2001) 74.
[84] R. Zeng, Y. C. Guo, Y. Tanaka, J. Horvat, M. Ionescu, T. P. Beales, M. Appley, H. K. Liu, and S. X. Dou, Physica C 307 (1998) 229.
[85] S.X. Dou, Y. C. Guo, J. Yau and H. K.Liu, Supercond. Sci. Technol., 6, (1993) 195.
[86] T. Yoo, H. Chung, J. Ko, H. Kim, IEEE Transactions on Applied Supercond., 7 (1997) 1837.
[87] K. Heine, J. Tenbrink and M. Thoner, Appl. Phys. Lett., 55 (1989) 2442.
[88] J. Jiang and J.S. Abell, in High Temp. Supercond. U. Balachandran, P.J. McGinn, and J.S. Abell, eds., The Minerals, Metals & Materials Society, 1996 p3
[89] M. Xu, D.K. Finnemore, U. Balachandran and P. Halder, Appl. Phys. Lett. 66 (1995) 3359.
[90] T.R.Thurston, U. Wildgruber, N. Jisrawi, P. Halder, M. Suenaga and Y. L. Wang, J. Appl. Phys. 79 (1996) 3122.
[91] I. S. Oh and K. Mukherjee, Physica C, 227 (1994) 197.
[92] Q. Y. Hu, H. W. Weber, H. K. Liu, S. X. Dou and H. W. Neuller, Physica C, 252 (1995) 211.
[93] R.A. Outlaw, S.N. Sankaran, GB. Hofland, and M.R. Davidson, J. Mater. Res. 3 (1988) 1378.
[94] J.H. Park, Mater. Letters, 9 (1990) 313.
[95] J. Sato, T. Sasaoka, and S. Kuma, in Advances in Superconductivity VI, edited by T. Fujita and Y. Shiohara, eds., (Springer, Tokyo, 1994) p. 679
[96] W. Gao and J. Vander Sande, Materials Science and Engineering, B10 (1991) 247
[97] K. Nomura, T. Sasaoka, K. Kato, S. Kuma, H. Kumakura, K. Togano, and N. Tomita, in Advances in Superconductivity VI, T. Fujita and Y. Shiohara, eds., (Springer, Tokyo, 1994).
[98] Kanisada, T. Koizomi, M. Sato and Y. Yamada, IEEE Trans. Magn. 30 (1994) 1675.
[99] R. Zeng, Y. C. Guo, Y. Tanaka, J. Horvat, M. Ionescu, T. P. Beales, M. Appley, H. K. Liu and S. X. Dou , Physica C, 307 (1998) 229.
[100] Y. Yamada, M. Satou, and S. Murase, in Advances in Superconductivity V, edited by Y. Bando and H. Yamauchi, eds., (Springer, Tokyo, 1993) p717.
[101] M. Ishizuka, Y. Tanaka, H. Maeda, Physica. C 252 (1995) 339.
[102] K. Noaki, S. Ichimura, T. Kurotaki, K. Oguti and Y. Nishi, Proc. 5th Int. Symp. on Superconductivity (ISS' 94)
[103] J. Tenbrink, M. Wilhelm, K. Heine and H. Krauth, IEEE Trans. Magn. 3 (1993) 1123.
[104] S. H. Jang, J. H. Lim, J. H. Kim, B. K. Ji, J. Joo, W. Nah, J. S. Volf. H. K. Liu and M. Apperley, IEEE, trans. Appl. Supercond. (2003), in press.
[105] R. Zeng, Ph.D thesis (1999), University of Wollongong, p148.
[106] A. Oota, J. Iwayna, P. Songsak, T. Saigou and M. Funakura, Physica C, 1993 (214) 9.
[107] Z. Han, and T. Preltoft, Applied Superconductivity, 2 (1994) 201.
[108] Q. L i, K. Brodersen, H.A. Hjuler and T. Fretloft, Physica C, 217 (1993) 360.
[109] W. G Wang, H. K. Liu, Y. C. Guo, P. Bain, S.X. Dou, Appl. Supercond. 2(7, 8), (1996) 1.

[110] J. H. Ahn, H. K. Liu, S. X. Dou, Physica C, 351 (2001) 371.
[111] J. MacManus-Driscoll, J. Bravman, R. J. Savoy, G. Gorman, and R. B. Beyers, J. Am. Ceram. Soc. 77 (1994) 2305.
[112] P. Morgan, R. M. Housley, J. R. Porter and J. J. Ratto, Physica C, 176 (1991) 279.
[113] P. Morgan, J. Piche, and R. Housley, Physica C, 191 (1992) 179.
[114] Q. Y. Hu, H. K. Liu and S. X. Dou, Physica C, 250 (1995) 7.
[115] W. G. Wang, J. Horvat, H. K. Liu and S. X. Dou, Physica. C, 29 (1997) 1.
[116] J. A. Parrell, D. C. Larbalestier, G. N. Riley, Q. Li, W. L. Carter, R. D. Parrella and M. J. Mater. Res., 69 (1996) 2915.
[117] H. F. Poulsen, T. Frello, N. H. Andersen, M. D. Bentzon and M. Zimmermann, Physica C, 298 (1998) 265.
[118] L.R. Motowidlo, P. Haldar, S. Jin and N.D. Spencer, IEEE Trans. Appl. Supercond., 3 (1993) 942

Chapter 3. Introduction to earlier stage work

The research work that is the subject of this thesis follows on from earlier stage work including the fabrication of the tapes, sample preparation and XRD characterization [1]. In this Chapter, the preliminary work that is relevant to the current thesis is introduced.

The applications of high-T_c superconductors will depend on the ability to produce both high critical current and mechanically strong conductors. Because high-T_c superconductors are brittle oxide ceramics, fabricating reliable, robust and high critical current tapes or wires is a difficult proposition. Usually, silver and silver-alloy are used as sheath materials. The method for fabricating silver-sheathed $(Bi,Pb)_2Sr_2Ca_2Cu_3O_{10}$ (Bi-2223) superconducting composites includes powder production, silver-alloy tube preparation and packing, tape processing, and heat treatment. Among the various methods used to produce metal/superconductor composites the powder-in-tube technique has proved to be the most promising route for the production of superconducting wires and tapes.

The powder-in-tube process uses established metallurgical shaping techniques such as drawing and rolling that are readily scaled up for the mass production of long wires or tapes. The production of high-T_c superconductors involves a large number of process variables: chemical composition, powder properties, heat treatment parameters and deformation processing variables. This chapter focuses on the fabrication process and technical parameters of HTS tapes completed by other researchers.

3.1. 37-filament Bi-2223 tape Configurations

Ag and Ag-alloy sheathed tapes with 37 filaments were fabricated using commercial Bi-2223 precursor material (Merck Ltd) and powder-in-tube techniques. The sheath configurations of the tapes are shown in Table 3.1.

Table 3. 1. 37-filaments Bi2223 tape configurations

Tape number	Restack sheath	Precursor sheath
1	Ag	Ag
2	AgAu7wt%	AgAu7wt%
3	AgSb0.6wt%	Ag
4	AgAu7wt%	AgSb0.6wt%
5	AgSb0.6wt%	AgAu7wt%
6	AgMg0.2wt%	AgAu7wt%
7	Ag	AgSb0.6wt%

3.2. Fabrication of Ag and Ag-alloy sheathed Bi-2223 tapes

The powder-in-tube (PIT) technique was used to fabricate the tapes. The process included the preparation of Ag and Ag-alloy sheath tubes, packing with Bi-2223 precursor powder, degassing, drawing to form monocore wire, restacking the feed wires, drawing to produce multifilament wire, rolling to produce a tape, and heat treatment. The fabrication process is shown in Figure 3.1.

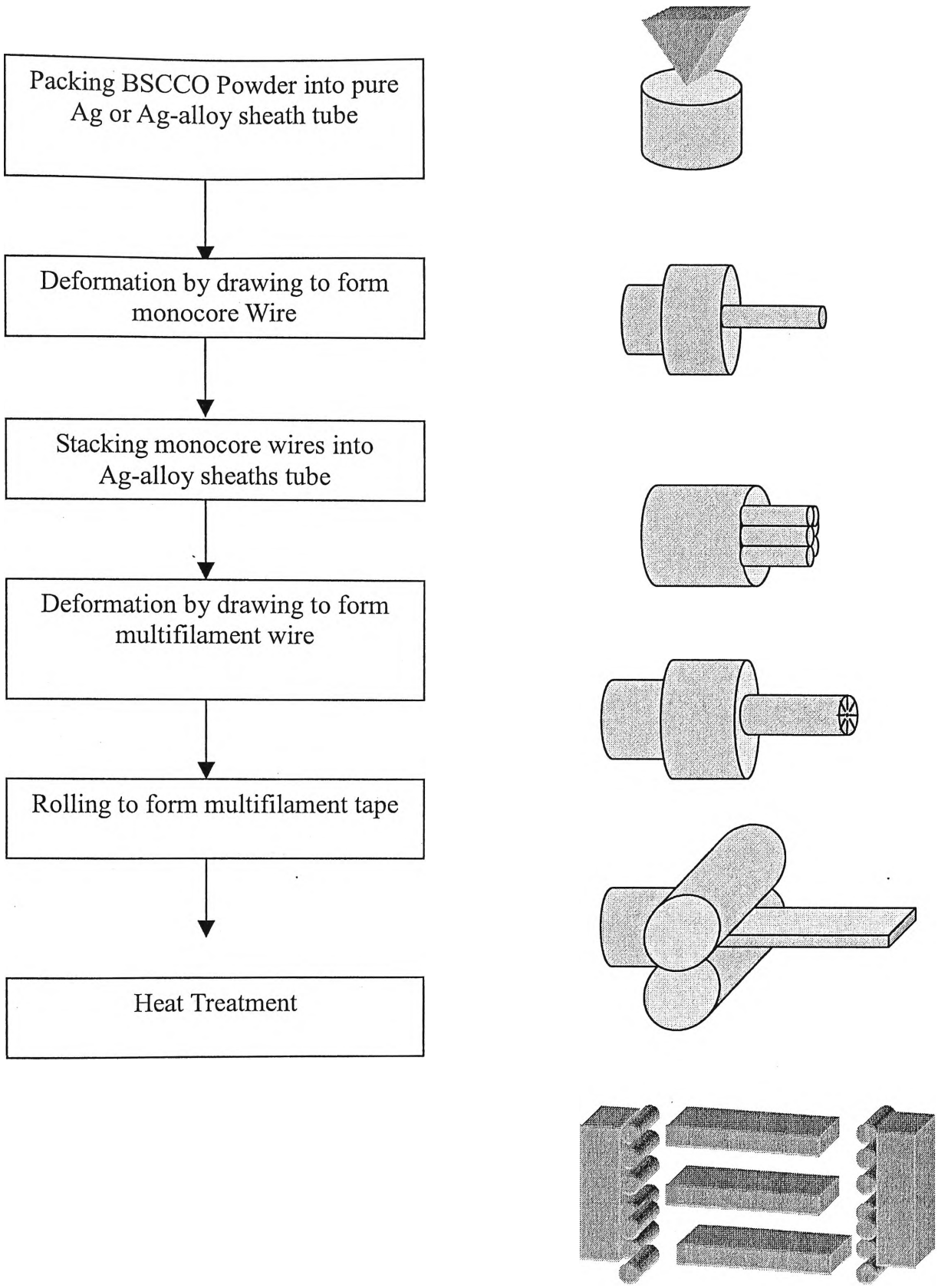

Figure 3. 1 The Fabrication of Multi-filament Tapes

3.2.1. Packing Bi-2223 Precursor Powder into the Tubes

In order to produce 10-15 m of tape, the BSCCO precursor powder was manually packed into Ag or alloy tubes 6.15 mm in diameter and 10 cm in length.

After packing, the filled tubes were given a thermal "degassing" treatment to remove entrapped gases in the compacted core. This process is shown as Figure 3.2.

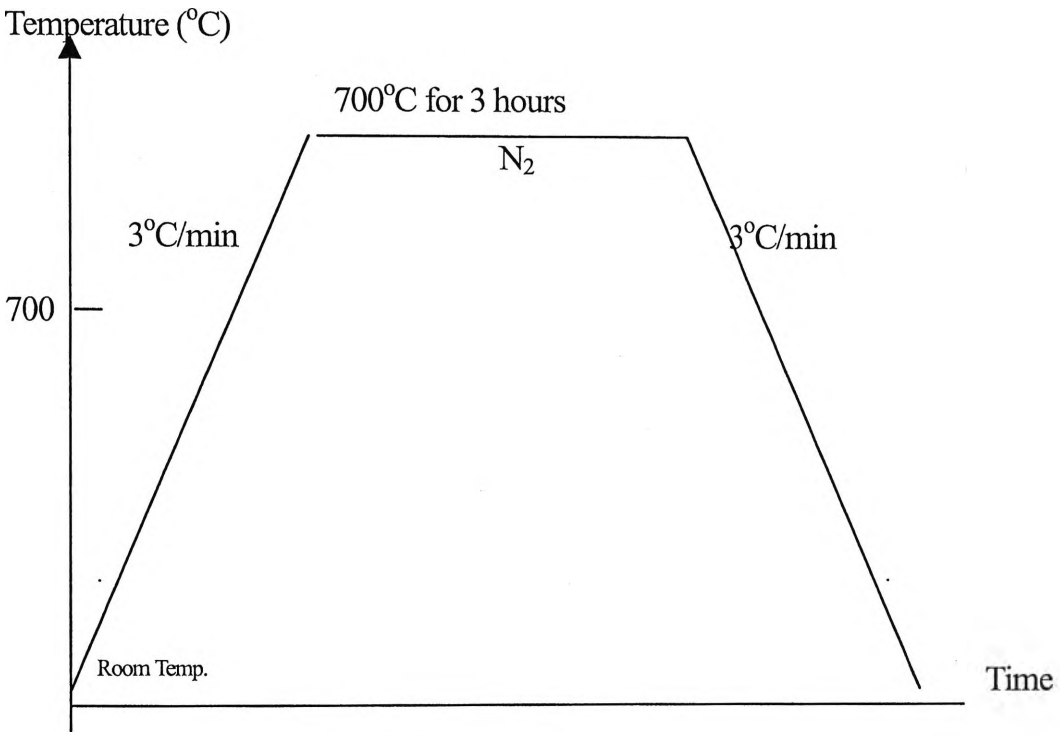

Figure 3. 2 The Degassing Process

3.2.2. Deformation Processing

The packed tubes were drawn into a diameter of 1.31 mm to 1.51 mm. The process is shown as follows:

6.15 mm → 5.68 mm → 5.21 mm → 4.80 mm → 4.48 mm → 4.01 mm → 3.76 mm → 3.48 mm → 3.18 mm → 2.96 mm → 2.77 mm → 2.52 mm → 2.30 mm → 2.15 mm → 2.01 mm → 1.91 mm → 1.79 mm → 1.61 mm → 1.51 mm.

The monofilament wire was then cut and bundled into groups of 37 filaments and inserted into the Ag or alloy restack tubes with a diameter of 6.15 mm The restacked tubes were then subjected to a second thermal degassing treatment. However, to prevent oxidation of the alloy sheaths of the tapes, N_2 gas was used to provide an inert atmosphere inside the furnace.

The multifilament wire was drawn to a final diameter of 1.54 mm using the same schedule as for the monofilament wire. The multifilament wire was then rolled into a tape using the schedule shown in Table 3.2. The final tapes with a thickness of 0.31 mm were subjected to a heat treatment-intermediate roll-heat treatment schedule.

Table 3. 2 Standard Rolling Schedule

Roll Number	Thickness (mm)	Reduction (%)
L1	1.05	31.8
L2	0.80	23.8
L3	0.65	18.8
L4	0.50	23.1
L5	0.40	20.0
L6	0.35	12.55
L7	0.31	11.4
Intermediate Roll	0.26	16.1

3.2.3 Heat Treatment

The heat treatment of the as-rolled tapes was a two-stage process. The first heat treatment was done in air, and the schedule is shown in Figure 3.3. The main dwell period was 50 hours, and a range of dwell temperatures were examined (832°C, 834°C, 838°C, 840°C, 842°C, 846 °C). The second heat treatment stage was performed after the tapes were given a single intermediate roll pass of approximately 10% following the first heat treatment stage. The schedule for the second stage is shown in Figure 3.4.

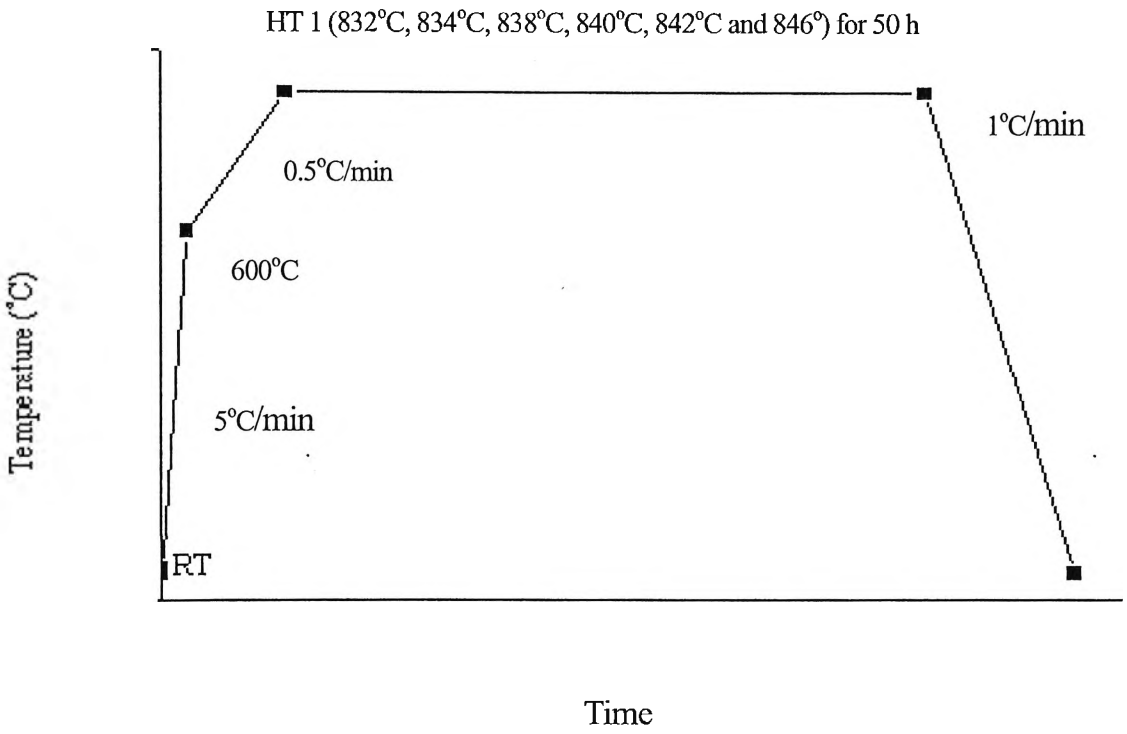

Figure 3. 3. The first heat treatment process

The second stage heat treatment was performed in low oxygen pressure (7.5wt% of oxygen and 92.5wt% of nitrogen). The schedule of the second heat treatment is shown in Figure 3.4.

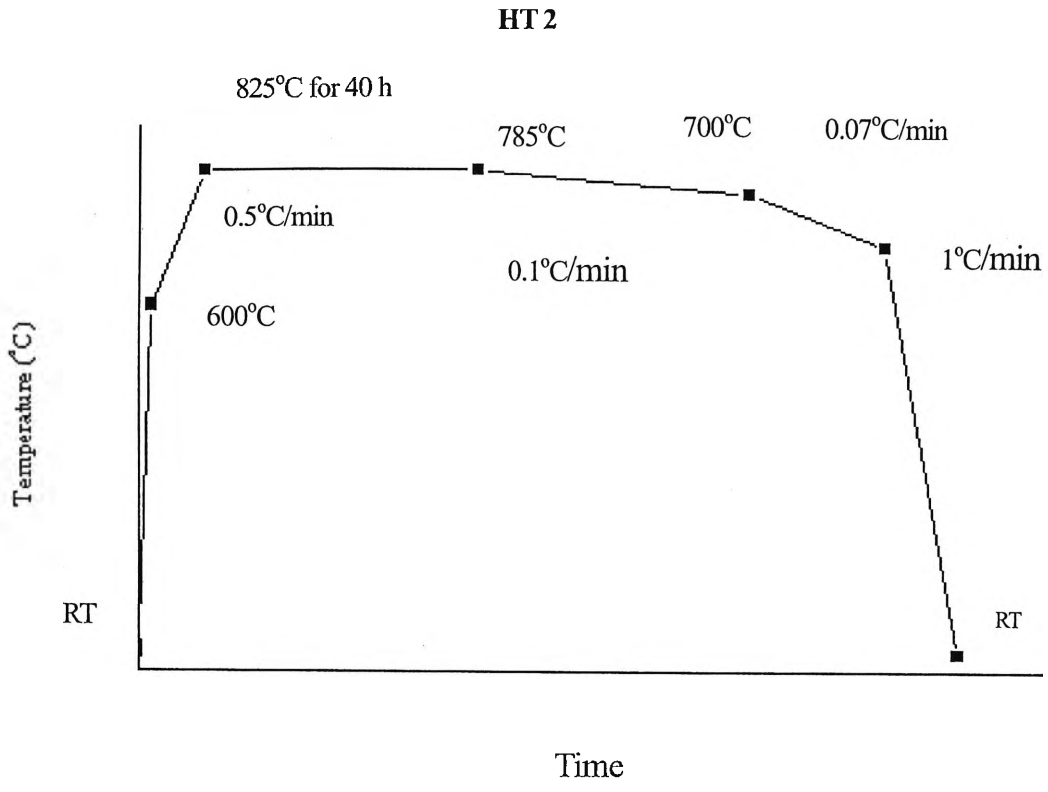

Figure 3. 4 The second heat treatment process

3.3. X-ray Diffraction (XRD)

Samples of heat-treated tapes for XRD were prepared by peeling one side of the sheath away from the tape to expose the BSCCO material within. A Phillips PW 1730 XRD Generator was connected to a computer that logged the data collected. The radiation used was CuKα with a wavelength of 1.5418 Å. Samples were examined over an angle range of $2\theta = 3^{o}$ to 70^{o}, which covers the major characteristic reflections for all superconducting phases in the BSCCO system. The x-ray diffraction patterns selected from $2\theta = 20^{o}$ to 26^{o} for Ag and Ag-alloy sheathed tapes after HT 1 and HT 2 are shown in Figure 3.5. It was found that so far as the amount of Bi-2212 was concerned, AgSb/AgAu>AgAu/AgAu>Ag/AgSb>Ag/Ag for the tapes after HT 2 (a peak at between 23^{o} to 24^{o}) and there was more 2201 phase (a peak at 22^{o}) for the tape with the AgSb sheath after HT 1 than others. The peak at 24^{o} showed Bi-2223 phase.

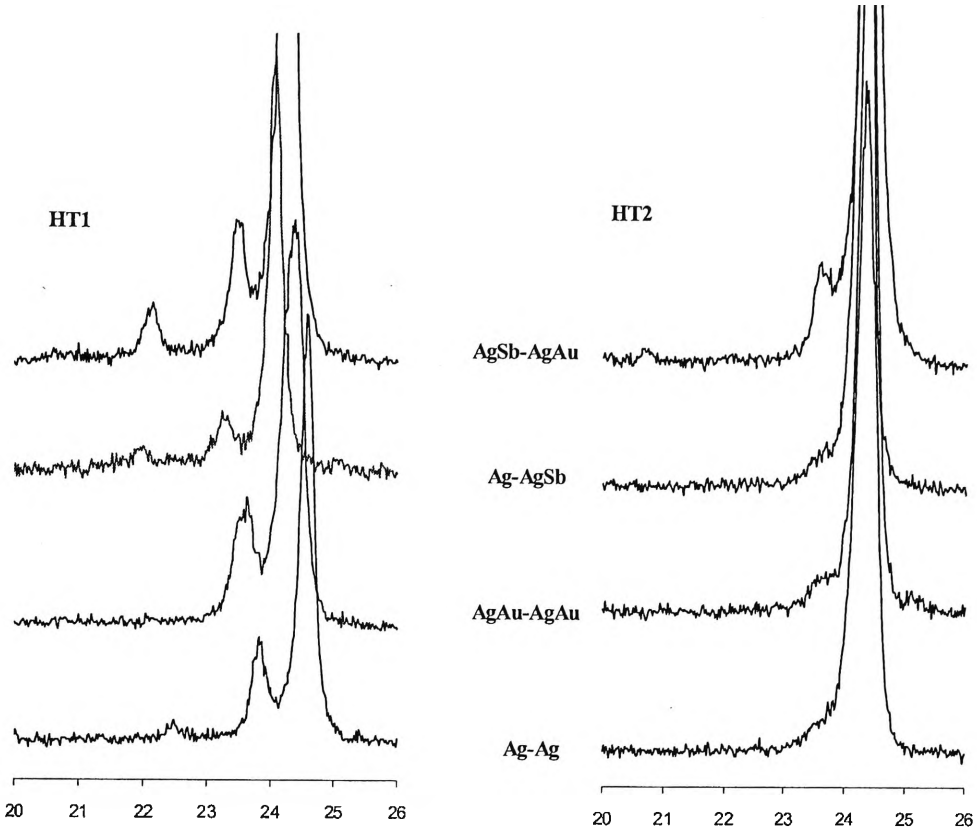

Figure 3. 5 XRD of Ag and Ag-alloy sheathed Bi-2223 tapes after HT1 and HT2

Reference

[1]. J. Volf, Unpublished manuscript, 2002

Chapter 4. Experimental Work

The effects of different Ag alloy sheath materials on the electrical properties, mechanical properties and microstructure of Bi-2223 HTS tape were studied. The electrical measurements included the critical current, I_c, at 77 K in self-field, and the normalized J_c in magnetic fields up to 1 T at 77 K. The mechanical properties, including the hardness, tensile strength and bending strain, were measured. The microstructures and phase were analyzed by X-Ray diffraction (XRD), Optical Microscopy (OM), Scanning Electron Microscopy (SEM) and Energy Dispersive X-ray.

4.1. Electrical Properties

4.1.1. Critical Current Measurement

Critical Current (I_c) and Critical Current Density (J_c) are the most important properties of high T_c superconductors for electrical power applications, where $J_c = I_c/S$, S is the cross-sectional area carrying the current. S can be of the superconductor only or it can be for the entire tape cross section, i.e. the engineering critical current density $J_e = I_c$/total tape area is the most useful parameter for engineering applications. A standard four-probe method using a 1 μV/cm criterion was used to measure the critical current at 77 K in self-field and the magnetic field up to 1 T. The technique is shown schematically in Figure 4.1. A DC current supply (Hewlett Packard 6680A), with a limit of 800A and a digital multimeter (Keithley DMM 196 and Keithley 2000/2001) with a standard resolution of 0.1 μV were used for the critical current density measurements. The cross sectional area of the tapes was measured using a CCD-IRIS Black and White Video Camera at Australian Superconductor.

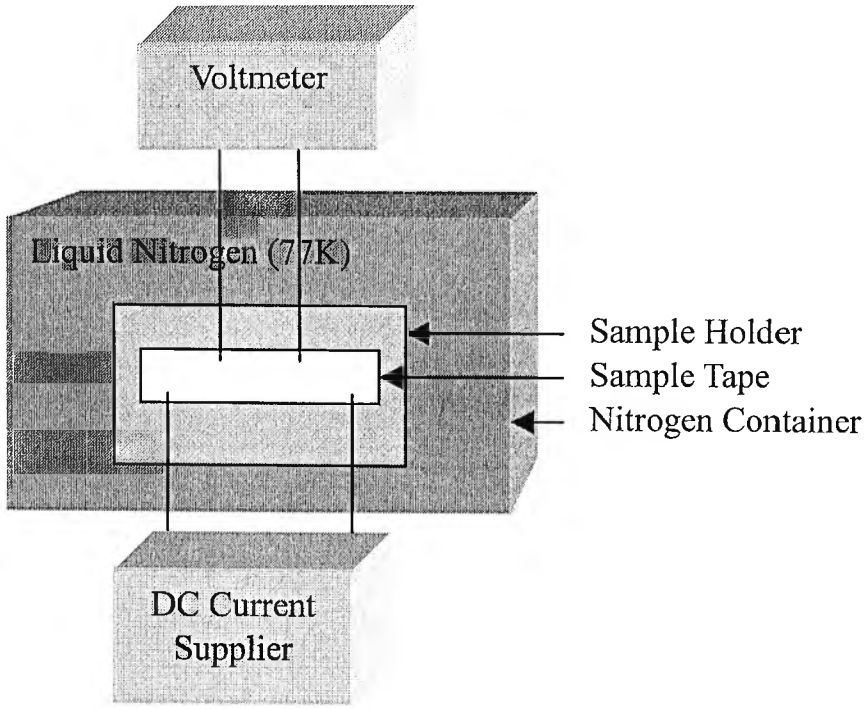

Figure 4.1. Illustration of the 4-probe I_c measurement technique

4.1.2. Critical Current Density (J_c) – Magnetic Field (H) Dependence Measurement

The critical current density (J_c) – magnetic field (H) dependence of the tapes was determined at 77 K, using a four-probe method and a 1 μV/cm criterion. The same DC supply and voltmeter used to measure I_c were used. The external magnetic field (in the range of 0 - 1.0 Tesla) was applied with the magnetic field both parallel (H⊥c) and perpendicular (H//c) to the surface (a-b plane) of the tape. I_{c0} was measured first, then the current was returned to 0 A, and the magnetic field was increased from about 2 mT to 1 T with different intervals. As each magnetic field was applied, I_c was measured. Figure 4.2 shows the instrument used for the J_c –field dependence measurement.

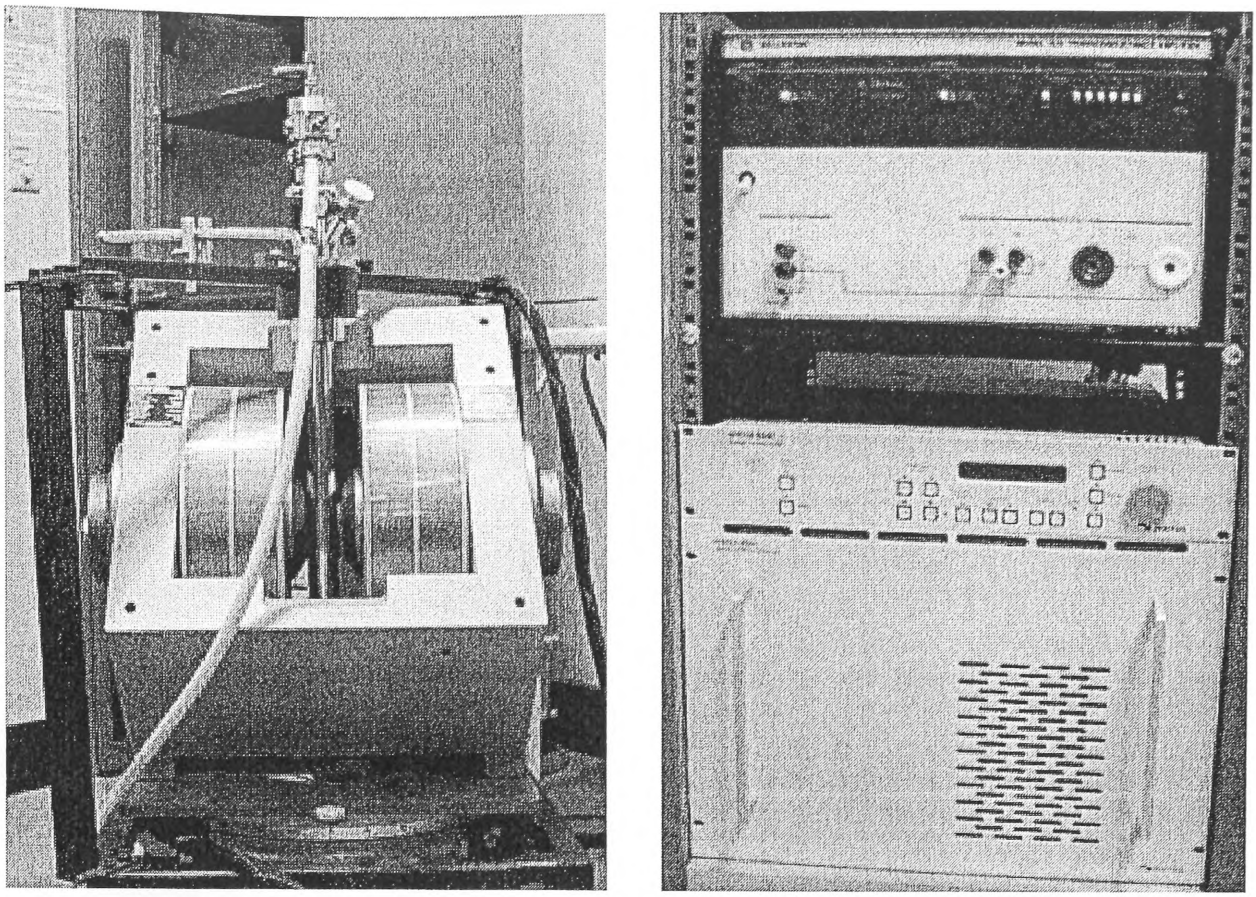

(a) (b)

Figure 4.2. The instruments for J_c field dependence measurements (a) electromagnet to provide the external magnetic field, (b) power supply

4.2. Mechanical Properties

An objective of this work was to examine the effect of the alloying elements Sb, Mg and Au on the mechanical properties of HTS tape. Three mechanical properties were examined: Hardness, Bending Strain and Tensile strength.

4.2.1. Sheath Hardness

Hardness measurements were performed using a Leco Microhardness Testing Machine (M-400-Hl) at room temperature with a load of 10 g. Tape samples were

mounted in epoxy and polished to a 1 μm finish prior to measurement. The measurements were taken across a transverse section of the tapes starting at a position adjacent to the filaments and proceeding in a direction towards the edge of the tape at the intervals of 25 μm (Figure 4.3). The error in the hardness measurement was estimated to be 3%.

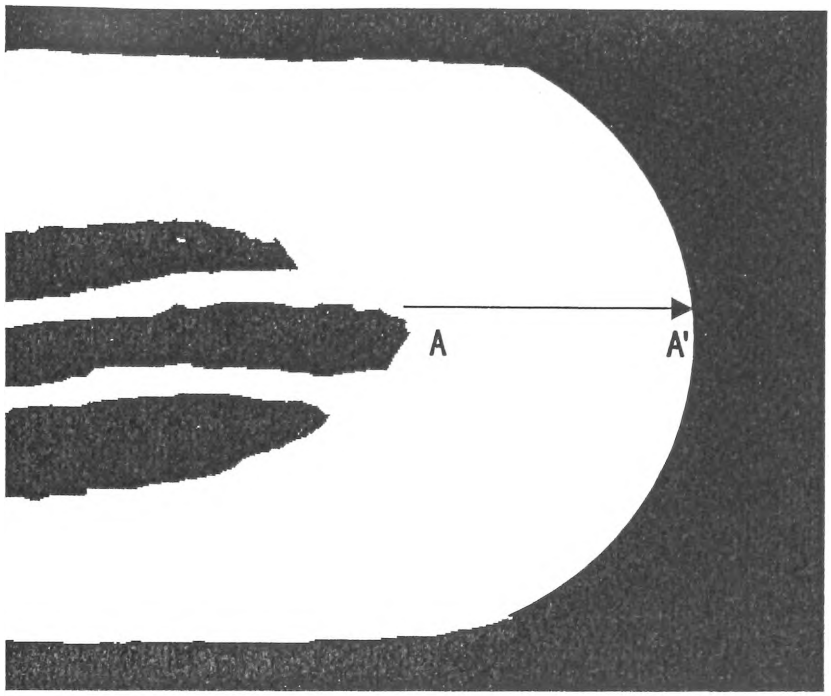

Figure 4.3. A line shows the region in the tape cross-section in which the micro-hardness distribution was examined.

4.2.2. Tensile strength

The tensile strength was measured using a Lloyd Instruments LRX Plus fitted with a 1 kN load cell at room temperature. The tests were done at the Australian Superconductors Company. Samples (6 cm long) with HT1 = 840°C were tested.

4.2.3. Bending Strain

The bend strain tolerance was investigated by measuring the I_{co} of tapes 1-7 with HT1 = 840°C at 77 K and self-field and the I_c after one-way bending of the sample around progressively smaller diameter formers in the range of 110 mm to 20 mm. The samples were straightened after each bend cycle. The percentage bend strain was calculated by $\varepsilon = t/\Phi_f \times 100$, where t is the tape thickness and Φ_f is the former diameter.

In the course of bend testing, tapes were bent at room temperature in one direction to a certain curvature then straightened. The critical current was measured by the four-probe method.

4.3. Microstructure Analysis

X-ray diffraction (XRD), optical microscopy (OM), and scanning electron microscopy (SEM) were used in the phase and microstructure analysis.

4.3.1. XRD for Phase Analysis

Although the actual XRD scans were performed in early stage work, the calculated results on phase content (%) from X-ray diffraction data form an integral part of the discussion (in Chapter 6) so a brief description of the technique and its limitations is included here for completeness.

X-ray Diffraction (XRD) analysis is usually conducted to identify the major and minor phases and evaluate the degree of grain alignment (texture) in the superconductor core of Bi-2223/Ag tapes after heat treatment. It is also very common to use XRD for monitoring the Bi-2223 phase formation and texture evolution during the process of

heat treatment.

Although XRD is a convenient way to get the chemical phase composition there are some limitations to the technique. Accurate determination of species or composition is only possible if the volume ratio of a chemical phase exceeds a few percent and the grain size is at least 1 μm. The X-ray diffraction pattern was taken on a longitudinal cross section of the tapes.

4.3.2. Optical Microscopy

The microstructure of the alloy sheaths was examined by LEICA optical microscopy as shown in Figure 4.4. The sample preparation procedure was as follows: mounting samples of tape in epoxy, polishing to a 1μm finish, etching for 15 - 20 seconds using a solution of H_2O (100ml), 25%NH_3 (50ml) and 30wt%H_2O_2 (10ml). A LEICA Research Microscope with 20 times magnifications was used in the analysis.

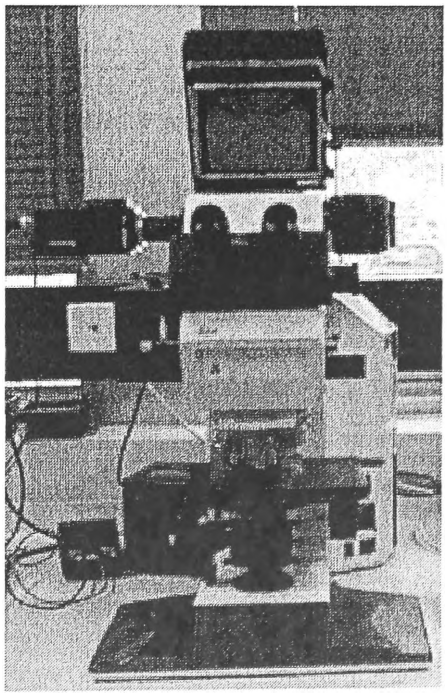

Figure 4. 4. LEICA Optical Microscopy

4.3.3. Scanning Electron Microscopy (SEM)

A LEICA Cambridge Stereoscan S440 SEM equipped with X-ray analytical capabilities (Figure 4.5) was used for microstructural observations. Samples for SEM were mounted in epoxy so that both longitudinal and transverse cross sections were visible. The samples were polished to a 1 μm finish and coated with Au. A QBSD detector was used in the analysis.

To analyze the phase composition of tape 4, EDS (Energy Dispersive Spectroscopy) analysis was used.

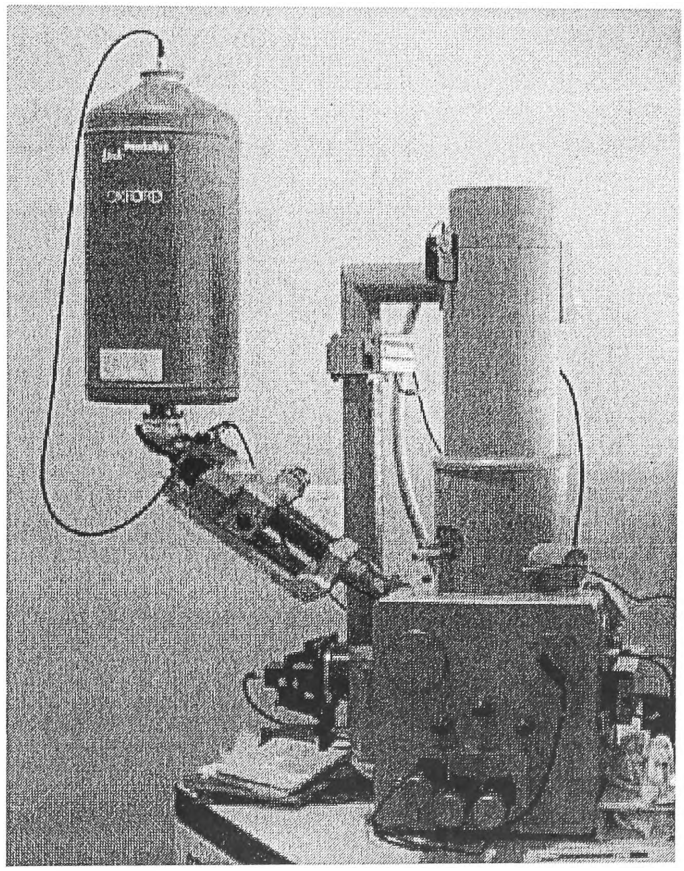

Figure 4. 5. LEICA Cambridge Stereoscan SEM S440

Chapter 5. Results

In this Chapter, the results on phase compositions calculated from X-ray diffraction data, critical current, J_c dependence on the magnetic field at 77K, bend strain tolerance, tensile strength, hardness and microstructure of different Ag and Ag alloy sheathed Bi-2223 HTS tapes are reported.

5.1. Phase compositions

After completion of tape processing the composition of the BSCCO cores in the tapes was characterized using X-Ray diffraction (XRD). Assuming that a %Bi-2223 + b %Bi-2212 + c %Bi2201 + d %Bi3221 = 100%, the volume fractions of the phases were calculated from the ratios of the peak intensity (I_{2223} (0010), I_{2212} (008), I_{2201} (006), and I_{3221} (300)) of each respective BSCCO phase to the sum of the respective intensities. The results of this phase analysis are shown in Tables 5.1 to Table 5.4 for a range of first heat treatment temperatures.

Table 5. 1 Phase composition of the BSCCO core in completed tapes when HT 1= 834 °C)

	Tape 1		Tape 2		Tape 3		Tape 4		Tape 5		Tape 6		Tape 7	
	HT 1	HT 2	HT 1	HT 2	HT 1	HT 2	HT 1	HT 2	HT 1	HT 2	HT 1	HT 2	HT 1	HT 2
Bi-2223	82.0	91.7	80.6	82.6	82.6	82.5	83.3	81.0	77.5	91.7	83.3	84.0	82.6	94.3
Bi-2212	12.3	5.5	12.1	11.6	13.2	11.7	13.3	14.0	18.6	4.6	14.2	10.1	9.9	4.7
Bi-2201	1.6	~0	1.6	~0	2.5	~0	2.5	0.8	~0	~0	0.8	~0	2.5	~0
Bi-3221	2.5	5.5	4.0	4.1	0.8	4.9	0.8	4.1	3.9	3.7	1.7	5.9	6.6	0.9

Table 5. 2 Phases content (%) from X-ray (HT 1: 838 °C)

	Tape 1		Tape 2		Tape 3		Tape 4		Tape 5		Tape 6		Tape 7	
	HT 1	HT 2	HT 1	HT 2	HT 1	HT 2	HT 1	HT 2	HT 1	HT 2	HT 1	HT 2	HT 1	HT 2
Bi-2223	85.3	94.3	82	81.1	83.6	84.7	69.4	82.9	83.9	91.6	86.2	84.0	87.7	96.2
Bi-2212	10.1	3.8	9.8	17.8	7.8	12.7	16.0	12	10.7	5.6	6.9	10.9	5.3	2.9
Bi-2201	0.9	~0	1.6	~0	2.6	~0	9.7	0.9	1.8	~0	1.7	0.8	1.8	~0
Bi-3221	3.7	1.9	6.6	2.4	6.0	2.5	4.9	4.3	3.6	2.8	5.2	3.4	5.3	1

Table 5. 3 Phases content (%) from X-ray (HT 1: 840°C)

	Tape 1		Tape 2		Tape 3		Tape 4		Tape 5		Tape 6		Tape 7	
	HT 1	HT 2	HT 1	HT 2	HT 1	HT 2	HT 1	HT 2	HT 1	HT 2	HT 1	HT 2	HT 1	HT 2
Bi-2223	90.9	93.75	92.6	81.7	90.9	95.2	31.8	76.7	90.9	96.2	89.3	80.8	89.3	97.1
Bi-2212	0.08	3.13	0.06	15.4	0.06	3.8	57.8	18.3	7.2	2.88	8.03	10.6	8.03	1.92
Bi-2201	0.01	~0	0.01	~0	0.03	~0	10.4	2.5	1.8	~0	2.68	~0	2.68	~0
Bi-3221	0	3.13	0	2.88	0	1	0	2.5	0	0.96	0	8.65	5.2	0.96

Table 5. 4 Phases content (%) from X-ray (HT 1: 842 °C)

	Tape 1		Tape 2		Tape 3		Tape 4		Tape 5		Tape 6		Tape 7	
	HT 1	HT 2	HT 1	HT 2	HT 1	HT 2	HT 1	HT 2	HT 1	HT 2	HT 1	HT 2	HT 1	HT 2
Bi-2223	86.4	95.7	83.3	84.3	88.5	95.2	20.9	86.4	82.0	93.5	89.3	88.5	87.0	94.8
Bi-2212	8.2	2.2	10.8	12.2	6.2	3.8	70.9	8.2	9.8	4.7	7.1	10.6	6.1	3.1
Bi-2201	0.9	~0	2.5	~0	1.8	~0	3.6	~0	2.5	~0	1.8	~0	1.7	~0
Bi-3221	4.5	2.2	3.3	3.5	3.5	1	4.5	5.5	5.7	1.9	1.8	0.9	5.2	2.1

5.2. Electrical Properties

5.2.1. I_c and Sheath Configuration

I_c values of Ag and Ag alloy sheathed Bi-2223 tapes at 77K are shown in Figure 5.1. It is

obvious that I_c of all the tapes is very low when HT 1 = 846 °C compared with HT 1 = some other temperature, which means HT 1 = 846 °C is too high for all the tapes. The highest I_c appears when HT 1 = 842 °C for tape 7, 832 °C for tape 5, 840 °C for tapes 2, 3 and 4, 834 °C for tape 6, and 838 °C for tape 1. The results indicate that tapes having different configurations of the precursor and restack sheath materials need suitable temperatures for the first heat treatment (HT 1) when other procedures are the same.

Comparing the I_c in Figure 5.1 with the XRD analysis results shown in Tables 5.1-5.4, it is clear that when the volume fraction of Bi-2223 >90%, Bi-2212 ~ 5%, Bi-2201~ 0% and Bi-3221 is at a very low level, normally the tapes demonstrate higher I_c.

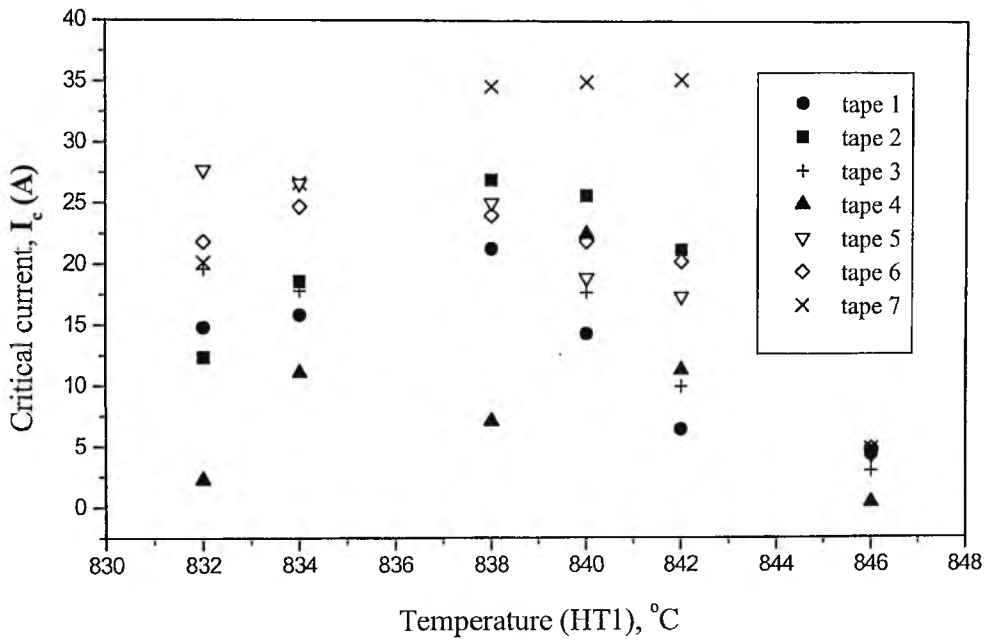

Figure 5. 1. I_c of short tapes 1-7 after HT 2 measured at 77 K and 0 T

5.2.2. Normalized J_c - Field Dependence and the Sheath Materials

The Jc-field dependence of each tape was measured, with the field perpendicular (H//c)

and parallel to the tape surface (H//ab) at 77 K for the different tapes (1, 3, 5, 6 and 7 with HT1 = 838 °C, and 2 and 4 with HT1 = 842 °C). The reason why these tapes were chosen is because they presented comparatively high I_c values in self-field. Figures 5.2 and 5.3 show the relationship between the normalized J_c and the applied magnetic field.

Comparing the normalized J_c dependence on magnetic field of the tapes at 77 K and H//ab, the normalized J_c of tape 5 decreases more quickly in higher field than that of tape 6 indicating that Mg in the restack sheath strengthens the superconducting materials much more than Sb.

Tapes 3 and 7 show the similar behaviour as they have the same sheath materials and only the configurations are different.

The normalized J_c of tape 4 decreases more quickly than for tape 2 indicating that Sb in the precursor sheath is not good as Au in the precursor sheath.

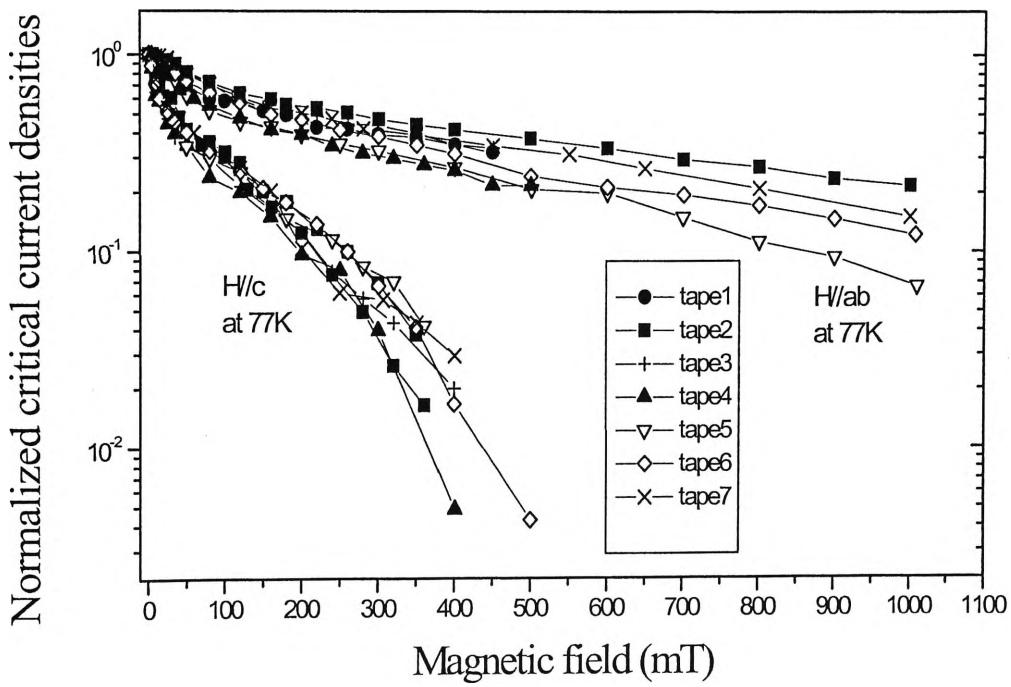

Figure 5. 2. Normalized J_c Dependence on the Magnetic Field of Tapes 1, 3, 5, 6 and 7 with HT1 = 838°C, Tapes 2 and 4 with HT1 = 840°C at 77 K

5.3. Mechanical Properties

5.3.1. Bending Strain and the Sheath Materials

The results of the one-way bending test for tapes 1 – 7 with HT1 = 840 °C are shown in Figure 5.3. It can be clearly seen that the bending properties of the tapes are quite different.

Tape 6 possesses the highest ε_{crit} of 0.73% and shows the best performance of I_c tolerance to bending strain, as Mg in the restack sheath that strengthens the superconducting materials.

The critical bend strains, ε_{crit} (bend strain when $I_c/I_{co} = 0.95$), of tapes 1 and 7 are approximately 0.3% as they have the same restack sheath (Ag). For tape 3 and tape 5, both of the same restack sheath – AgSb, the critical bend strains are 0.42% and 0.47%, higher than that for the tape 1. For tape 2 and tape 4, also with the same restack sheath – AgAu, the critical bend stains are 0.28% and 0.25%, also lower than that of tape 1.

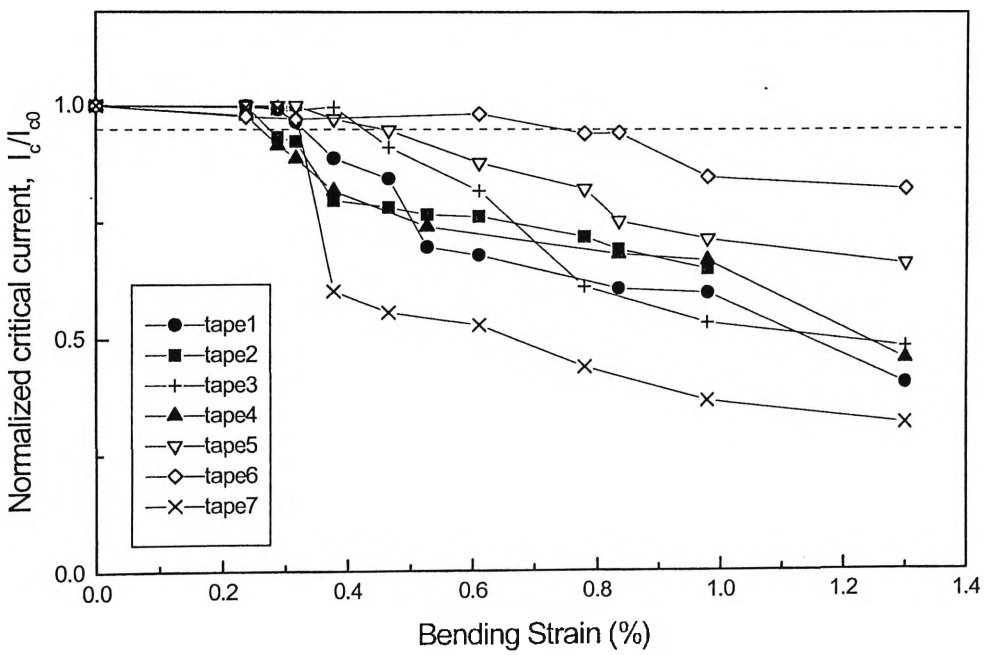

Figure 5. 3. Relative J_c/J_{co} as a function of bending strain (first heat-treatment at 840°C).

5.3.2. Hardness Profiles and the Sheath Materials

The hardness profiles in the sheath materials of the tapes (with HT 1 = 840 °C) are shown in Figure 5.4. It shows that tape 6 has a high level of hardness ~90 Hv due to the alloy element Mg in the restack sheath. Tapes 3 and 5 show a middle level of hardness ~70 Hv, because Sb is in the restack sheath. The other tapes show a lower level of hardness 50~60 Hv, as they have Ag or Au in the restack sheath.

From these results we can know that the sequence of the alloys' hardness from high to low is AgMg0.2wt%, AgSb0.6wt%, AgAu7wt% or Ag.

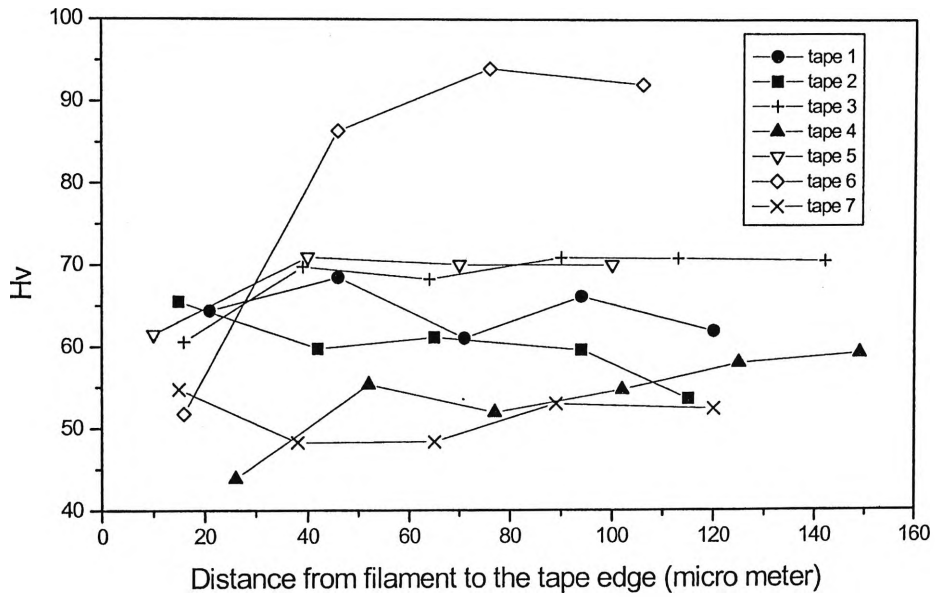

Figure 5. 4. Hardness profiles in the sheath materials of the tapes 1-7

5.3.3. Tensile Profiles and the Sheath Materials

The tensile profiles in the sheath materials of tapes 1-7 (with HT1 = 840 °C) are shown in Figure.5.5. It can be seen that the best strengthening effect is shown by tape 6 in which the restack sheath contains Mg. The next best strengthening effects are shown by tape 3 and tape 5

in which the restack sheaths contain Sb. The lowest strengthening effect is shown by tapes 7, 2 and 4, which have similar performance to tape 1 (pure Ag sheath), indicating that the use of Au has negligible effects on the tensile strength.

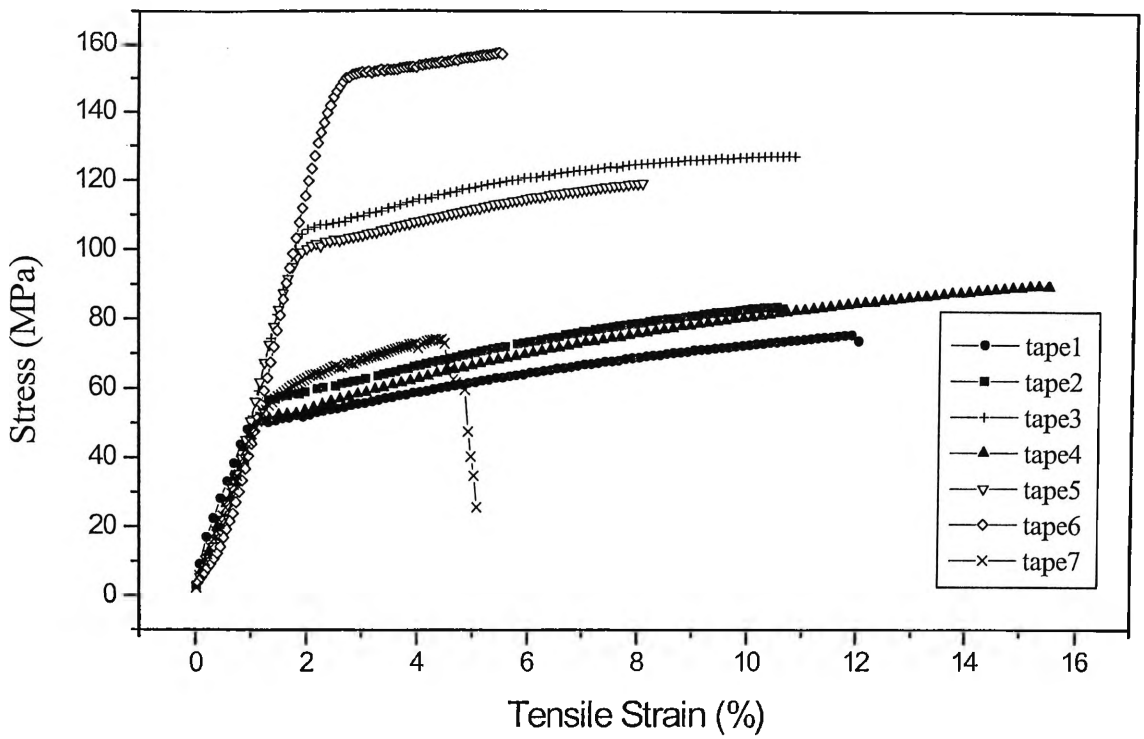

Figure 5.5. Tensile strength properties of the tapes measured at room temperature

5.4. Microstructure Analysis

5.4.1. Optical Microscope Analysis

Using an optical microscope, one can get the microstructure images of the sheath materials. Figures 5.6. - 5.12 show optical micrographs of tapes 1-7 with HTI = 834°C.

In Figure 5.6, the optical micrograph of tape 1 with pure Ag as precursor and restack sheath material shows big metal particles and little diffusion of outgrowths. In Figure 5.7, for tape 2

with AgAu7wt% alloy as precursor and restack sheath material, the micrograph shows a very smooth surface in the cross section because Au is difficult for the solution to etch. For tape 3 with AgSb0.6wt% as restack material and Ag as precursor material, Figure 5.8 shows much smaller metal particles than in tape 1. This means that Sb plays an important role in enhancing the hardness of the tape. For Tape 4, with AgAu7wt% alloy as restack material and AgSb0.6% as precursor material, Figure 5.9 shows that the smooth restack part is not etched by the solution, but in the precursor sheath there are numerous black dots which are Sb oxide. For Tape 5, with AgSb0.6% alloy as restack material and AgAu7wt% as precursor material, Figure 5.10 shows that there are many very small metal particles in the restack sheath and also black dots of Sb-oxide. The thick black dots at the interface between the restack and precursor materials may imply the diffusion of the alloy. For tape 6 with AgMg0.2% alloy as restack material and AgAu7wt% as precursor material, Figure 5.11 shows that there are small metal particles and some diffusion of the alloy material in the restack sheath. Figure 5.12 shows the micrograph of tape 7, with pure Ag as restack material and AgSb0.6% alloy as precursor material. Note that there are very big metal particles and very heavy diffusion of alloy material in the precursor sheath. Jang et al. reported that the average grain diameter of Ag was measured to be 48.0 μ m, while those of the AgAu, AgSb and AgMg sheaths were 29.3, 26.0, and 3.9 μ m, respectively [1].

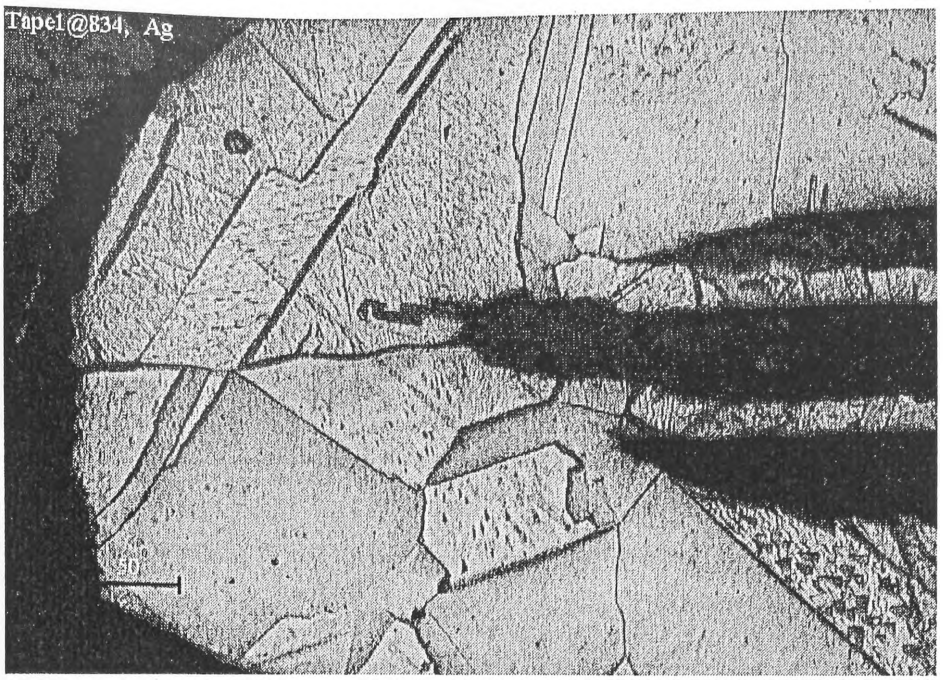

Figure 5.6. Optical Microscope Image of Tape 1 (HT1 = 834 °C) with 20 Magnification

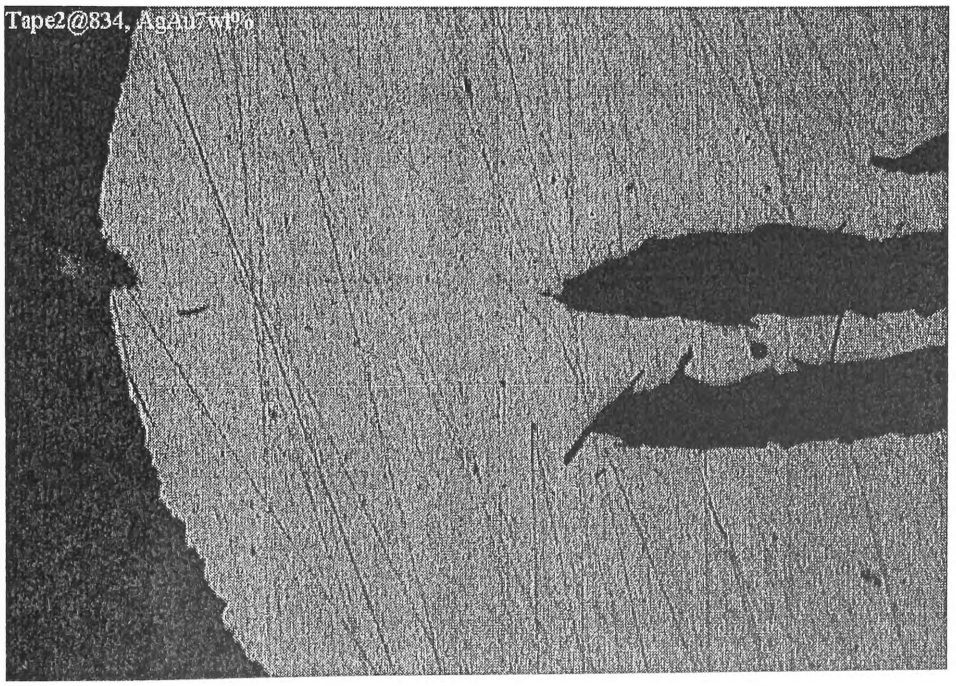

Figure 5.7. Optical Microscope Image of Tape 2 (HT1 = 834 °C) with 20 Magnification

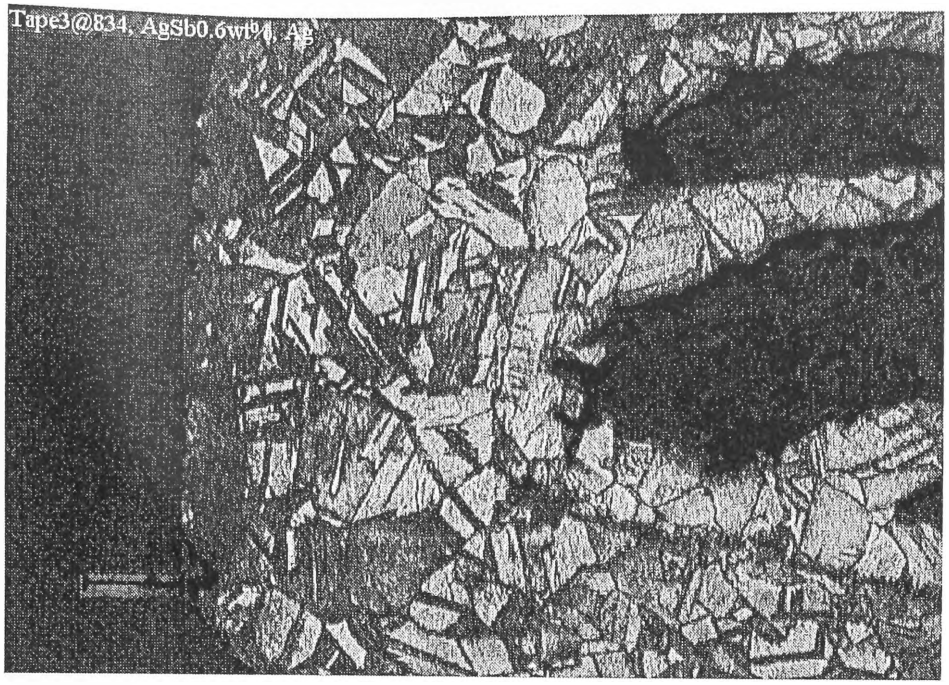

Figure 5. 8. Optical Microscope Image of Tape 3 (HT1 = 834 °C) with 20 Magnification

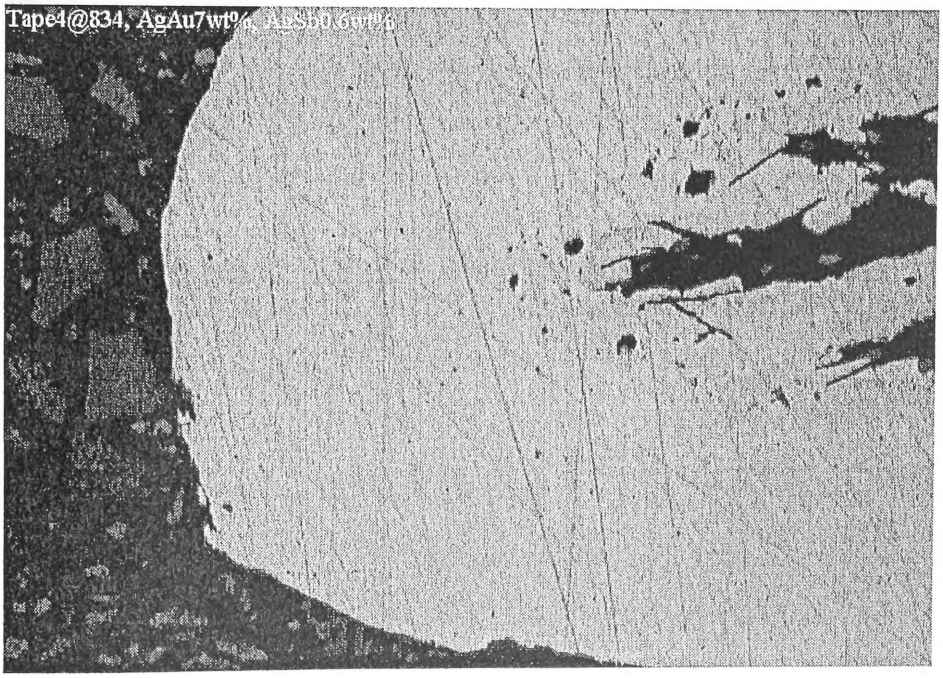

Figure 5. 9. Optical Microscope Image of Tape 4 (HT1 = 834 °C) with 20 Magnification

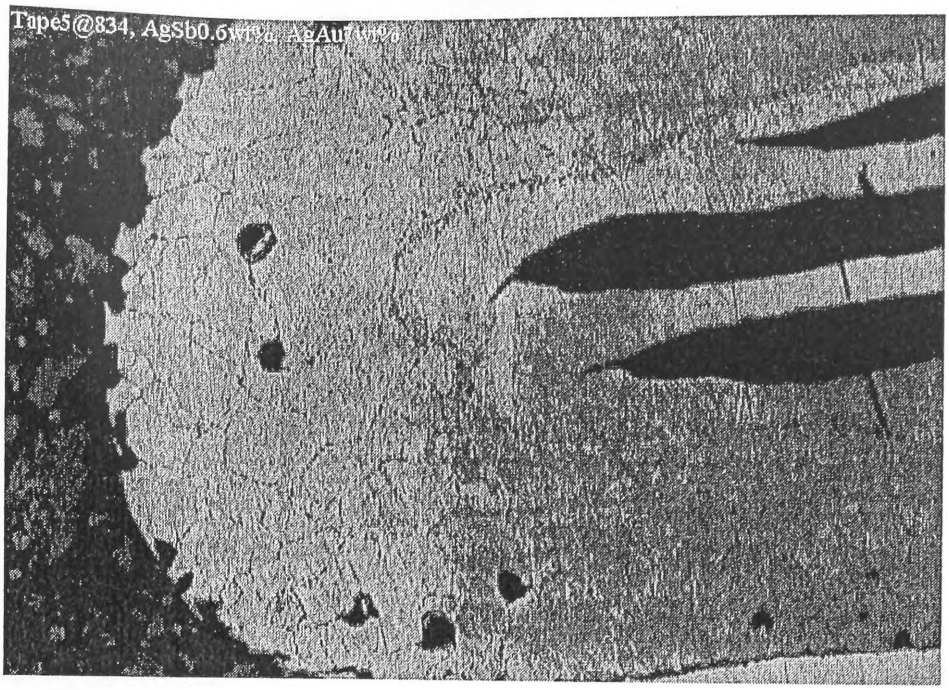

Figure 5.10. Optical Microscope Image of Tape 5 (HT1 = 834 °C) with 20 Magnification

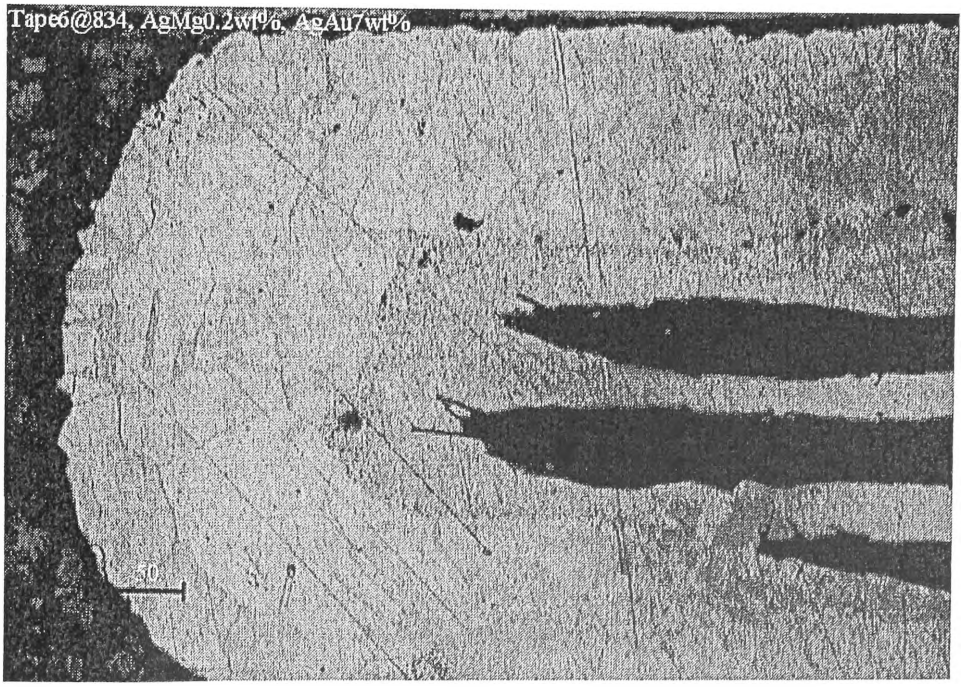

Figure 5.11. Optical Microscope Image of Tape 6 (HT1 = 834 °C) with 20 Magnification

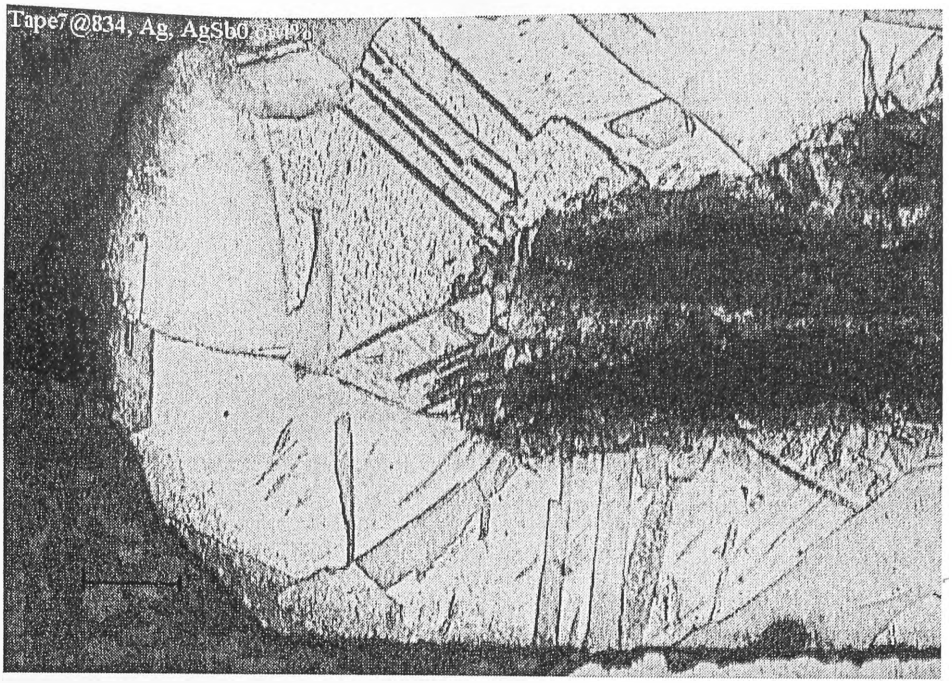

Figure 5.12. Optical Microscope Image of Tape 6 (HT1 = 834 °C) with 20 Magnification

5.4.2. Scanning Electron Microscopy Analysis

Figures 5.13 - 5.19 show SEM images of the seven green tapes. The SEM images of tape 1 and tape 2 show many holes in the filaments, while tapes 3, 4 and 5 have fewer holes in the filaments, and there are almost no hole in tape 6. The image of tape 7 shows that some filaments are joined together.

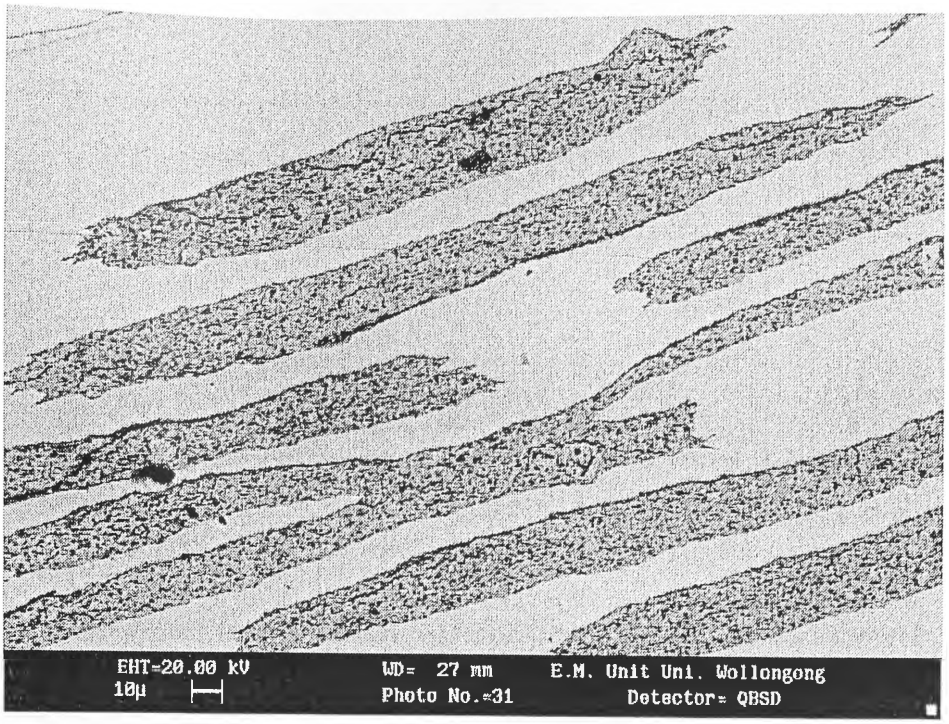

Figure 5. 13. SEM Image of Green Tape 1

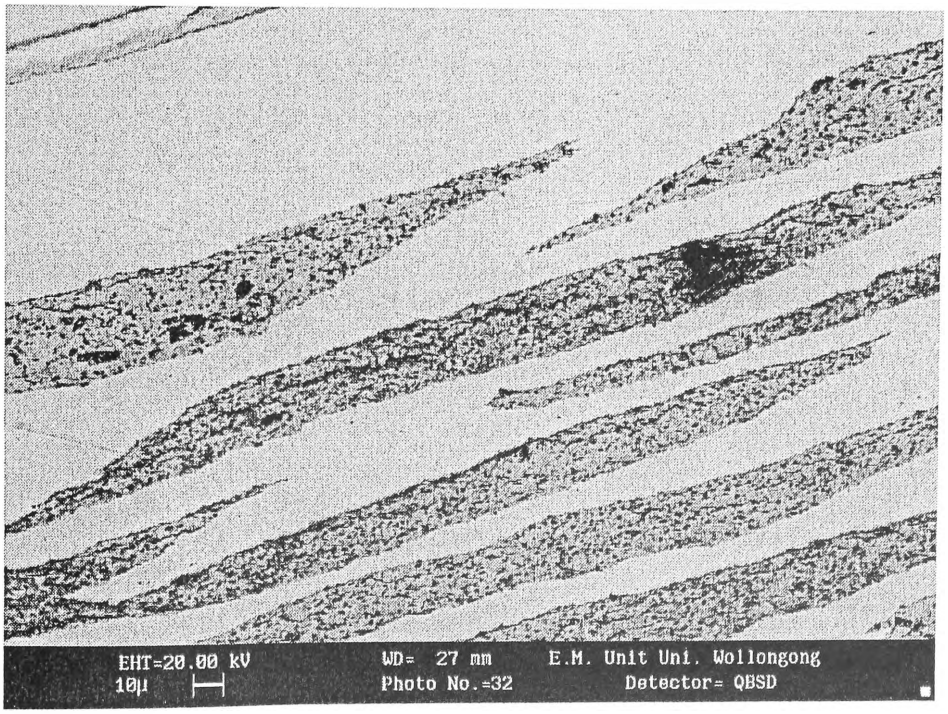

Figure 5.14. SEM Image of Green Tape 2

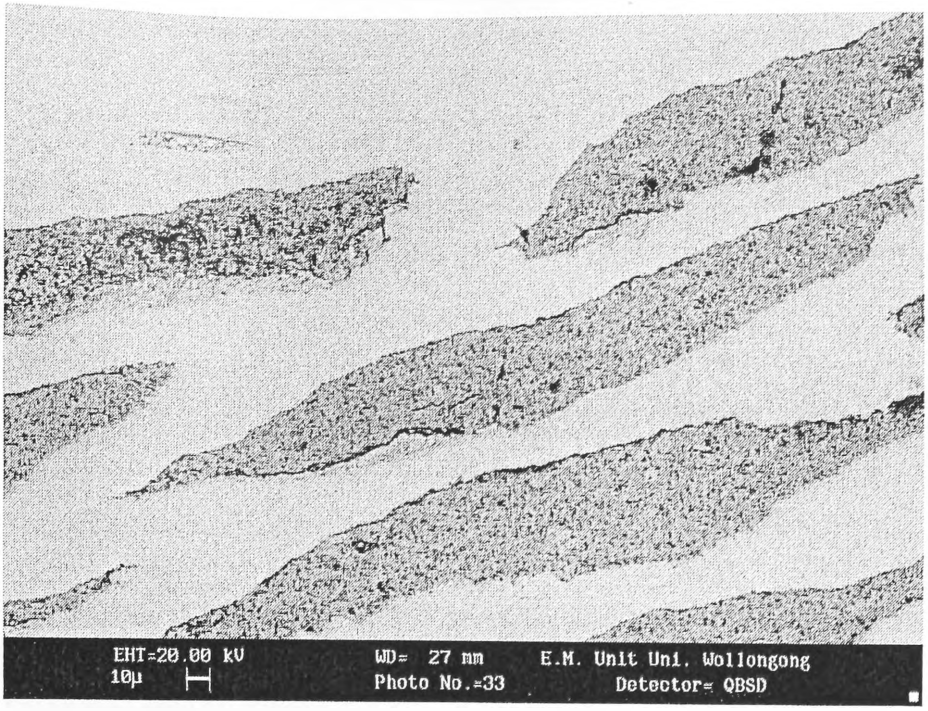

Figure 5.15. SEM Image of Green Tape 3

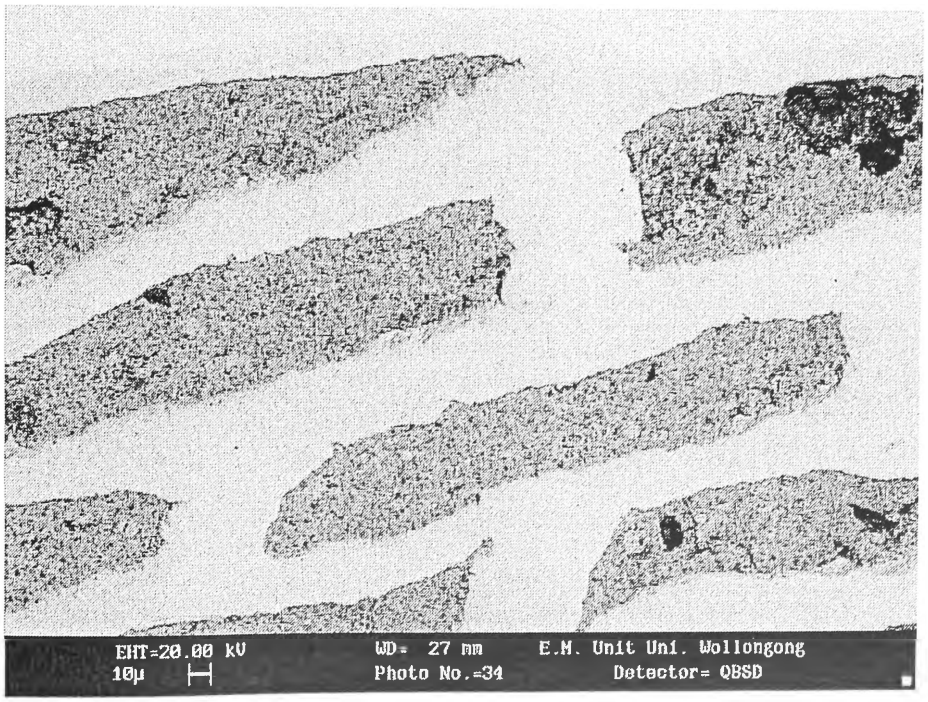

Figure 5.16. SEM Image of Green Tape 4

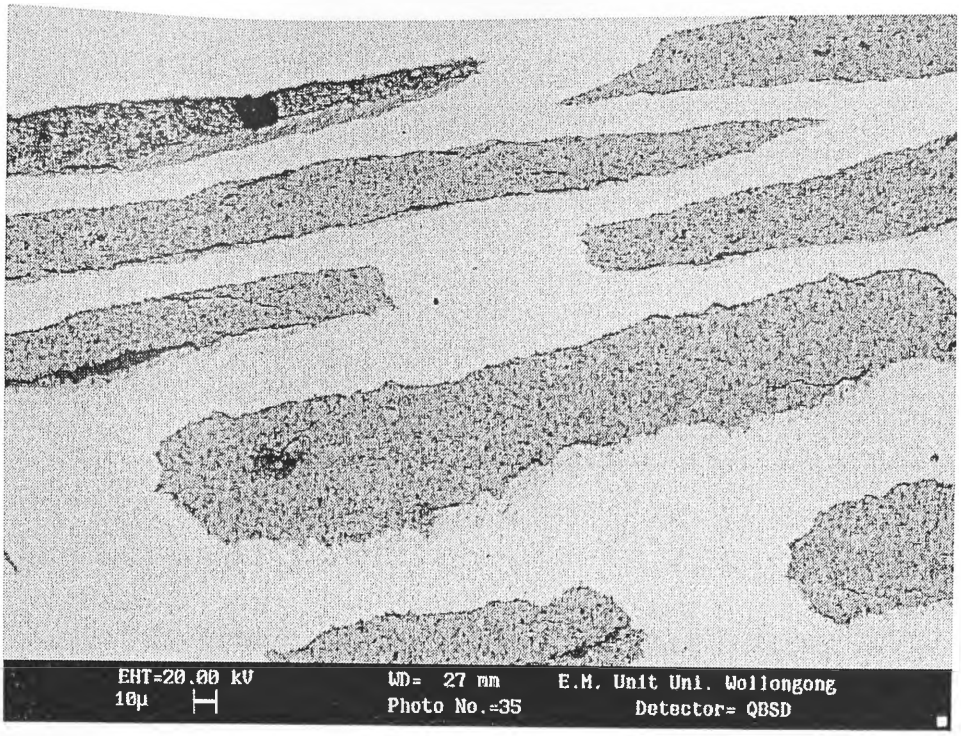

Figure 5. 17. SEM Image of Green Tape 5

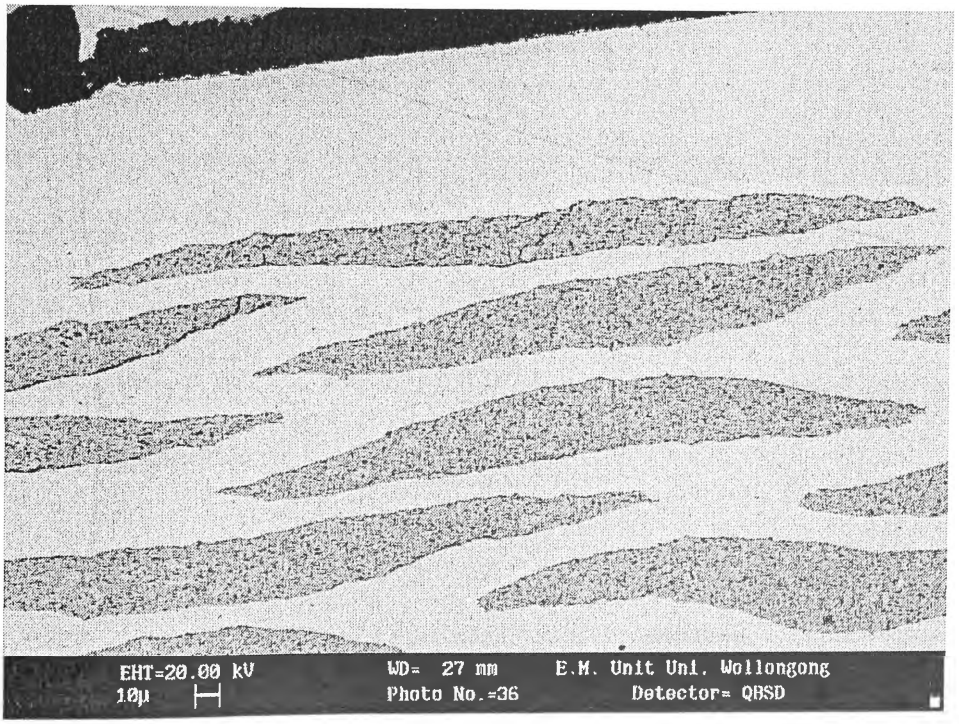

Figure 5.18. SEM Image of Green Tape 6

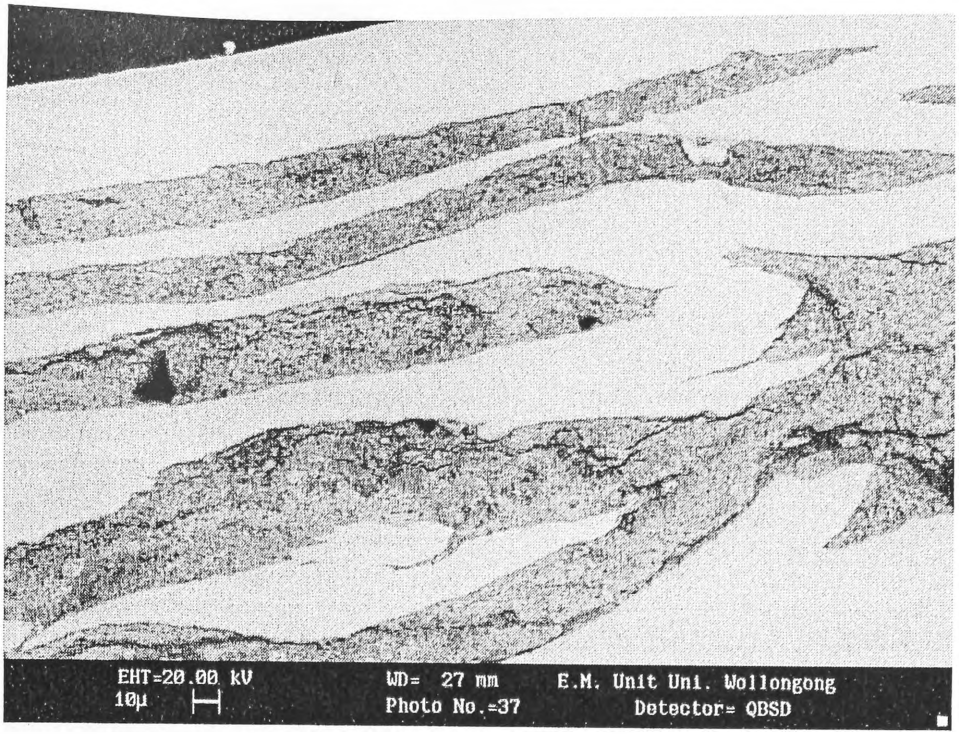

Figure 5.19. SEM Image of Green Tape 7

Figures 5.20 –5.26 show SEM images of tapes 1-7 after the first heat-treatment at 840°C. It can be clearly seen that there is considerable liquid phase in tape 4; less in tapes 3, 5 and 6; and very much less in tape 1, 2 and 7. The second phase in tapes 1, tape 2 and tape 7 is much less than in tape 4, and less than in tapes 3, 5 and 6. The particle sizes of tapes 3, 5 and tape 6 are smaller than in tapes 1, 2 and 7. In tape 4, the filaments are all melted together and have lost the regular aligning.

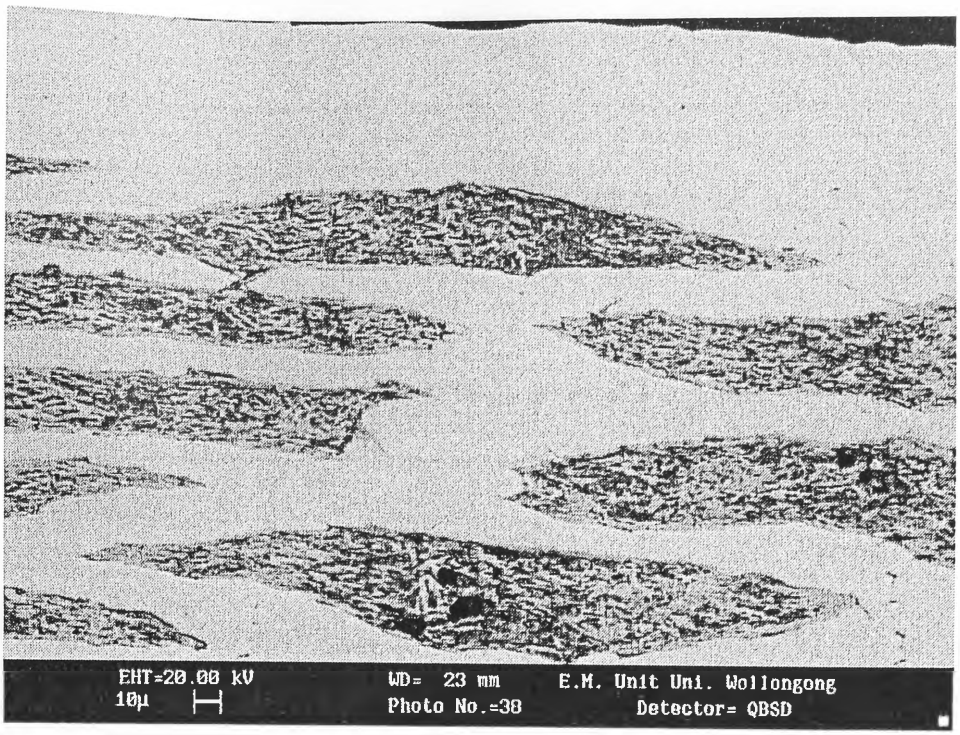

Figure 5.20. SEM image of tape 1 after the first heat-treatment (HT1 = 840°C)

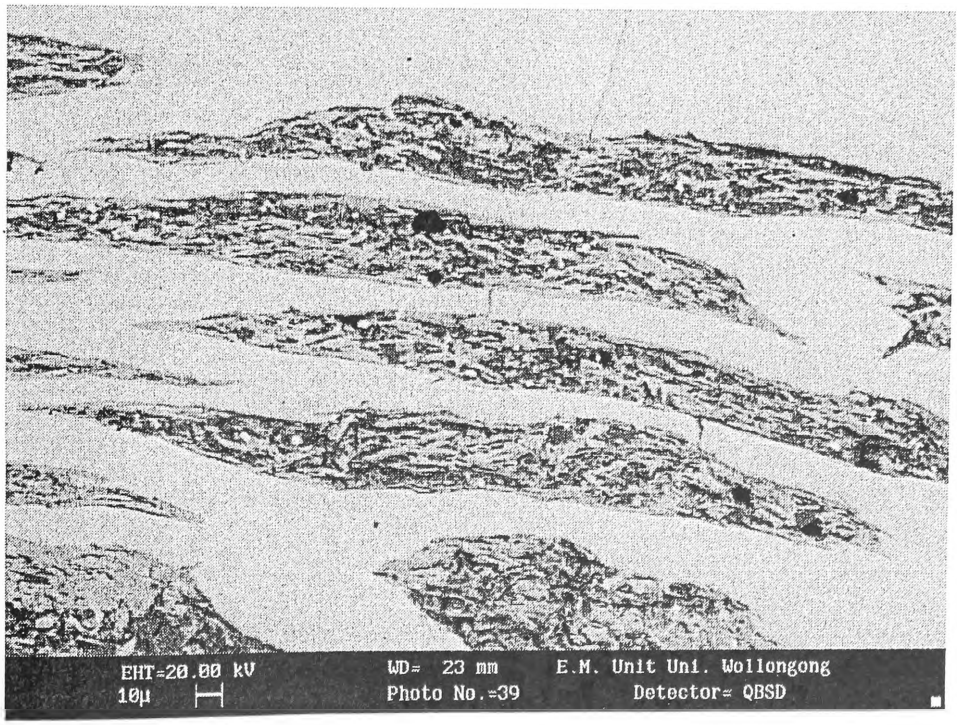

Figure 5.21. SEM image of tape 2 after the first heat-treatment (HT1 = 840°C)

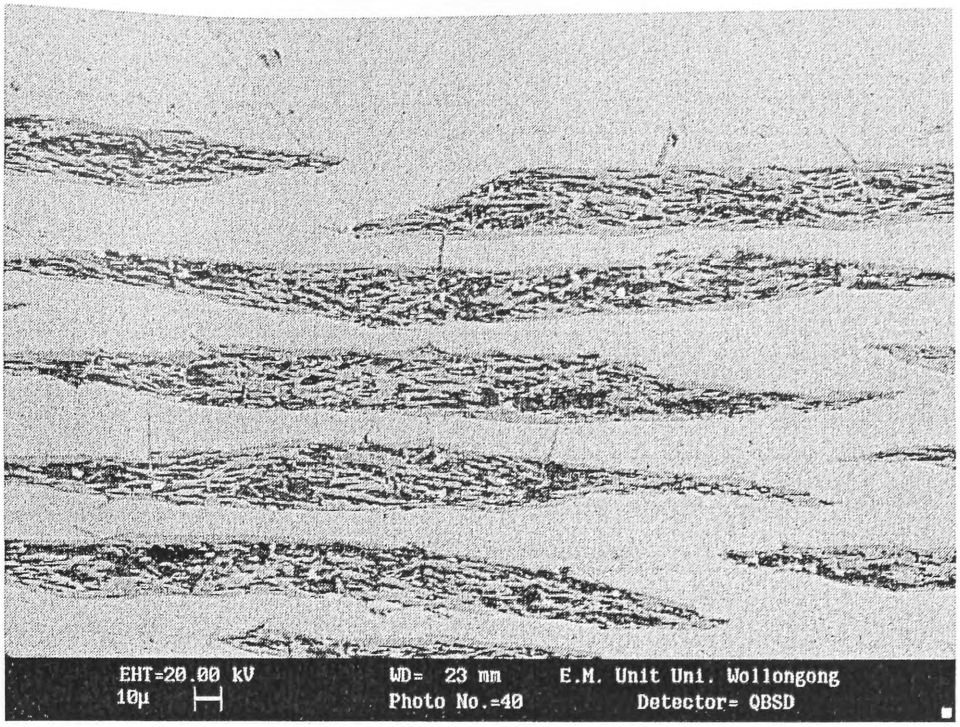

Figure 5. 22. SEM image of tape 3 after the first heat-treatment (HT1 = 840°C)

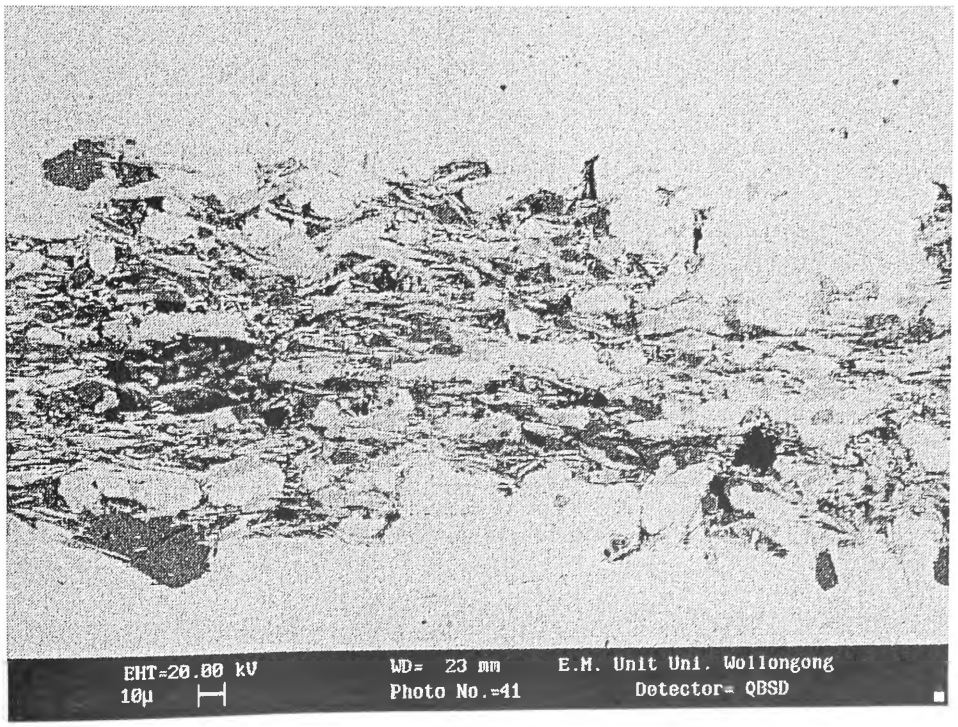

Figure 5. 23. SEM image of tape 4 after the first heat-treatment (HT1 = 840°C)

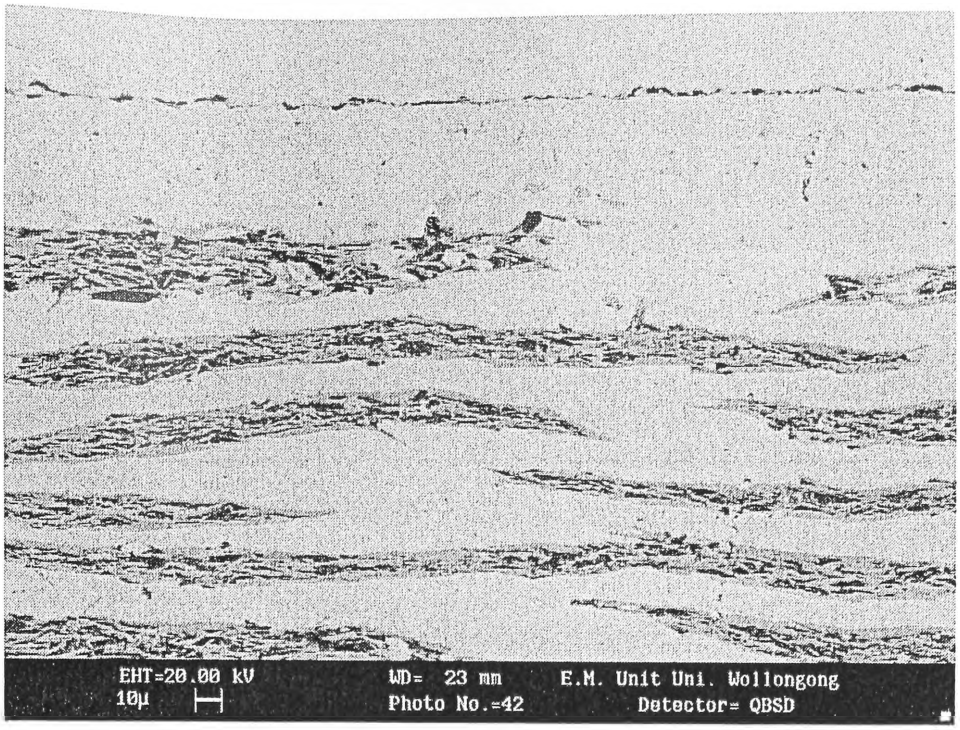

Figure 5. 24. SEM image of tape 5 after the first heat-treatment (HT1 = 840°C)

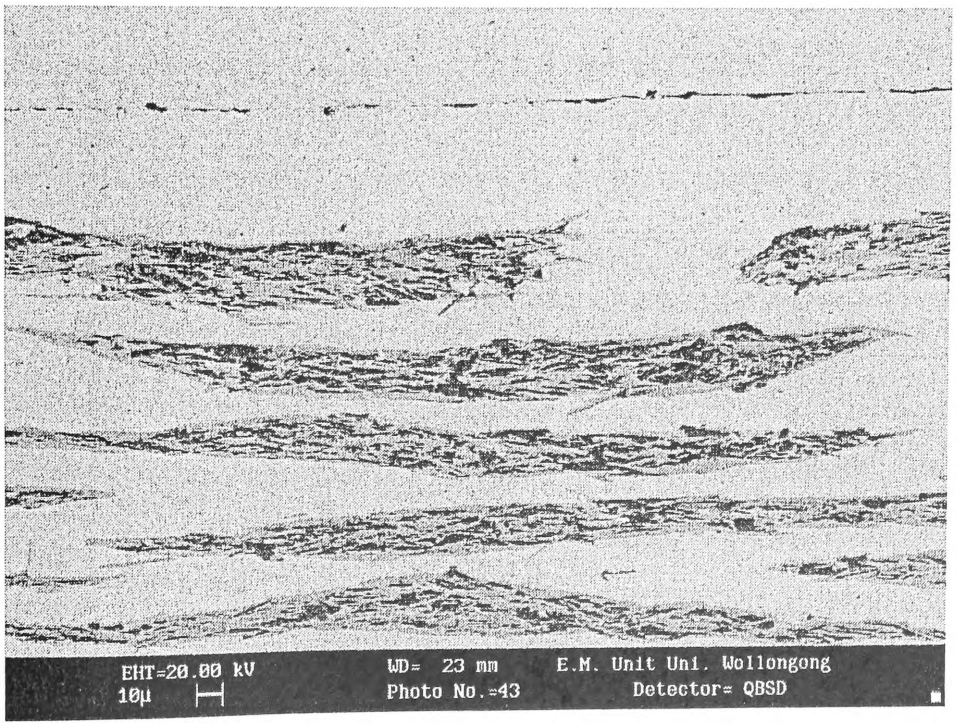

Figure 5. 25. SEM image of tape 6 after the first heat-treatment (HT1 = 840°C)

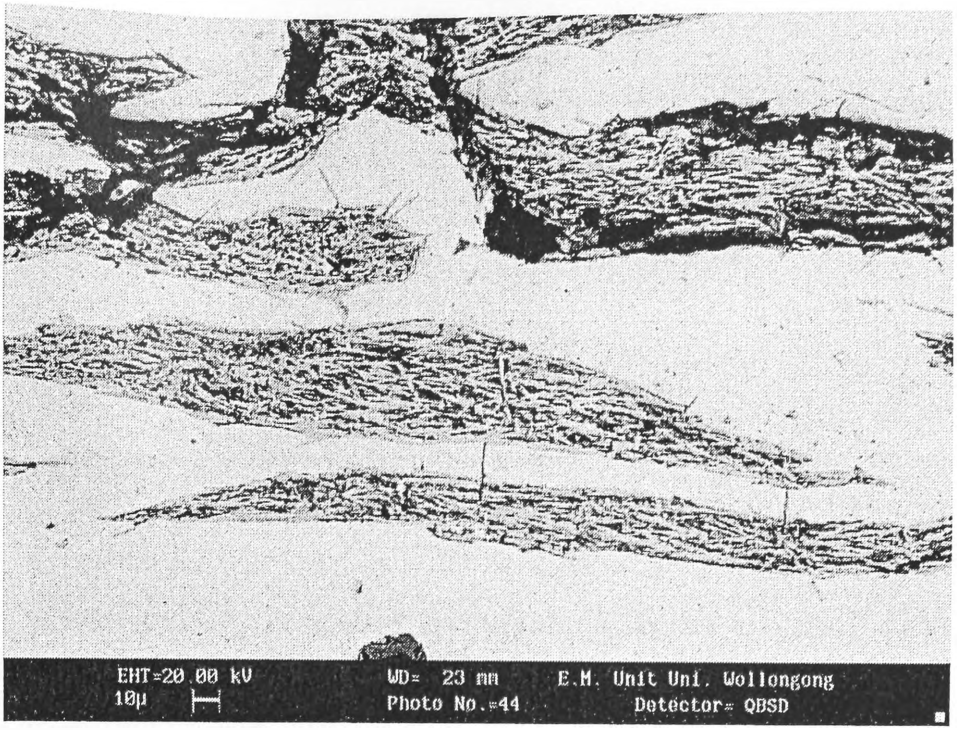

Figure 5. 26. SEM image of tape 7 after the first heat-treatment (HT1 = 840°C)

Figures 5.27 – 5.33 show SEM images of the final tapes 1-7. After intermediate rolling and HT2, the cores become denser and better aligned compared with the tapes after HT1. The amount of second phase in tapes 1, 2 and 7 is less than in tapes 3, 5 and 6. Tape 4 contains more impurity phase. Compared with the tapes after HT1, the amount of second phase decreases in each tape. In Figure 5.33, it can be seen that Bi-2223 phase (grey) crystals has a high volume content (>90%), while there is a very small amount of Bi-2212 (thin white layer), and impurity phases of CuO and Ca_2CuO_3 (black).

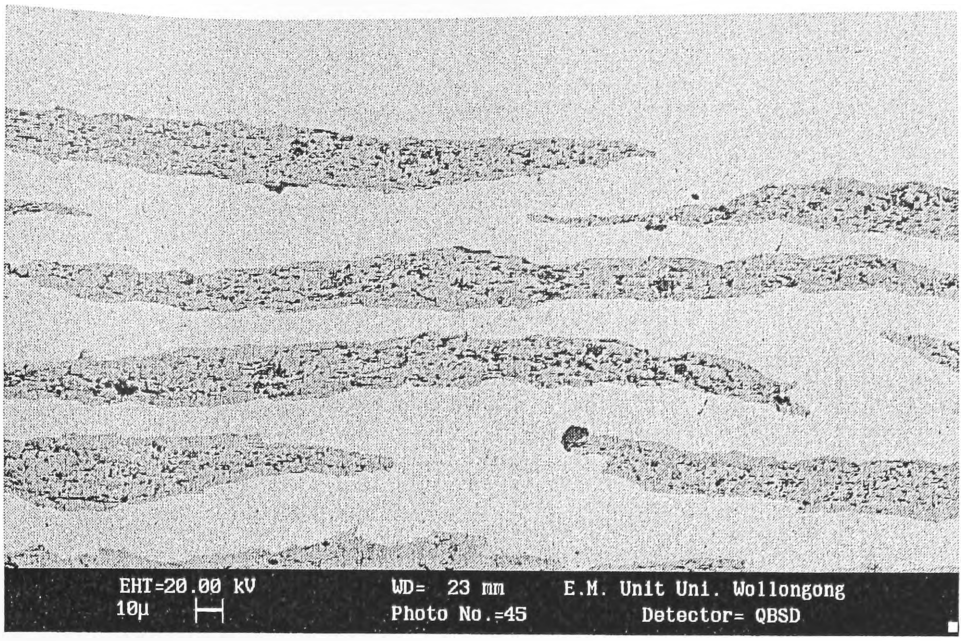

Figure 5. 27. SEM image of tape 1 after HT2

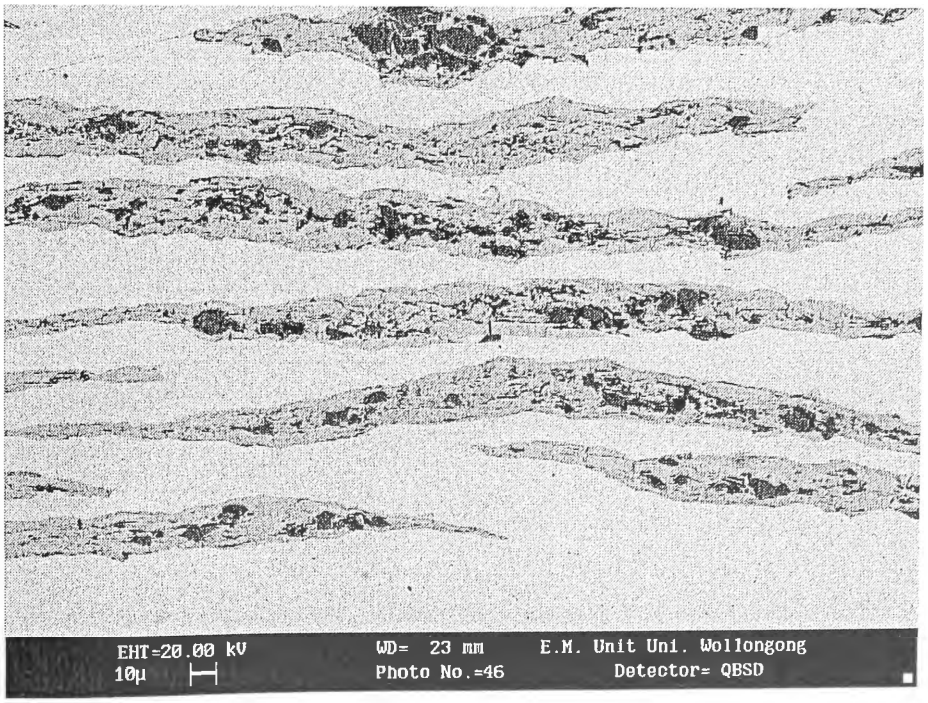

Figure 5.28. SEM image of tape 2 after HT2

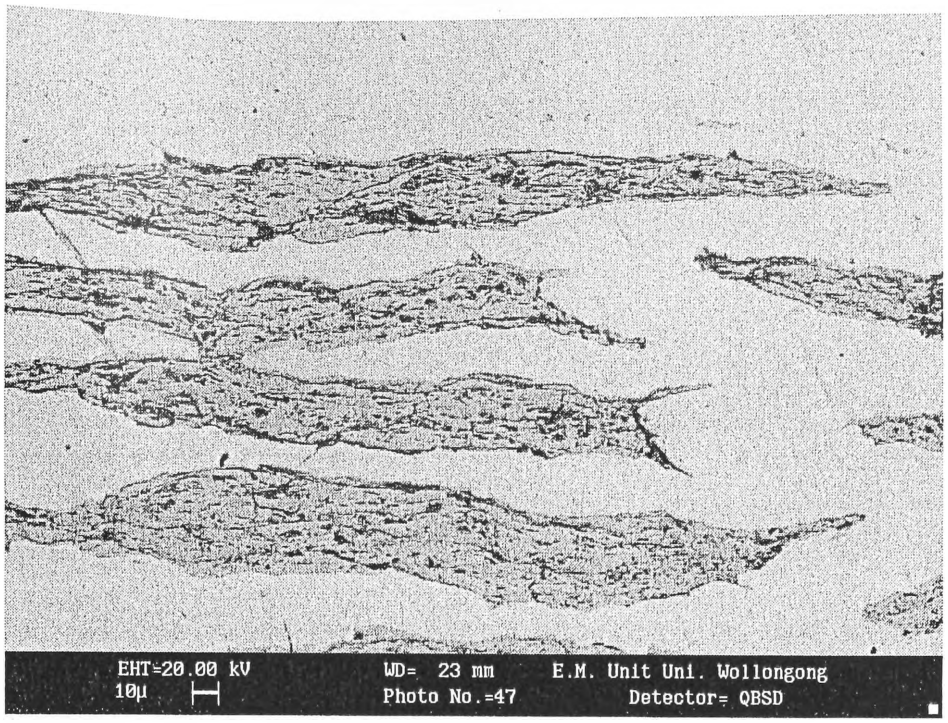

Figure 5. 29. SEM image of tape 3 after HT2

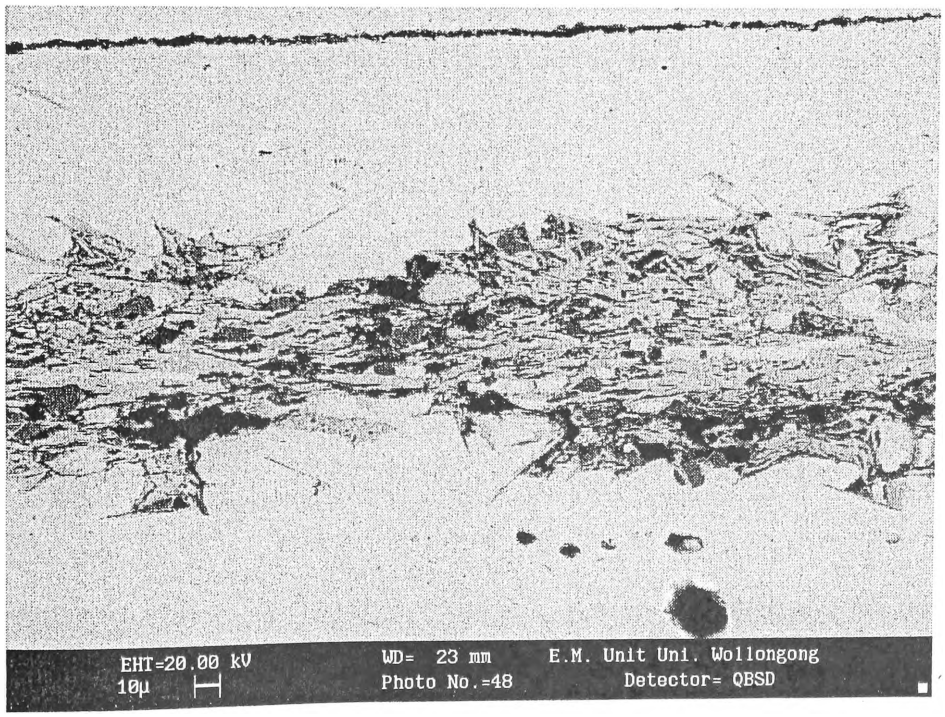

Figure 5. 30. SEM image of tape 4 after HT2

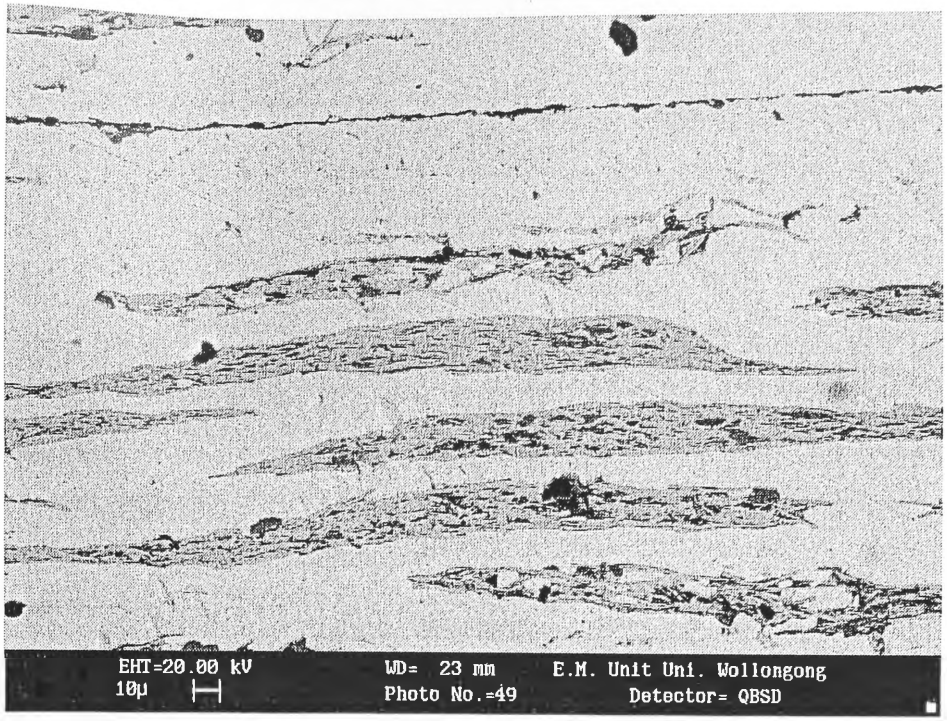

Figure 5. 31. SEM image of tape 5 after HT2

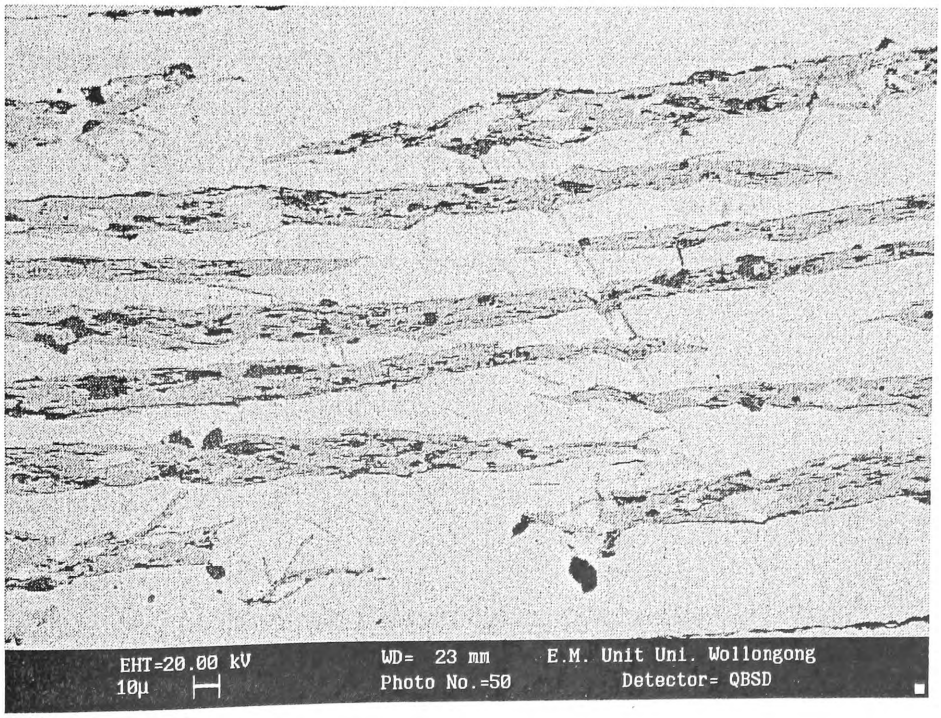

Figure 5. 32. SEM image of tape 6 after HT2

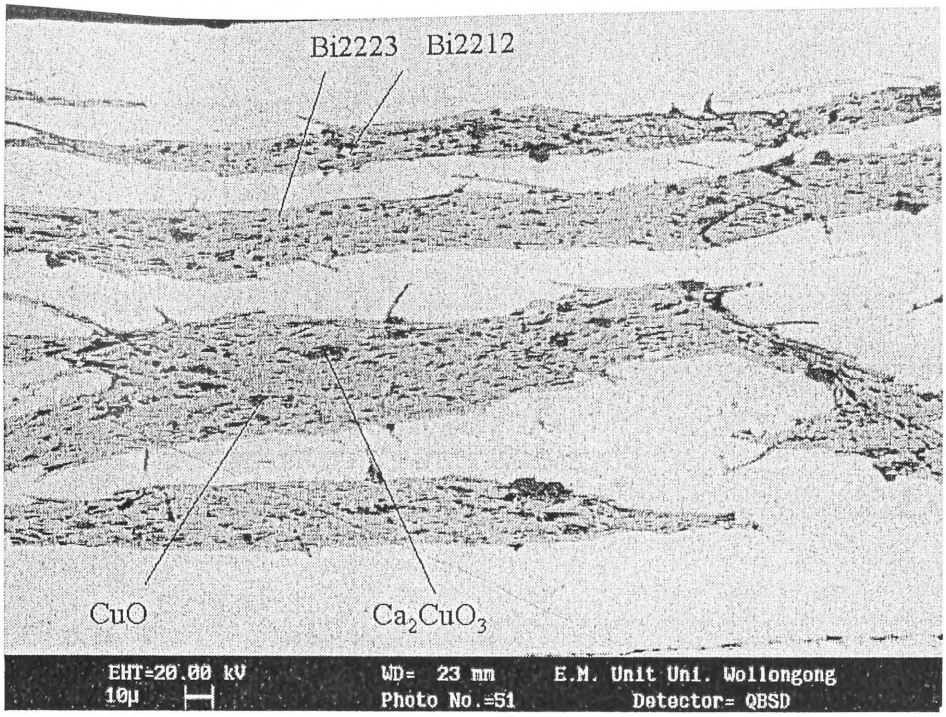

Figure 5. 33. SEM image of tape 7 after HT2

Reference

[1]. S.H. Jang, J. H. Lim, J. H. Kim, B.K. Ji, J. H. Hoo, W. S. Nan, J.S. Vol, H. K. Liu, and M. Apperley, IEEE, Trans. Appl. Supercond., 2003, in press.

Chapter 6. Discussion and Conclusion

Table 6.1 summarizes the properties of the Ag and Ag-alloy sheathed Bi2223 tapes studied. Optimized I_c (at 77 K, 0 T), J_c/J_{c0} (at 77 K, 0.4 T), bending strain, the ranking of hardness and tensile strain, and the volume fraction of Bi-2223, Bi-2212 and Bi-3221 phases are given.

6.1. Phase composition

Tables 5.1-5.4 show the volume fractions of the Bi-2223, Bi-2212, Bi-2201 and Bi-3221 phases for the tapes after HT 1 = 834°C, 838 °C, 840 °C and 842 °C, and after HT 2. It is seen that after HT 1 about 80% of core was converted into Bi-2223 phase with the rest remaining phases in most cases, because the major phase was Bi-2212 in the green tapes and there was almost no Bi-2223 phase. The main purposes of sintering are to convert Bi-2212 into Bi-2223 and to achieve grain growth and grain connectivity [1]. With HT 2, the fraction of Bi-2223 phase reached about 95%, Bi-2201 was converted into superconducting phase during sintering at lower temperature (810 °C - 825 °C) [2], and slow cooling eliminated Bi-3221 [3].

From the X-ray patterns shown in Chapter 3, it can be seen that AgAu alloy has more effect on Bi-2223 phase formation than AgSb alloy. After HT 1, XRD patterns show more Bi-2201 phase in the tape with the AgSb sheath than in the others, indicating that the Sb reduced the melting point of the precursor. There is more Bi-2212 phase in the tapes with AgAu sheaths, indicating that Au decreased the reaction rate from other phases transferring to the Bi-2223 phase.

Table 6.1. The Main Properties of Ag and Ag-alloy Sheathed Bi-2223 Tapes

		Tape 1	Tape 2	Tape 3	Tape 4	Tape 5	Tape 6	Tape 7
Configuration	Restack	Ag	AgAu7wt%	AgSb0.6wt%	AgAu7wt%	AgSb0.6wt%	AgMg0.2wt%	Ag
	Precursor	Ag	AgAu7wt%	Ag	AgSb0.6wt%	AgAu7wt%	AgAu7wt%	AgSb0.6wt%
Optimize I_c (77 K, 0 T)	Value	21.315	25.699	29.375	22.535	27.718	24.720	35.208
	HT 1 Temp. °C	838	840	840	840	832	834	842
	J_c (10^4A/cm^2)	0.895	1.08	1.23	0.94	1.17	1.03	1.47
	J_e (10^4A/cm^2)	0.11	0.13	0.15	0.11	0.14	0.13	0.18
J_c/J_{c0} (77 K, 0 T)	H ⊥ c (%)	35	42	34	25	27	33	37
	Rank	2	1	3	4	4	3	2
	H // c (%)	1.7	1.7	0.6	2.9	2.3	0.5	2.2
	Rank	3	3	2	4	2	1	4
Bending Strain		0.33	0.28	0.43	0.25	0.47	0.68	0.32
Rank of Hardness		3	3	2	4	2	1	4
Rank of Tensile Strain		4	3	2	4	2	1	3
Volume Fraction of Bi-2223		94.3	84.3	95.2	82.9	91.8	84.1	94.8
Volume Fraction of Bi-2212		3.8	12.2	3.8	12.0	4.6	10.0	3.1
Volume Fraction of Bi-2201		0	0	0	0	0	0	0
Volume Fraction of Bi-3221		1.9	3.5	1	4.9	3.7	5.9	2.1

6.2. Electrical Properties

6.2.1. Optimized Critical Current I_c (at 77 K, 0 T)

From Table 6.1, it can be seen that the values of the optimum critical current I_c are mainly consistent with the XRD observations. When the volume fractions of Bi-2223, Bi-2212, Bi-2201 and Bi-3221 phases are at the level of Bi-2223 ~ 83-95%, Bi-2212 ~ 5%, Bi-2201 ~ 0% and Bi-3221 < 2%, the tapes show the highest I_c and J_c (as all the tapes have the same cross section area).

SEM observations of the cross section of the tapes (Figures 5.27—5.33) reveal that the amount of second phase in tapes 7, 2, and 3 is much less than in tape 4. The superconducting grain sizes of tapes 3, 5, and tape 6 are smaller than in tapes 1, 2 and 7.

Since growing Bi-2223 depends on a reaction between Bi-2212 and melting impurity phases like Ca_2PbO_4 and Ca_2CuO_3, and partial melting is important to the formation of Bi-2223 [4], the heat-treatment is very important to form pure Bi-2223 phase. With different Ag-alloys as restack and precursor sheath materials, the first heat-treatment temperature (HT 1) needs to be varied.

For tapes 1 and 2, using the same alloy as both precursor and restack matrix, their optimum I_cs occur at 838°C and 840 °C respectively and their I_c-temperature curves are shaped like a reversed U. For tapes 4 and 7, using AgSb alloy as the restack sheath and AgAu or Ag as the precursor sheath, the optimum I_c values occur at 840 °C and 842 °C, respectively. The I_c-temperature curve of tape 4 is wavy, and that of tape 7 forms a high I_c platform from 838 °C to 842 °C. For tapes 5 and 6, with AgAu alloy as the restack sheath, the optimum I_cs are lower at 832 °C and 834 °C, respectively. This result may mean that Sb can increase the optimized heat-treatment temperature.

From Figure 5.1, it is observed that the I_c's of tape 4 with different HT 1 (except HT 1 = 840°C) are very low under 10 A. SEM images (Figure 5. 24) strongly support this result because

they show that the oxide core has grown into the Ag-alloy sheath in the form of branches or spikes. Some oxide core branches connect together and form Ag-islands. In contrast to this, the outgrowths in tapes 2, 5, 6, and 7 are less than in tapes 3 and 4. Since high critical current densities depend on grain alignment [5] and high compression of a well-aligned plate-like grain structure in the core part [6 - 9], the SEM photos and XRD phase analysis can explain the results on the I_cs.

Also it is made clear that when AgAu alloy is used as restack material and AgSb alloy is used as precursor material, Sb composite can cause a serious reaction with the core oxide to form branches and spikes that can decrease I_c of the tape. But with pure Ag as the inner precursor material and AgSb alloy as the restack material as in tape 3, the reaction is not as serious as in tape 4. This result is consistent with some other research [10].

6.2.2. Normalized J_c - Field Dependence and the Sheath Materials

Figure 5.2 shows the relationship between the normalized J_c and the applied magnetic field, with the field perpendicular (H//c) and parallel to the tape surface (H//ab) at 77 K for the different tapes 1, 3, 5, 6 and 7 with HT1 = 838°C, and tapes 2 and 4 with HT1 = 842°C. Table 6.1 gives the value of J_c/J_{co} at 0.4 T at 77 K. It can be seen that the tapes 1, 2 and 7 with the restack sheath material Ag or AgAu, present better tolerance to magnetic fields parallel to the tape surface (H//ab), while tapes 4, 5 with restack and precursor materials of AgAu and AgSb matrix present better tolerance to magnetic fields perpendicular to the surface (H//c). Tape 7 with Ag as the restack material and AgSb as precursor material shows good tolerance to magnetic fields in both directions. These results mean that there is no conclusive correlation between alloy tapes or configuration and I_c performance in magnetic field. However, both XRD analysis and SEM images indicate that the best J_c-field dependence found in tapes 7, 2 and 1 are related to them having the highest fraction of Bi-2223, the lowest volume fraction of second

phases, the best grain connection, the best alignment and the least outgrowths.

6.3. Mechanical Properties

6.3.1. Bend Strain and the Sheath Materials

From the results of the one-way bending strain test for tapes 1 – 7 with HT1 = 840°C (Figure 5.3 and Table 6.1) it can be seen that the critical bending strain, ε_{crit}, of tapes 1 and 7, with Ag as the restack material, was at rank 3 among the 4 ranks of the seven tapes. The ε_{crit} of tapes 3 and 5, with AgSb as the restack material, was at rank 2. Tapes 2 and 4, with AgAu alloy as the restack material, were at rank 4 among the 4 ranks which means that the tape with AgAu restack material is the weakest in terms of bending. Tape 6, with AgMg as the restack material, possessed the highest ε_{crit} of 0.73%, displaying the best performance of I_c tolerance to bending strain.

Combining these results with the optical microscope images shown in Figures 5. 6 – 5.12, it can be inferred that tape 6 displays the best performance I_c tolerance to bend strain because the sheath of tape 6 has the smallest grains. The optical microscope images of tapes 2 and 4 do not show very clear grains because Au is hard to etch. However, Au is a very soft metal that cannot firmly support the core. The optical microscope images of tapes 3 and 5 also show very small grains, but the bending strain tolerances of these two tapes are not as good as for tape 6. The thick black dots, especially numerous in tape 3, may indicate that there is a reaction between Sb and oxygen that produce some Sb oxides. The Sb oxides reduce the tolerance to bending strain. Because there is much more Sb oxide in tape 3 this can explain why the tolerance to bending strain of tape 3 is weaker than that of tape 5. The optical microscope images of tapes 1 and 7 show very large grains that can explain why tapes 1 and 7 cannot endure to bending. The black dots at the interface between the precursor and restack materials indicate a reaction of Sb and

oxide that reduces the tolerance to bending of tape 7. This is why the ε_{crit} of tape 7 is less than that of tape 1.

From these results it can be concluded that tapes with like restack sheath materials had similar bend strain properties and that the improved tolerance to bending strain could be related to the mechanical properties of the sheath materials.

6.3.2. Hardness Profiles and the Sheath Materials

The hardness of the sheath materials shown in Figure.5.4 indicates that tape 6 with Mg in the restack sheath shows the highest hardness, while the sheaths of tapes 3 and 5, containing AgSb as the restack material show the next level of hardness; the lowest level of hardness appears in tapes with Au or pure Ag in the restack sheath.

For tape 6, the hardness is lower near the filaments (precursor sheath-AgAu alloy), and it increases towards the tape edge, reaching a plateau at the restack sheath (AgMg alloy). This is consistent with the literature [11]. Generally, the higher the concentration of solute atoms, in this instance Mg, the higher the volume fraction of the precipitated phase and consequently the higher the maximum hardness. Similar situation occurs in tapes 3 and 5 with the element Sb in the restack sheath.

The sequence of the sheath hardness from highest to lowest: AgMg0.2wt%, AgSb0.6wt%, AgAu7wt% or Ag is strongly supported by the optical microscope images. These results are consistent with the bending strain performance revealed in section 6.3.1. Harder restack sheaths, such as those with Mg or Sb, provide a mechanism by which the tolerance of the Bi-2223 to bending strain and its tensile strength and hardness can be improved. The reason for the differing alloy performance could be that during the sintering Mg is more easily oxidized to MgO and results in a harder sheath. Sb is also oxidized to oxide and increases the hardness of the sheath, but Au is very stable and cannot increase the hardness of the sheath. Mg greatly

increases hardness and strengthens the superconducting cores, so the best I_c tolerance to bending strain is contributed by Mg.

6.3.3. Tensile Strength and the Sheath Materials

From Figure 5.5 and Table 6.1, it can be seen that the tensile strength result is consistent with the hardness and bending results. The strongest tensile strength is found in tape 6, with the element Mg in the restack sheath, which ranks among the seven tapes, followed by tapes 3 and 5 containing AgSb as the restack material. The lowest level of tensile strength is found in tapes 1, 2, 4 and 7 with Au or pure Ag in the restack sheath.

These results can be explained very clearly by the optical microscope images on the sheath materials of these tapes. It is also consistent with some other research on mechanical properties of Ag-alloy sheathed Bi-2223 tapes. Mg and Sb have been introduced to form oxide particles for hardening tapes [12] and can enhance the tensile strength and tolerance to bending strain of the tapes.

The strength of pure Ag can be improved by the addition of an alloy element through solid solution strengthening and oxide dispersion strengthening. The alloy element in the Ag matrix will affect the lattice through the different sized alloy atoms. This lattice distortion acts to hinder dislocation movement and strengthen the matrix [12 -15]. A fine dispersion of oxide particles of an appropriate alloy element in the Ag matrix may improve the mechanical properties of Ag sheathed Bi-2223 tapes [16]. Mg or Sb exhibits limited solid solubility in Ag and is oxidised during the sintering process. Therefore, the fine dispersed oxide particles raise the tensile strength.

6.4. Conclusion

Ag, AgAu7wt%, AgSb0.6wt% and AgMg0.2wt% alloys were used as precursor and restack sheath materials for fabricating 37 filament Bi-2223 tapes using a PIT technique with a two-stage heat treatment process.

Analysis of the I_c and volume fractions of the Bi-2223, Bi-2212, Bi-2201 and Bi-3221 phases indicated that volume fractions of Bi-2223 ~ 83-95%, Bi-2212 ~ 5%, Bi-2201 ~ 0% and Bi-3221 < 2% normally result in tapes with the highest I_c.

The normalized J_c dependence on magnetic field of the tapes at 77 K at H//c and H//ab were compared. The relationship between J_c and magnetic field was characteristic of multifilamentary Bi-2223 tapes fabricated using a PIT technique. No conclusive correlation between alloy type or configuration and I_c performance in magnetic fields was established.

The sequence of the critical bend strains, ε_{crit} of the tapes is 0.73% for tape 6, 0.42% and 0.47% for tapes 3 and 5, ~0.3% for tapes 1 and 7, and 0.28% and 0.25% for tapes 2 and 4. Tapes with like restack sheath materials had similar bending strain properties. The variation in the bend strain tolerance of the tapes was consistent with the results of the hardness and tensile strength measurements. It was observed that the sequence of the sheath hardness and tensile strength from highest to lowest was AgMg0.2wt%, AgSb0.6wt%, AgAu7wt% or Ag corresponding to the ranking of bend strain tolerance.

SEM images show the process of Bi-2223 grain growth and grain connection by comparison of green tapes, tapes after HT 1 and tapes after HT 2. Higher density and better grain alignment in the superconducting core are responsible for higher J_c values.

Optical micrographs of the sheaths show the Ag and Ag-alloy particle sizes and oxide particles of MgO or Sb_2O_3. These oxides may result in lattice distortions and improve the mechanical properties. Also, the grain size in AgSb and AgMg sheath significantly restricts grain growth more than Au does in an Ag matrix. It is believed that the smaller grain size in the Ag alloys contributes to the higher strength of alloy-sheathed tape compared to that of Ag tape.

Through the results and discussion it is known that in general, using AgMg and AgSb

alloys as the precursor and restack materials of Bi-2223 tapes can extraordinarily improve the mechanical properties of HTS tapes, but doesn't definitely improve the electrical properties. The improved mechanical properties are probably due to strengthening mechanisms such as solid solution hardening, dispersion hardening, or grain size strengthening.

References

[1] H. K. Liu, M. Ionescu, and Y. C. Guo, in Handbook Adv. Elec. and Photonic Mat. and Devices—High Superconductors and Organic Conductors, H. S. Nalwa, eds., 2001, pp71-127.

[2] Y. C. Guo, J. Horvat, H. K. Liu, and S. X. Dou, Appl. Supercond. 5 (1997) 163.

[3] W. G Wang, J. Horvat, B. Zeimetz, H. K. Liu, and S. X. Dou, Physica C 291 (1997) 1..

[4] T. Hatano, K. Saota, S. Ikeda, K. Nakamura, and K. Owaga, Jpn. J. Appl. Phys. 27 (1988) L2055.

[5] Y. B. Yamada, B. Oberst and R. Flukiger, Supercond. Sci. Technol., 4 (1991) 165

[6] D. C. Larbalestier, X. Y. Cai, Y. Feng, H. Edelman, A. Umezawa, G N. Riley Jr., and W. L. Carter, Physica C 221 (1994) 299.

[7] G Grassp, B. Hemsel, A. Jeremie, and R. Flukiger, Physica C 241 (1995) 45.

[8] A. Sivakov, A. V. Lukashenkoo, D. Abraimov, P. Muller, A. V. Ustinov, and M. Leghissa, Appl. Phys lett. 76 (2000) 2597

[9] A. G Sivakov, A. V. Lukashenkoo, O. G Turutanov, I. M. Dmitrenko, D. V. Abraimov, P. Muller, and A. V. Ustinov, Physica B. 284-288 (2000) 2071.

[10] R. Zeng, Ph.D Thesis (1999), University of Wollongong, p148.

[11] R. E. Read-Hill, Physical Metallurgy Principles, 2nd ed. Monterey: Wadsworth, 1973.

[12] J. Trnbrink, M. Wilhelm, K. Heine and H. Krauth, IEEE Trans. Magn. 3 (1993) 1123.

[13] K. C. Goretta, J. l. Routbort, R. L. Thayer, J. P. Carroll, J. Wolfenstin, K. Kessler, and J. Schwartz, Physica C, 265 (1996) 201.

[14] W. Goldacker, E. Mossang, M. Quilitz, M. Rikel, IEEE Trans. Appl. Supercond. 7 (1997) 1407.

[15] P. X. Zhang, H. Maeda, L. Ahou, C. S. Li, Z. Z. Duan, H. L. Zheng, IEEE Trans. Appl. Supercond, 9 (1999) 2770.

[16] B. Ullman, A. Gabler, M. Quilitz, and W. Goldacker, IEEE Trans Appl. Supercond. 7 (1997) 2042.

Betta Bookbinding & Printing
M & D Morrisey 02 42612998
26 Fields St
Kanabooka NSW 2530